Technische Universität München
Lehrstuhl für Nanoelektronik

Alternative fabrication techniques for organic electronic devices

Philip Morten Alexander Schmidt

Vollständiger Abdruck der von der Fakultät für Elektrotechnik und Informationstechnik der Technischen Universität München zur Erlangung des akademischen Grades eines

Doktor-Ingenieurs

genehmigten Dissertation.

Vorsitzende:	Prof. Dr.-Ing. Sandra Hirche
Prüfer der Dissertation:	1. Prof. Paolo Lugli, Ph.D.
	2. Assoc. Prof. Aldo Di Carlo, Ph.D.

Die Dissertation wurde am 14.09.2016 bei der Technischen Universität München eingereicht und durch die Fakultät für Elektrotechnik und Informationstechnik am 29.05.2017 angenommen.

"If you try and take a cat apart to see how it works,
the first thing you have on your hands is a non-working cat."

-Douglas Adams

Abstract

Organic electronics are a fast developing and promising field of research. The number of possible applications is constantly growing. Commonly used fabrication methods like spincoating or ink-jet printing are not suitable for every purpose. In this thesis alternative fabrication methods for organic electronic devices are investigated.

First the feasibility of spraycoated transparent conductive organic electrodes was investigated. Also a lithography process using the same material system was developed and used to fabricate fully organic electrolyte gated transistors. Spraycoating of transparent conductive organic electrodes has later been used to fabricate organic photodetectors. The fabricated photodetectors had an external quantum efficiency of 62% and on-off-ratios of nearly 4 orders of magnitude. A responsivity of 0.25 A/W at 530 nm was reached.

In a next step the applicability of spraycoating in the fabrication of full solid state organic potentiometric sensors and the fabrication of CNT-FET based ISFETs was demonstrated. Both systems are based on spraycoated ion-selective membranes.

In a last step the feasibility of nanoimprinting and nanotransferprinting for the fabrication of nanostructured organic solar cells was investigated, resulting in nanotextured organic solar cells with a 16,8 % higher power conversion efficiency than not structured devices.

Contents

1 Introduction

Organic electronics have gained a huge increase in attention in the recent years. They offer a wide variety of possible applications. The by far most popular one is the field of organic optoelectronic devices. The most prominent examples from this field are organic solar cells and organic light emitting diodes. Both kinds of devices attracted a lot of attention in the scientific community. But also organic chemical sensors, bio-sensors and organic RFID devices are the aim of research.

Organic electronic devices do not outperform their inorganic counterparts. Therefore they will mostly not be a replacement but lead to new products, as they offer major advantages like flexibility and low-cost production. The low-cost production potential mainly emerges from the solution processability of organic devices. Solution processability describes the possibility to process a material in its liquid state. This ability allows the use of processing technologies well known from the printing and painting industry. Good examples are ink-jet printing, screen printing and spray coating. Compared to standard fabrication technologies used in the semiconductor industry, like thermal evaporation and other vacuum based processes, these long known technologies require relatively little equipment. Thus they allow a more cost effective way of fabrication.

A wide variety of different fabrication techniques is used for the fabrication of organic devices. The most common techniques are the previously mentioned

ink jet printing and the mainly in laboratory scale production used spin coating. Spray coating and nanotransferprinting which are not common in the fabrication of organic devices would provide a valuable addition to the already established technologies. The main focus of this thesis is the evaluation of these alternative fabrication methods for organic devices. Especially the device fabrication using the fabrication methods spray coating and nanotransferprinting will be examined in detail. Spray coating will be used to fabricate indium-tin-oxide free organic photodiodes and all solid state potentiometric sensors. nanotransferprinting will b e used to fabricate nanopatterned organic solar cells.

Chapter 2 will give a brief overview of the physical background of solar cells, organic semiconductors, plasmonics and the used materials. In chapter 3 the used fabrication techniques are described in detail.

In chapter 3 the fabrication methods used in this thesis are described in detail.

Chapter 4 focuses on the fabrication of conductive organic electrodes by the use of the polymer poly(3,4-ethylenedioxythiophene):Polystyrene sulfonate. In this chapter the a conductivity increasment by chemical doping as well as the fabrication of fully carbon transistors with a lithography process.

In chapter 5 the fabrication of indium tin oxide free organic photodiodes by spray coating is demonstrated. The diodes use a conductive organic electrode as described in chapter 3 to replace the commonly used indium tin oxide.

The first all solid state organic potentiometric sensors fabricated completely by spray coating is demonstrated in chapter 6. The sensors are based on a carbon nanotube electrode covered with an ion-selective membrane. Also the fabrication of ion-selective field effect transistors with a spray coated membrane is demonstrated.

In the last chapter of this work, chapter 7, the fabrication of nanotextured organic solar cells by nanoimprinting and nanotransferprinting is demonstrated.

2 Physical background and materials

The following chapter covers the physical and technical background on which this work is based. First organic electronics will be addressed, followed by details about solar cells. Also the most important materials used in this thesis will be described in detail.

2.1 Physics of solar cells

Every second radiation with the energy of approximately $752\,\mathrm{W/m^2}$ reaches the earth surface. Since the description of the photoelectric effect by Albert Einstein in 1905 [1] lots of effort has been invested to use this physical principle to tap this unlimited amount of energy which is supplied by the sun. This resulted in a huge variety of different kinds of photovoltaic cells. All these cells have in common that they are based on the so called inner photoelectric effect. This effect describes the transfer of an electron from one energy level to another triggered by the absorption of light. This will be described in the following section in more detail.

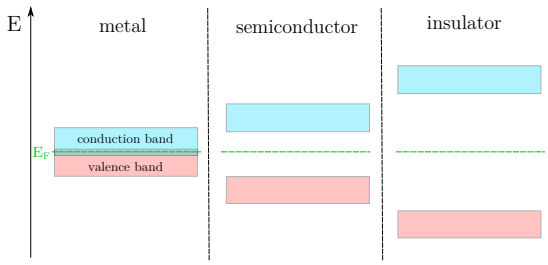

Figure 2.1: Schematic overview on the band structure of different kind of solids

2.1.1 Semiconductors

If an atom is hit by a photon it is possible that this photon is absorbed. The energy of the photon is in this case transferred to an electron, which due to this additional energy is transferred to a higher energy state. The photon can only be absorbed if its energy is high enough to lift the electron above the gap between the two energy levels. If two atoms form a molecule these energy levels form molecule orbitals with discrete energy levels. In a large periodic molecule or crystal made of thousands of atoms these allowed energy levels are so close together that they can be considered as a continuum or in other words a band. Still there are some energy states which are forbidden. These forbidden zones divide the continuum into separated bands. The width of such a band gap is defined as the energy difference between the two neighbouring gaps.

$$E_G = \Delta E = E_2 - E_1 \tag{2.1}$$

With the energy of the band gap E_G, the energy of the valence band E_2 and the energy of the conduction band E_1.

Now if a photon is absorbed the electron is transferred from one band to another. In a band with higher energy electrons interact less with the cores of

the atoms forming the crystal and therefore can move freely along the crystal. In other words they can contribute to the charge transport. If a band can contribute to the charge transport or not depends on its filling level and how strong the electrons filling the level are bound to their atoms. An empty band can not contribute due to the lack of charge carriers. A band which is full, respectively in which all possible states are occupied, can also not contribute to the transport as well. Only partly filled bands can. The highest band in which electrons are present at absolute zero temperature is called valence band. The electrons filling this band are usually strongly bound, not allowing them to contribute in the charge transport. But if an electron is transferred into a higher band, which is not or only partly filled, it can move freely. For this reason these energy bands are called conduction bands.

The distance between the valence and the conduction band divides all solids into three groups as depicted in figure 2.1: metals, semiconductors and insulators. In metals the valence and conduction band are overlapping. No energy is required to transfer an electron from the valence to the conduction band, making the metal a good conductor. Semiconductors have a small gap between the bands. To transfer an electron to the conduction band energy is required, which can for example be provided by light absorption, as mentioned earlier, or by thermal energy. The last group are the insulators. These have a large gap between the valence and the conduction band, which usually can not be overcome.

2.1.2 The photovoltaic effect

When an electron is transferred to the conduction band, it leaves an empty spot in the valence band. This empty spot, usually called electron hole or simply

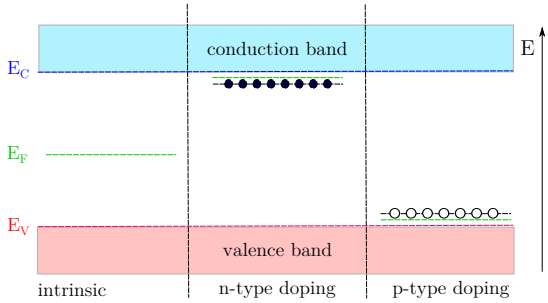

Figure 2.2: Band structure of different kinds of doped semiconductors compared to an intrincis semiconductor

hole, can be treated as a particle with a positive charge and a negative effective mass which can move through the band like an electron. By doping the crystal with atoms having more or less valence electrons than the atoms the rest of the crystal is made of the concentration of holes and unbound electrons can be increased. This results in the addition of new energy levels as depicted in figure 2.2. If the dopant adds more electrons, or in other words negative charges, one speaks of a n-type doping. If holes are added, one speaks of a p-type doping respectively. In an intrinsic (undoped) semiconductor the number of positive and negative charges is the same and can be described according to equation 2.2.

$$n = p = n_i \tag{2.2}$$

With the concentration of conducting electrons n, the concentration of conducting electron holes p and the intrinsic concentration of charge carriers of the material n_i. But if the semiconductor is non-intrinsic (doped) it becomes:

$$n_0 \cdot p_0 = n_i^2 \tag{2.3}$$

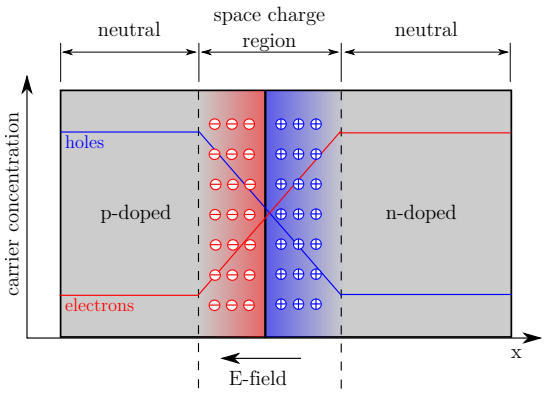

Figure 2.3: Schematic of a p-n-junction with zero voltage bias at thermal equilibrium. Electron concentration is shown by red line, while hole concentration is shown by blue line

When p- and n-doped areas are brought together, electrons from the n-doped part close to the interface tend to diffuse into the p-doped part while holes from the p-doped part close to the interface diffuse to the n-doped part. As the electrons leave positively charged and the holes leave negatively charged ions a space charge region or depletion layer is formed (see figure 2.3).

If now a forward bias is applied (p-doped region is connected with the positive pole and the n-doped region is connected with the negative pole) the electrons in the n-type region and the holes in the p-type region are pushed towards the junction. The thickness of the depletion layer and the potential barrier is reduced with increasing forward bias. If the forward bias is increased further the depletion layer eventually becomes thin enough that the electric field can not hold back the charge carriers from moving across the p-n-interface. This reduces the electric resistance of the junction.

The current-voltage behaviour of such a junction is displayed in figure 2.3. It can be described with the Shockley ideal diode equation (also called the diode law):

$$I = I_s \left(e^{\frac{V_D}{nV_T}} - 1 \right) \tag{2.4}$$

With reverse bias saturation current I_s, the voltage across the diode V_D, the thermal voltage V_T and the ideality factor n. The shape of current voltage behaviour is depicted in figure 2.4. The red curve shows the behaviour if the semiconductor is not illuminated with light. As previously described, if a forward bias is applied the semiconductor becomes conductive at a certain point. This point is called the the turn-on voltage or threshold voltage V_d. At lower voltages the diode stays non conductive. If a reverse bias is applied, a similar behaviour occurs. The diode stays non conductive until the so called breakdown voltage V_{br}. Here the current rises dramatically. Between turn-on and breakdown voltage only a very small current flows. It is called saturation current I_s and is caused by thermally generated charge carriers. In photodiodes this current is also called dark current.

If now this diode is illuminated with light additional excitons are generated by photoexcitation. These excitons are separated by the built in field and drift to the n-doped respectively p-doped area, generating a potential difference or in other words a voltage. If now both parts are connected through a wire, a current starts to flow to equalize the accumulated charges. This current can now be extracted, making the photosensitive diode a solar cell.

When characterizing a solar cell one usually focuses on the following parameters (see figure 2.4):

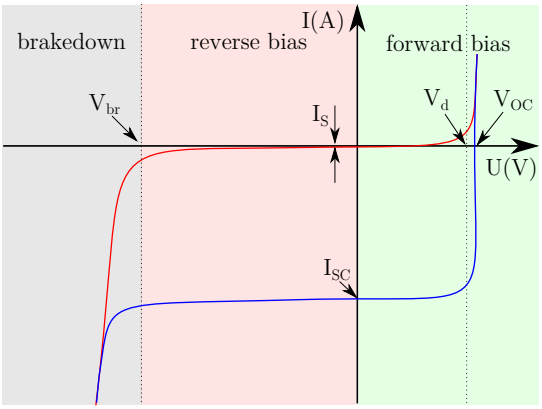

Figure 2.4: I-v-characteristics of a diode (p-n-junction) in the dark (red) and under illumination (blue). With the reverse bias saturation current I_s, the turn-on voltage of the diode V_d and the breakdown voltage V_{br}

- The open circuit voltage V_{oc}, the potential that is generated if both poles are not connected (open circuit).
- The short circuit current I_{sc}, the current that flows if both poles are connected without any electrical resistance.
- The maximum power point M_{pp}, the point were the solar cell produces the highest power. Product of V_{pp} and I_{pp}.
- The maximum power point voltage V_{pp}.
- The maximum power point current I_{pp}.
- The solar cell area a_{sc}.

These parameters allow to calculate the most important parameter of a solar cell: The power conversion efficiency η_{sc} (see equation (2.5)).

$$\eta_{sc} = \frac{V_{pp} \cdot I_{pp}}{P_L \cdot a} = \frac{M_{pp}}{P_l \cdot a_{sc}} \tag{2.5}$$

With the incident light power P_L and the solar cell area a_{sc}. η_{sc} defines how much of the incoming light is actually converted into electrical energy that can be extracted from the solar cell. Another important parameter is the fill factor FF a solar cell.

$$FF = \frac{M_{pp}}{V_{oc} \cdot I_{sc}} \tag{2.6}$$

FF is the ratio between the maximum power point and the product of the open circuit voltage and short circuit current (an "'ideal solar cell"'). Cells with a high fill factor usually have a low series resistance and a high shunt resistance and therefore low internal losses.

2.2 Organic electronics

Organic electronics have been the aim of lots of research [2–4]. The history of organic electronics begins with the groundbreaking work of Heeger *et al* in the late seventies which was awarded by the Nobel price in Chemistry of 2000 [5]. After this a vibrant development started resulting in a large field of applications, ranging from organic field effect transistors (OFET) for biosensing or radio-frequency identification (RFID) applications [6–8] over organic light emitting diode (OLED) [9] to organic photovoltaic devices [10, 11].

The biggest advantage of organic electronics is the easy processability. Organic semiconductors can usually be processed in liquid, allowing cost effective production techniques like ink-jet printing, spin coating or, as also described in this work, spray coating. Another advantage is the lack of use of rare earth

metals which suffer from limited availability and increasing costs. While never reaching the effectiveness of inorganic devices, organic devices pave the way for semitransparent, flexible, low cost or even single use electronics.

A lot of these above mentioned applications are based on organic semiconductors whose properties are rooting in physical principles which are described in detail in the following sections, starting with the most fundamental principle of conjugated polymers.

2.2.1 Conjugated polymers

A conjugated system is defined as a system usually made of carbon atoms with alternating single and double bonds. During the bond formation, the carbon atoms form 3 sp^2-hybrid orbitals with an angle of 120° between them. Perpendicular to this hybrid orbital an unchanged p-orbital remains. The in plane sp^2 hybrid orbitals will form strong bonds called σ-bonds in which the electrons are highly localized. These σ-bonds are the "backbone" of the polymers, but due to the strong binding energy they do not contribute to the conductivity. The remaining p-orbitals perpendicular to the σ-bonds overlap and form so called π-orbitals, which are connected. As the degree of overlap is low, the binding energy is low, allowing the electrons to move freely along the chain. The electrons in these orbitals can no longer be assigned to a certain atom and are therefore considered delocalized. According to the molecular orbital theory this overlapping orbitals can be considered as a molecular orbital in which the π-electrons can move freely. This is considered as the origin of the semiconducting behaviour of the organic semiconductor.

When two atoms form a bond, the electron wavefunctions of the atoms overlap, splitting the all energy levels of the isolated atoms into pairs of two levels,

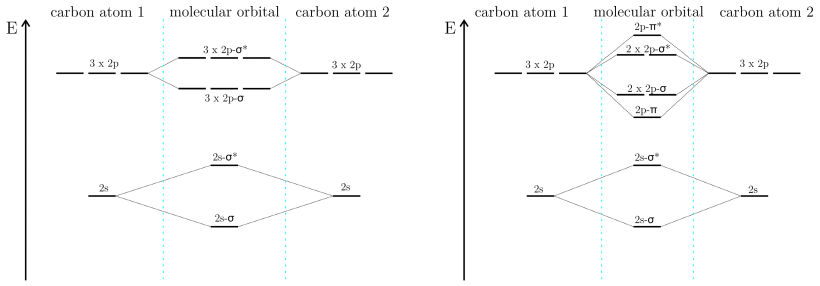

Figure 2.5: resulting molecular orbitals of binding carbon atoms. a) without hybridization b) with hybridization

which belong to the molecule instead. One of these is lower in energy and one higher than the original atomic levels, called antibinding and binding. As electrons tend to fill levels with low energy first, the binding levels are filled first, leaving the antibinding levels empty. This lowers the overall energy of the molecule and thereby increases the binding energy of the molecule. As the binding levels or orbitals are usually filled they are referred to as highest occupied molecular orbital (HOMO), while the usually empty antibinding orbitals are referred to as lowest unoccupied molecular orbital (LUMO). Due to the increased splitting of the energy levels with increasing chain length a band-like structure similar to that of inorganic semiconductors develops, with the gap between HOMO and LUMO as bandgap.

When the polymer chain is exposed to light, photons with energy higher than the bandgap of the conjugated polymer can be absorbed. The photon energy lifts an electron from the HOMO to the LUMO level, leaving a hole on the HOMO level. This way an electron hole pair bound by Coulomb forces is created, which can be considered as a quasiparticle and is called exciton. While these excitons are usually on the same molecule or polymer (intrachain) [12], in

some cases excitons on neighbouring molecules have been reported [13]. This energy is in organic semiconductors, other than in inorganic semiconductors, higher than the thermal energy at room temperature [14]. These excitons are usually called Frenkel excitons, while the weakly bound excitons in inorganic semiconductors are called Wannier -Mott excitons [15]. A more detailed discussion on these excitons can be found elsewhere [16].

To separate the two charges an energy greater than these Coulomb forces binding the exciton together has to be provided. In organic solar cells this is usually accomplished by the introduction of a electronegative acceptor material as described later (see section 2.2.3).

2.2.2 Charge transport

Once separated the charges have to be transported to the electrodes. ompared to inorganic semiconductors organic semiconductors show a mostly amorphous, in the best case highly polycrystalline character. Besides consisting of separated, only weakly bounded polymer chains organic semiconductors show structural defects like chain twists and kinks or chemical impurities. For this reason the charge transport differs from inorganic semiconductors. Instead of band transport like in crystalline inorganic semiconductors the charge transport is described better as hopping between localized states.

To describe this charge transport behaviour Bässler *et al.* [17] suggested a statistical transport model using the Miller-Abrahams hopping rate. In this model the density of states for electrons in the LUMO, respectively holes in the HOMO, is described as a Gaussian distribution.

$$D(E) = \frac{N}{\sqrt{2\pi\sigma^2}} \cdot 10^{-\frac{(E-E_0)^2}{2\sigma^2}} \tag{2.7}$$

With the density of states for electrons $D(E)$, the density of monomer states N, $E - E_0$ the energy relative to the center of $D(E)$ and width of the Gaussian density of state distribution σ. Hopping of charge carriers can occur as inter or intra molecule transport. This hopping process, which also includes phonon interaction [18], is the main reason for the low charge carrier mobility in organic semiconductors.

2.2.3 The principle of a bulk heterojunction

As explained earlier excitons generated in an organic semiconductors can be separated by the introduction of a second organic semiconductor. A very easy way to achieve this would be the fabrication of a bilayer device. But as the exciton diffusion range is usually in the range of 10 nm [16] such a solar cell fabricated layer by layer could only separate excitons that are generated within this short distance to the interface (see figure 2.6 a). Cells fabricated in such a way have only very limited efficiency due to the high losses of either the light passing through the very thin device or the high recombination losses in thicker devices.

A possibility to overcome this is the fabrication of bilayer devices with an optimized structure (see figure 2.6 b). In such a solar cell the two organic semiconductors are structured in a way that excitons can, in the ideal case, always reach an interface where they can separate. Common examples for this are interdigitating comb-like structures. In these kinds of structures a grating structure is formed (for example by nanoimprinting) with lines that are only a few 10 nm wide. Excitons can now easily reach an interface where they separate. After separation the charges are transported through the corresponding

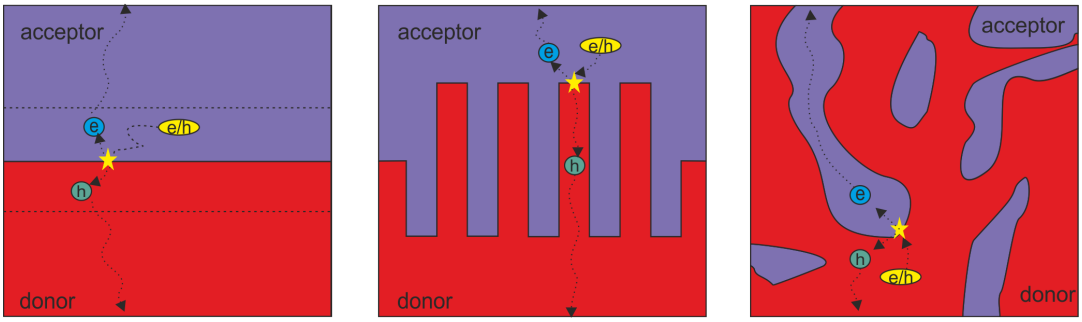

Figure 2.6: a) bilayer device b) bilayer device with optimized structure c) bulk heterojunction

semiconductor to the electrodes. This approach faces high difficulties from the production point of view.

The third and most common approach is the so called bulk heterojunction (see figure 2.6 c). In such a configuration both kinds of semiconductors are mixed during the production process. In the drying process after applying this mixture on a sample a phase separation occurs. Both organic semiconductors form a random network of separated fingers and islands. The size of these fingers and islands is usually in the range of tens of nanometers. Detailed studies about the morphology of bulk heterojunctions can be found elsewhere [19]. The main drawback of a bulk heterojunction compared to a bilayer cell with optimized structure is the formation of isolated semiconductor islands. After an exciton separation charge carriers can be caught in such islands with no transportation path to the corresponding electrode.

2.3 Materials

In this section the most important materials used in this work will be described in detail. Information about the other used materials can be found elsewhere.

2.3.1 Poly(3-hexylthiophen-2,5-diyl)

Sulfur heterocyles, or thiophenes, can polymerize to long polythiophene chains. These chains can become conductive when doped by adding or removing electrons from their conjugated π-orbitals but are usually not soluble in common solvents. A solubility can be achieved by adding suitable alkyl side groups (e.g. hexyl, methyl, ethyl) to the thiophenes [20]. In case of poly(3-hexylthiophene) (P3HT) this group is a hexyl group (see figure 2.7 a). During the synthesis of P3HT the thiophene rings polymerize between the 2- and 5- positions of the rings (see figure 2.7 b), allowing three different coupling mechanisms:

- 2,5' : head–tail (HT)
- 5,5' : tail–tail (TT)
- 2,2' : head–head (HH)

The higher the percentage of HT coupling in the polymer the higher is the inter- and intramolecular order. If it is higher than 95%, the P3HT is called regioregular P3HT (rr-P3HT). Due to its higher carrier mobility compared to regiorandom P3HT (rra-P3HT) it is preferred in device applications [21]. The valence band, respectively the HOMO level are 4,9-5,2 eV under the vacuum level. The conduction band is 2,9-3,3 eV below vacuum level. The resulting band gap is therefore 1,9 eV (see figure 2.7 c) [22, 23]. Typical hole mobilities

are $1 \times 10^{-6}\,\mathrm{cm}^2/(\mathrm{V\,s})$ [24]. The P3HT used in this work has been received from Rieke Metals Inc.

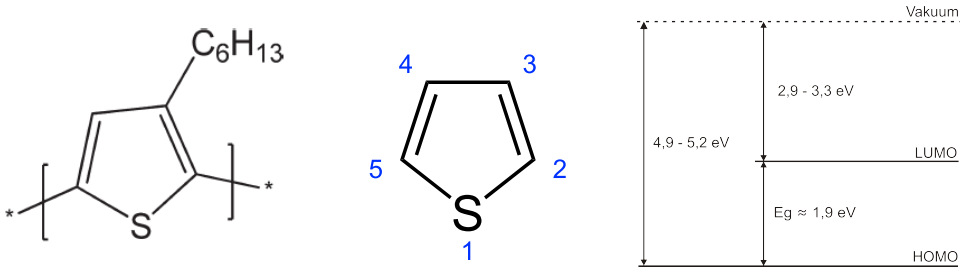

(a) (b) (c)

Figure 2.7: Poly(3-hexylthiophen) a) Chemical structure [21] b) Energy diagram with the HOMO and LUMO level in relation to the vacuum level

2.3.2 [6,6]-phenyl-C61-butyric acid methyl ester

[6,6]-phenyl-C61-butyric acid methyl ester (PCBM) is a fullerene derivative first syntecised by Hummelen *et al* in 1995 [25]. It consists of the buckyball called C_{60} molecule and a functional methyl-ester-group making it soluble in common aromatic solvents like chlorbenzene, dichlorebenzene or toluene. After first being used by Yu *et al* as electron acceptor material in a bulk heterojunction solar cell in 1995 [26] it became commonly used in organic solar cells or organic photodetectors [16, 27–30]. It has a HOMO-level of 6,1-6,8 eV, a LUMO-level of 3,7-4,1 eV, resulting in a band gap of approximately 2,7 eV [22, 23] and electron mobilities of $1 \times 10^{-7}\,\mathrm{cm}^2/(\mathrm{V\,s})$ [24]. See figure 2.8 for its chemical structure and band structure. The PCBM used in this work has been received from Solenne B.V.

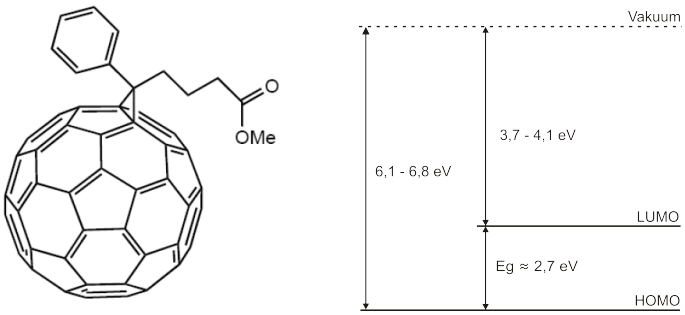

(a) (b)

Figure 2.8: [6,6]-phenyl-C61-butyric acid methyl ester [22] a) chemical structure b) Energy diagram with HOMO and LUMO level in relation to the vacuum level

2.3.3 Poly(3,4-ethylenedioxythiophene):Polystyrene sulfonate

Poly(3,4-ethylenedioxythiophene):poly(styrenesulfonate) (PEDOT:PSS), a conductive polymer, is widely used in organic optoelectronic devices like organic photodiode (OPD), organic solar cell (OSC) and OLED. Its success is based on its superior properties like high transparency, high thermal stability and easy processability [31]. The material is based on the conductive conjugated polythiophene poly (3,4-ethylenedioxythiophene) or PEDOT. If mixed with the polystyrene derivative poly (styrenesulfonic acid) or PSS it gets soluble in water, forming a polyelectrolyte complex (PEC) [32], thereby allowing it to be used in cost effective fabrication methods like spin and spraycoating. As a drawback, the conductivity of the polymer decreases with rising PSS content. While this is not critical or even favourable when used as hole conduction layer in photodiodes (see chapter 5), it becomes an issue when PEDOT:PSS is used as transparent conductive electrode. To make PEDOT:PSS suitable for this purpose, the conductivity can be increased by chemical doping which is described

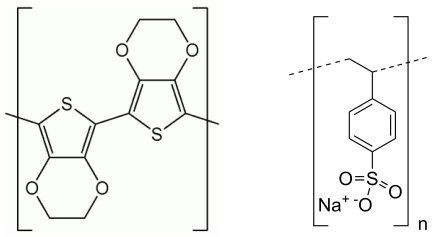

(a) (b)

Figure 2.9: Chemical structure of PEDOT:PSS a) poly(3,4-ethylenedioxythiophene) (PEDOT) [32] b) polystyrene sulfonate (PSS) [32]

later (see chapter 4.1). PEDOT:PSS has a work function of 5.2 eV and a band gap of approximately 1.5 eV[23]. Its chemical structure is depicted in figure 2.9. In this work the formulations Clevios P VP CH 8000, Clevios P VP AI4083 and Clevios PH 1000 by Haraeus were used.

As mentioned earlier PEDOT:PSS is widely used as interlayer in organic devices. A main reason for this is that by such an interlayer, the hole extraction and injection into the active layer of the device increases due to a reduction of the energy barrier [33], leading to a higher quantum efficiency. Also it has been stated that the PEDOT:PSS interlayer planarizes the indium tin oxide (ITO) layer often used in such devices [34]. This avoids local shorts caused by spikes on the ITO layer.

2.3.4 Polydimethylsiloxane

Polydimethylsiloxane (PDMS) is a silicone based organic polymer which belongs to the group of silicones. It is optically transparent, mostly inert, non inflammable and non toxic. Due to its properties it is used in a wide range of

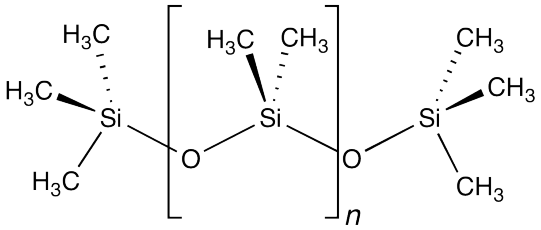

Figure 2.10: Chemical structure of Polydimethylsiloxane [35]

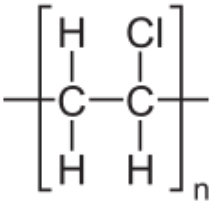

Figure 2.11: Chemical structure of polyvinyl chloride [37]

applications. It is used in foods, as conditioners in shampoos, in medical devices as well as in soft lithography [35]. In this work the PDMS formulation Silgard 184 from Dow Corning is used. The two component system consists of a liquid polymer base and a curing agent. After mixing both components they form a flexible elastomer which can be used immediately after the curing process is finished.

2.3.5 Polyvinyl chloride

Polyvinyl chloride or PVC, first synthesized by Eugene Baumann in 1872 [36], is after polyethylene and polypropylene one of the most produced and used polymer in the industry. Without the addition of plasticizers PVC is usually rigid. In this form it is commonly used for construction purposes like window frames. Also common is its use in the food industry as packaging material (i.e.

bottles) and the use in credit or debit cards. By the addition of a plasticizer the rigid material can be made more flexible [37]. In this flexible form it is used for inflatable products, leather imitation, electric cable insulation and clothing.

3 Fabrication technologies

In this work a multitude of fabrication technologies has been used. The following chapter aims to describe the techniques used in detail, beginning with details about the nanoimprinting and nanotransferprinting techniques and followed by spraycoating. The aim of this chapter is rather to deliver a base for the discussions in the later chapters than to present a complete review of the individual topics.

3.1 Optical lithography

Optical lithography is one of the most used processes in micro-technology. The vast majority of chips and microsystems is produced with this technology. For this process a sample covered with a photosensitive resist is exposed to light through a photomask. This makes the exposed areas soluble in a developer or, in case of a negative resist, insoluble. In a following step the sample is immersed into a developer solution. This solution dissolves the parts of the resist exposed to light, leaving only the unexposed parts at the sample which resemble the structure of the photomask.

The main drawback of this process is the need of expensive photomasks and the resolution limitation by the diffraction of light. The smallest possible feature

size which can be fabricated by a given photolithografic system can be calculated according to the following equation:

$$CD = \kappa_1 \frac{\lambda}{NA} \tag{3.1}$$

Where CD is the critical dimension, κ_1 a factor depending on the lithography system and photoresist, λ the wavelength of the used light and NA the numerical aperture. While κ_1 is in an up-to-date system around 0,4 (with a theoretical minimum of 0,25), NA can rise up to 0,93 (with a theroetical maximum for non immersion systems of 1)[38]. As all of these parameters are already close to the theoretical maximum, the next step would be a reduction of the wavelength of the light used. Modern systems use ArF excimer laser with a wavelength of 193 nm. A further reduction of the wavelength in next generation lithography systems is difficult, as for lower wavelength completely new optical systems have to be developed. An alternative approach to fabricate smaller structures is nanoimprint lithography.

3.2 Nanoimprint lithography

For photonic devices often large area nanostructures in the sub 25 nm region are needed. This need can not be fulfilled by commonly used optical lithography which is limited by the diffraction of light. Electron beam lithography on the other hand can reach the needed resolution but is slow and cost-intensive. A way to overcome these problems is Nanoimprint lithography (NIL), a nanopatterning technology that provides the possibility to achieve resolutions similar to that of high precision electron beam lithography, while allowing a fast large area fabrication of micro- and nanostructures at the same time. By the use of

prefabricated stamps instead of shadow masks it allows to overcome the resolution limit of optical lithography without the need to pattern each sample individually with electron beam lithography. It was first introduced by Chou *et al* in 1996 [39] and is getting more and more attention especially in research groups as it offers the possibility to fabricate large numbers of nanopatterned samples at reasonable costs.

Stamps for nanoimprinting are usually fabricated by electron beam lithography or eUV-lithography. These stamps, so called master stamps, are than replicated using specialized replication polymers like OrmoStamp from Microresist. The stamp replicas are than used for the actual imprinting process avoiding any damage to the master stamp caused by the imprint process. The stamps are covered with an antisticking layer to lower adhesion to the stamp [40]. For details on the stamp replication process see section 3.3.2.

3.2.1 Imprint process

The target substrate is covered with a thermoplastic imprint resist via spin coating. In this work only mr-I8020R from microresist was used for this purpose. Before spin coating the samples are baked at 200 °C to remove residual water vapor. After letting the sample cool down to room temperature the samples are covered with the resist and a spin speed is chosen that will result with a layer thickness defined by height of the structures on the used stamp. The right chose of layer thickness is important to reduce the residual layer thickness. After the sample is coated with resist the stamp is placed on top (see figure 3.1). Consecutively the sample is heated and pressure is applied. To achieve a conformal contact sample and stamp are usually covered with a foil or membrane and pressurized gas is filled in the room between foil and imprinter. By this a

conformal pressure all over the stamp is achieved. The resist is heated above its glass transition temperature and starts to flow into the structures on the stamp.

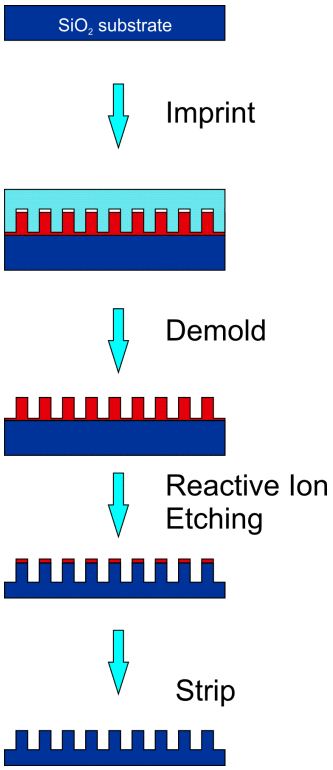

Figure 3.1: Schematic overview of the single steps in an imprint process.

Then the stamp is cooled down under the glass transition temperature of the resist and the stamp is removed. Another common technique is UV-NIL. In this case the imprint resist is not hard like in the previously described thermal NIL but stays liquid to some extent. The stamp is pressed into the liquid resist which is cured by UV exposure afterwards. The main advantage of this technique is the minimized heat load to the sample. As the curing by UV light is only a

matter of seconds, the imprint process is much faster because the heating and cooling steps can be skipped.

In both cases a negative of the stamp structure is transferred into the resist. The residual layer of resist in the structures can now be removed by reactive-ion-etching. After this step the sample can be further etched down, using the structured resist as etching mask, or other surface modifications are possible like metal evaporation or growth of nanowires.

3.2.2 Imprint parameters

The imprint process can be strongly influenced by the imprint temperature, the imprint time and the adhesion between sample, resist and stamp. Also important for later processing is the height of the residual layer.

In a thermal imprint process the imprint temperature is defined by the glass transition temperature T_g of the imprint resist. T_g is the temperature where a polymer is transferred from its solid form into a liquid. This is necessary to allow the resist to flow into the cavities on the imprint stamp. The more the imprint temperature is above this temperature, the less viscous is the imprint resist, allowing it to flow faster into the cavities. For this reason a sufficient high imprint temperature has to be chosen. In the case of the imprint resist used in this work (mr-I8020R from Microresist) is was 160 °C.

The duration of an imprint, the so called imprint time t_f, is also critical. It depends on the imprint Force F, the polymer viscosity η_0, the area of the imprinted structure (in this case simplified to length L and width s), the residual layer height h_f and the original thickness of the imprint resist h_0. See the following equation [41].

$$t_f = \frac{\eta_0 L s^3}{2F}\left(\frac{1}{h_f^2} - \frac{1}{h_0^2}\right) \tag{3.2}$$

The equation shows that the imprint force and viscosity only have a small influence ($t_f \approx 1/F$). Much stronger is the influence of the structure size of the imprint as well as the desired residual layer height in relation to the original resist thickness. By choosing a resist layer thickness close to the structure height of the stamp the residual layer which can be achieved in a reasonable amount of time can be minimized.

3.3 Nanotransfer printing

A closely related approach of nanotexturing is the so called Nanotransfer printing (nTP). Its main advantages are the mild process conditions like low temperature, low pressure, lack of need for expensive equipment (beside the mastermold) and the possibility of large scale production. Besides this, nTP offers the possibility of processing under inert gas atmosphere, especially favourable for easily degrading organic semiconductors like P3HT.

3.3.1 Transfer process

The main difference between nTP to nanoimprinting is that, contrary to nanoimprinting, there is no resist patterned on top of a substrate but an already structured layer is transferred onto the sample. These layers are transferred by the use of a nanotextured stamp similar to that used in nanoimprinting (see section 3.2). Commonly a flexible Polydimethylsiloxane (PDMS) copy is used instead

of a rigid stamp to achieve a better covering of the sample. A general overview on the process is depicted in Figure 3.2.

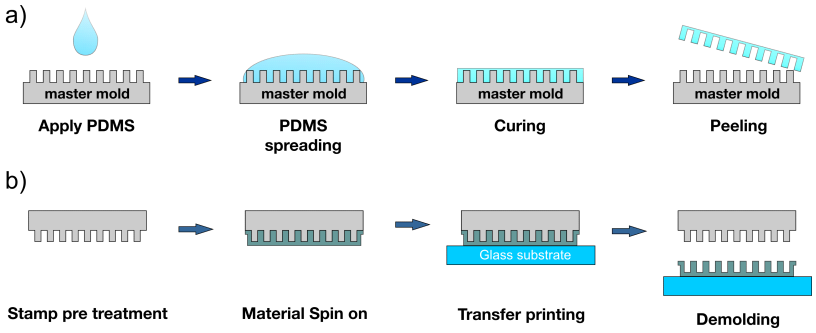

Figure 3.2: Schematic overview on the nano transferprinting process with flexible PDMS molds. a) Fabrication of the flexible transfer stamp b) Transferprinting process using the flexible stamp

As shown in the figure, first the stamp is covered with the desired material. Afterwards it is brought in contact with the sample. Pressure is applied to achieve a conformal contact between stamp and sample and the sample is heated to improve adhesion to the sample. As last step the stamp is peeled off leaving a layer with the desired structure on the sample. The most critical parts during this rather easy fabrication process is the adhesion between transferred layer and stamp as well as the adhesion between layer and substrate. For a transfer the adhesion between substrate and layer has to be higher than the adhesion between layer and stamp. This is often achieved by the application of anti-sticking layers onto the stamps before coating. Also critical is a conformal contact between sample and stamp. A transfer can only happen where the stamp gets in contact with the substrate. For this reason the use of flexible or "semi"-flexible stamps is common [42]. The obvious advantage of flexible stamps is that minor surface irregularities can be compensated. This is

especially favourable in case of the presence of dust particles on the substrate. When using a rigid stamp a single dust particle would result in a large area where no transfer happens. The more flexible the stamp is, the smaller this area gets. In an ideal case limiting it to the area of the dust particle itself. A drawback of flexible stamps is their weakness to compression. If too much pressure is applied, the stamps can deform with the result of a deformed transferred pattern. Usually the transfer process is carried out with copies to reduce costs as the stamps are covered with a material (i. e. is evaporated with a metal) and cleaning is mostly not possible [41].

3.3.2 Stamp fabrication

In this work two kinds of stamps have been used. For the transfer process flexible Polydimethylsiloxane (PDMS) copies of the master stamp have been used and for the imprint process (see section 3.2) "semi"-flexible copies have been used. As a starting point for both kinds of stamps a silicon master stamp with the desired structure fabricated with eUV-lithography and treated with an antisticking layer is necessary. The next step, the fabrication of a master copy with an inverse ('negative') of the original structure, is still identical for flexible an semi-flexible stamps. To obtain such a master copy several drops of the stamp replication polymer OrmoStamp [43–46] are applied on top of the silicon master. A 2" quartz wafer pretreated with an adhesion promoter (Ormoprime by microresist) is then placed on top. The OrmoStamp hybride polymer then spreads between the wafer and the silicon master and fills the structures on the master. Subsequently the OrmoStamp is cured by UV exposure in an Suss mask aligner for 60 s. After separation the cured and patterned OrmoStamp stays on the quartz wafer. After a hard bake of the copy at 130 °C for 30 min for 1 hour

is performed. The last step to finish the master copy is the treatment with an anti-sticking layer [40].

From this point the fabrication of flexible and 'semi'-flexible stamps differs. For flexible stamps the master copy is drop casted with PDMS (see section 2.3.4). Afterwards the master covered with PDMS is placed on a horizontally aligned hotplate and cured at 30 °C for 48 h. A low curing temperature is critical as PDMS tends to shrink when cured at high temperatures [47] and thereby the structure can be deformed. After curing the PDMS is peeled of the master and can be used for transfer or imprinting. See figure 3.2 for an overview of the fabrication process.

The fabrication process of the 'semi'-flexible stamps is pretty similar to that of the master copy. The main difference is that instead of a quartz wafer a 100 µm thin microscope cover slides are used. Instead of a relatively thick quartz wafer, these thin glass slides still retain a certain amount of flexibility. While not as flexible as PDMS stamps and not as rigid as stamps fabricated with quartz wafers, these 'semi'-flexible stamps combine the advantages of both kinds. They can compensate small surface irregularities, the non imprinted area in case of dust contamination is small, while still retaining the ability to withstand high pressures.

3.3.3 Stamp pretreatment

A big advantage of PDMS made stamps when used in nanoimprinting is their low surface energy [42]. This low surface energy results in a reduced 'sticking' of the imprinted material on the stamp, making the demolding step easier. When it comes to transfer printing this low surface energy can also be disadvantageous.

When a metal is transferred, it is usually deposited by thermal or e-beam evaporation on the transfer stamp. Both deposition techniques usually result in a smooth and closed layer even on samples with low surface energy. Organic semiconductors on the other hand are usually dissolved in an organic solvent during the deposition process and are therefore deposited as a liquid solution. Possible deposition processes are drop casting, spincoating, spray coating or immersing the stamp into the solution. Here the low surface energy is a problem. It makes a conformal coating of the stamp surface difficult if not impossible.

This problem can be overcome by the introduction of an oxygen plasma treatment of the transfer stamps [48, 49]. Such a treatment improves the wettability of the stamp by chemically changing its surface. See section 3.5 for details of the used plasma asher.

The treatment parameters have to be chosen carefully as a too long treatment time can result in a brittle SiO_2 layer on the PDMS stamp surface [48]. Such a layer is likely to form cracks during the deposition or transfer process, which will cause cracks in the transferred layers also. A high adhesion of the deposited layer on the stamp is not desired, as it will also cause difficulties in the later transfer process.

3.4 Spraycoating

Spraycoating is one of the most widely used technologies for coating surfaces. The application ranges from simple painting and art application to coating of pharmaceutical products. Its main advantage is the easy use, its reproducibility and, if used in large scale, its effective material use. Recently this technology has been established for fabricating organic transistors [50, 51], organic photodetectors [52–54], organic solar cells [55–57] and potentiometric sensors [145].

In this work a commercially available automated spray head (Krautzberger M10) has been used. It allows, unlike the often used hand held airbrush guns, exact control over spray parameters like spray time, sample to nozzle distance and material flow. This is necessary for reproducible results as the properties of the resulting films rely strongly on these parameters. Figure 3.3 shows a schematic drawing of the used spray setup. The used spray head is a dual fluid nozzle with external mixing. In this setup the flow of carrier gas and the ink solution can be controlled separately and mix in front of the nozzle. While in this work the carrier gas was always nitrogen, the ink formulation varies from polymer solutions to water based carbon nanotube (CNT) ink. The spray time is controlled by a 3/2-way automatic valve. For starting the deposition process the carrier gas flow is started first, shortly afterwards the ink flow is started by pneumatically moving a needle upwards that blocks the ink outlet. When the needle is moved upwards ink can flow throughout the nozzle and form a drop on the prefilming area at the tip of the nozzle. The material flow is controlled by the movement of the tapered needle. The more the needle is moved upwards the more material can flow through the nozzle. When the deposition stops the nozzle is closed first by moving down the needle again. This prevents dripping.

Besides the later explained spray parameters, the properties of the solvent used in the ink formulation influence the drop formation and spray pattern. The surface tension and viscosity of the solvent play a major role in the actual drop formation. The boiling point on the other hand controls the amount of solvent which evaporates before the drop reaches the surface of the sample. A low bowling point results in a rapid droplet drying, which can result in a high material loss if the sample to nozzle distance is too high, as the dried droplets are blown away as powder.

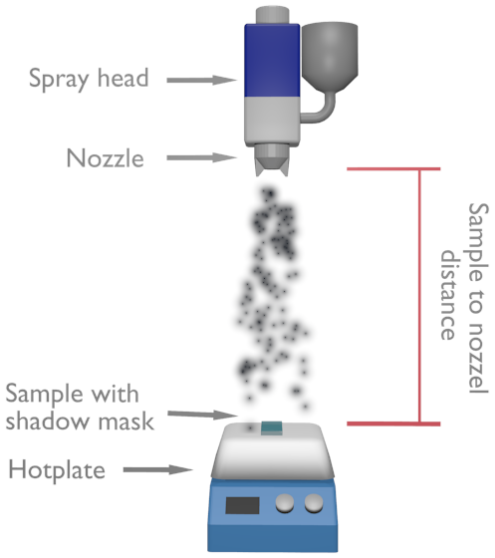

Figure 3.3: Schematic overview of the used spray setup

The other important spray parameters are the spray time t, the substrate-to-nozzle distance d, the substrate temperature T, the carrier gas pressure p and the material flow. t controls the thickness of the achieved layer which rises linearly with the spray time. As a spray coated layer consists of multiple single drops which are distributed randomly over the sprayed area, a certain minimum spray time is necessary to completely cover the designated area. The influence of d is more complexe. Only in a certain range a uniform film can be achieved. There are three possible domains: the wet domain, the intermediate domain and the dry domain. In the dry domain d is to small, the droplets coming from the nozzle still contain to much solvent and dry to slowly on the substrate. The result is a non uniform wet film with undefined thickness. If d is to big we are in the dry regime. In this case the droplets dry complete or

nearly completely before reaching the substrate and are mostly or completely blown away as powder. This results in a significant material loss as mentioned earlier. Between these two extremes is the intermediate domain. It allows the deposition of a uniform film with a defined layer thickness.

The substrate temperature T has a strong influence on d. Especially on the wet domain, as by an increased substrate temperature the drying process of the droplets is accelerated. In an ideal case the substrate temperature is close to the boiling point of the solvent used in the ink. The carrier gas pressure p influences the size of the droplets. The higher p the finer the ink gets atomized, or in other words the smaller are the resulting droplets. The last parameter is the material thickness, which increases the thickness of the resulting layer if increased.

It has to be mentioned that all parameters influence each other and can therefore not be considered individually, i.e. a higher substrate temperature or a solvent with a different boiling point will allow other parameters for d and vice versa.

Defined patterns can be sprayed by the use of shadow masks. These masks are placed on top of the sample and protect areas which should stay free from ink.

3.5 Plasma treatment

A neutral ionized gas is called plasma, it presents together with solid, liquid and gas the fourth state of matter. If such a plasma interacts with a surface it can modify the surface chemically and physically. Due to reactions of the sample surface with ions in the plasma a chemical modification of the surface is possible. Also surface etching and cleaning ("'plasma ashing"') are possible results of such

interactions. A good example is the plasma activation of polymers, which is a very common process in industry. For example polymer parts in the automotive industry are usually plasma treated to achieve a good wetting of the surface during the painting process [59]. As the PDMS stamps used in chapter 7 and the ITO-glass samples used in the same chapter are hydrophobic a plasma treatment is necessary to achieve a good covering.

For most industrial applications so called low pressure or cold plasmas are used. The pressure of the working gas is usually in the range of 1 mbar. To ionize the gas or in other words ignite the plasma a sufficient amount of energy has to be applied. This can be achieved by electric fields. Electrons in such a plasma can have up to 10 000 K while the much heavier ions remain at room temperature. The heat transfer from electrons to the plasma chamber walls is relatively low, therefore the term cold plasma [59].

In this work a Femto plasma asher by Diener electronics with oxygen as working gas was used, which uses microwaves with a frequency of 2.45 GHz to ignite the plasma. While always a working gas pressure of 0.3 mbar was used, the treatment time and plasma power were varied.

4 Conductive organic electrodes (PEDOT:PSS)

In the following chapter the use of the conductive polymer PEDOT:PSS as transparent electrode in organic electronic devices will be described in more detail. The main focus of this chapter is the fabrication of such electrodes for different application as well as the influence of different process parameters (spray and spincoating) on the film behaviour.

When fabricating organic electronics, especially optical devices, usually indium tin oxide or ITO is the material of choice. The big drawback of this material is the high price of indium. One possibility to replace this material is the use of electrodes consisting of an organic material.

Organic materials are known for being flexible, cheap and easy to process. One of these organic materials that is famous for its conductivity is PEDOT:PSS.

4.1 Conductivity enhancement by chemical doping and cross-linking

4.1.1 Conductivity enhancement

While being described as a good conductor, the conductivity of PEDOT:PSS is compared to i.e. metals still relatively low. One way to increase the conductivity of PEDOT:PSS is the reduction of the PSS content in the polymer (see also section 2.3.3). Good examples are the different PEDOT:PSS formulations used in this work. Clevios P VP CH 8000 has a PEDOT to PSS ratio of 1:20 and resistivity of $1 \times 10^5\,\Omega\,\mathrm{cm}$ to $3 \times 10^5\,\Omega\,\mathrm{cm}$, while Clevios P VP AI 4083 with a PEDOT to PSS ratio of 1:6 has a much lower resistivity of $500\,\Omega\,\mathrm{cm}$ to $5000\,\Omega\,\mathrm{cm}$. Even layers with a conductivity up to $1400\,\mathrm{S/cm}$ have been reported [60] using a PEDOT:PSS (Clevios Ph 1000) formulation with a even smaller ratio of 1:2.5 and ethylene glycol (EG) as additional solvent.

By adding a second solvent to the PEDOT:PSS solution its conductivity can be increased by several orders of magnitude. Usually solvents like glycerol, diethylen glycol sorbitol, dimethyl sulfoxide (DMSO), N-methyl-pyrrolidone or ethylene glycol (EG) are used for this purpose [29, 60–64]. It is believed that the solvents cause morphological changes in the resulting PEDOT:PSS layers which are the origin of this enhancement. Ouyang and others suggest that a change of the conformation of the PEDOT chains from coil to expanded coil lead to an increased intrachain and interchain charge carrier mobility which increases the conductivity [61, 63, 65]. The PSS which is insulating the PEDOT chains from each other is also partly removed by this solvents, which leads to highly conducting paths throughout the layer [60, 65, 66].

DMSO and EG enhanced PEDOT:PSS solutions have been used in a wide range of applications reaching from cell measurements [67] to organic solar cells and photodetectors [53, 68, 116, 70, 71]. In this work layers made of a formulation consisting of Clevios Ph 1000 and EG will be used as electrodes in organic photodetectors and organic transistors for ion sensing application (see chapter 5 and chapter 6).

4.1.2 Cross-linking

A big advantage of PEDOT:PSS is its good solubility in water. At the same time this is a big disadvantage in terms of layer stability and use in more complex processes like photolithography which are used to fabricate microstructures. Most common developers and/or etchants are water based and would therefore destroy/dissolve PEDOT:PSS layers if used in i.e. a lift off process. This can be solved by cross-linking the PEDOT:PSS layer. If a polymer gets cross-linked the individual polymer chains get linked to each other covalently and form a bulk material.

In this work 3-glycidoxypropyltrimethoxysilane (GPS) is used to cross-link PEDOT:PSS layers making them suitable to be used in standard lift off processes [72, 73]. The silane will be hydrolysed in the acidic conditions of the aqueous PEDOT:PSS solution forming silanol groups (Si-OH-groups). These groups will condense during drying and form a cross-linked silicon dioxide network. Therefore the GPS is not cross-linking the PEDOT:PSS itself, but making it insoluble to any kind of solvent due to the incorporation of an inorganic network [32].

4.2 Fabrication and characterization

Before the actual usage, the PEDOT:PSS layer has to be optimized for the particular purpose. In case of spraycoated organic photodetectors (see chapter 5) it was optimized towards a low sheet resistance R_{sheet} and a high optical transmission T_{opt}. An increasing layer thickness d_{sheet} will reduce R_{sheet} and at the same time decrease the transmission. For this reason a trade off point has to be found, where a low sheet resistance is reached but the transmission is still sufficiently high.

A solution consisting of the conductive PEDOT:PSS formulation Clevios Ph 1000 by Haraeus together with EG, deionized-water (DI-water) and the commercially available wetting agent Dynol 604 was used for this purpose. Ideal ratios by weight were already optimized and described by others [74]. Therefore a ratio of PEDOT:PSS to DI-water to EG of 2:2:1 where chosen. Additionally 0.3 wt% of the commercially available wetting agent Dynol 604 was added.

For characterization purposed layers were sprayed onto glass substrates with a size of 25x25mm which have been previously treated with an oxygen plasma to increase wettability (see section 3.4 and section 3.5 for details on spraycoating and plasma treatment). To achieve a homogenous covering of the sample and dry layers a sample to nozzle distance of 20 cm was chosen and the samples were heated to a temperature of 120 °C. After spraycoating the resulting layers were characterized by four-point-probe, transmission and profilometer measurements. Results are displayed in table 4.1.

Figure 4.2 a) shows the thickness of spraycoated PEDOT:PSS layers doped with ethylene glycol on glass substrates. The layers were fabricated as described in the previous section. As one can see the layer thickness rises almost linearly with spray time. This can be expected, as during spraycoating a constant

Table 4.1: Characteristics of spraycoated PEDOT:PSS layers doped with EG

spraytime (s)	layer thickness (nm)	R_{sheet} (Ωcm)	Transmission (%)
10	n.a.	1510	98,9
20	64	405	97,6
30	129	228	95,7
40	162	154	93,2
60	214	102	92,3
70	242	85	89,5
80	260	76	88,1
90	310	65	86
120	410	48	79,5
180	624	32	71,3
240	830	23	64,7

amount of material is applied over time, which is resulting in a linear rise of the layer thickness. The transmission of such PEDOT:PSS layers at a wavelength of 500 nm is displayed in figure 4.2 b). Thin layers with a thickness lower than 100 nm show a high transmission of over 95%. Even thicker layers of more than 800 nm have transmissions of more than 65%. This high transmission in the visible spectrum makes the material a suitable candidate for transparent electrodes.

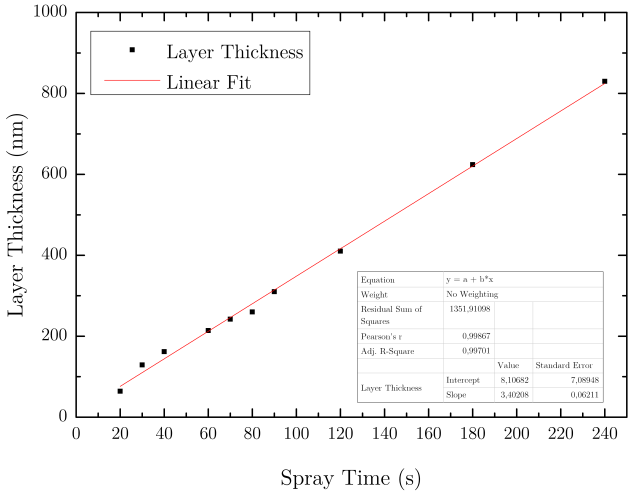

(a)

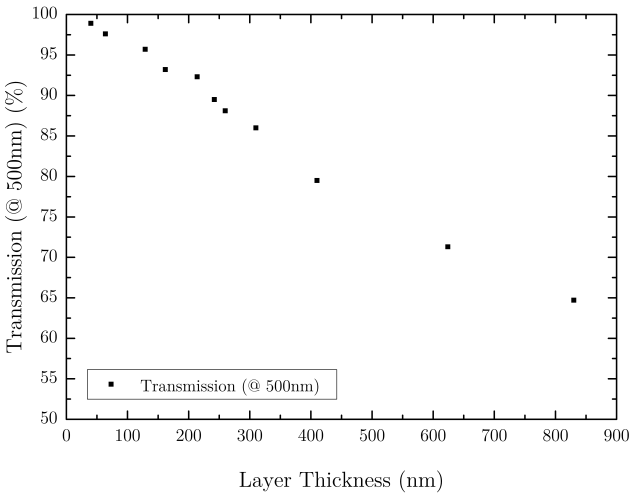

(b)

Figure 4.1: a) Layer thickness of spraycoated PEDOT:PSS layers doped with EG. b) Transmission at 500 nm for doped PEDOT:PSS layers with different thicknesses

Figure 4.2 a) shows the sheet resistance of the layers depending on the layer thickness, while 4.2 b) shows the optical transmission at a wavelength of 500 nm in dependence of the layer thickness. At a low layer thickness of around 60 nm the sheet resistance is with 405 Ω/cm relatively high. At thinner layers a even higher resistance can be measured (see table 4.1). These values have to be considered carefully as at very low spray times no conformal layer is formed. Due to the random distribution of droplets during the spray coating process a minimum spray time has to be granted to achieve a closed layer. At too low spray times an irregular network of droplets with an undefined layer thickness is formed. With rising layer thickness the sheet resistance is dropping rapidly under 100 Ω/cm until at a layer thickness of around 400 nm a saturation starts.

A good transparent electrode is defined by a high optical transmission while still maintaining a low sheet resistance. If the sheet resistance is plotted against the optical transmission (see figure 4.2 b)) a trade off point between these two properties can be chosen. For the devices used in chapter 5 this trade off point was chosen at a sheet resistance of 100 Ω/cm which provides a high optical transmission of 92,5% and refers to a layer thickness of 214 nm or a spray time of 60 s. A further increasement of the layer thickness would only provide a slight decrease of the sheet resistance but a strong decrease of the transmission. Making the layer thinner would only provide a moderate improvement of the already high transmission while increasing the sheet resistance dramatically.

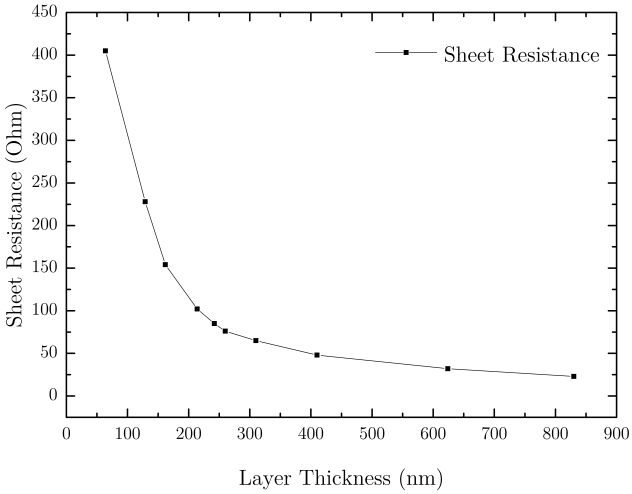

(a)

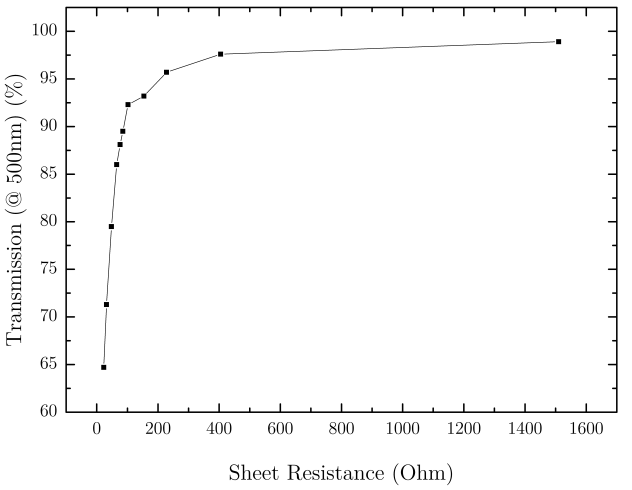

(b)

Figure 4.2: a) Sheet resistance of spraycoated PEDOT:PSS layers doped with ethylene glycol. b) Transmission at 500 nm for doped PEDOT:PSS layers in relation to the sheet resistance

4.3 Lithography

Conductive PEDOT:PSS can not only be used as spraycoated transparent electrodes, also a usage as electrode material in OFET is possible. In this case as substrates are often opaque, the transparency of the film is usually not important. On the other hand small structures in the micrometer range are necessary for good transistors. This can not be achieved by spraycoating with shadow masks as described in the previous chapter. For this reason the use of optical lithography becomes necessary (see section 3.1).

As described in section 4.1.2 it is difficult to use PEDOT:PSS in standard lift off processes due to the water containing chemicals which are usually used. To overcome this problem 0.25 % by weight of the crosslinker GPS were added to a PEDOT:PSS solution containing 5 parts of PEDOT:PSS Clevios Ph 1000 by Haraeus, 5 parts of isopropanol and 1 part of ethylene glycol. Isopropananol was added to decrease the contact angle of the solution and therefore increase the wettability of samples [75]. The solution was stirred for one hour at room temperature before usage.

Samples were structured using a standard lithography process as described in section 3.1. After resist application, exposure and development, the samples were spincoated with the PEDOT:PSS solution and annealed at 100 °C. After annealing the sample was placed in an acetone bath and sonicated, removing the resist and the PEDOT:PSS on top of it. A microscopic picture of an interdigitated structure fabricated this way is depicted in figure 4.3.

In general the process is possible on a wide variation of samples like glass plates and silicon wafers or polyimide (Kapton) or Polyethylene terephthalate (PET) sheets. Test performed on PET and Kapton substrates showed no dif-

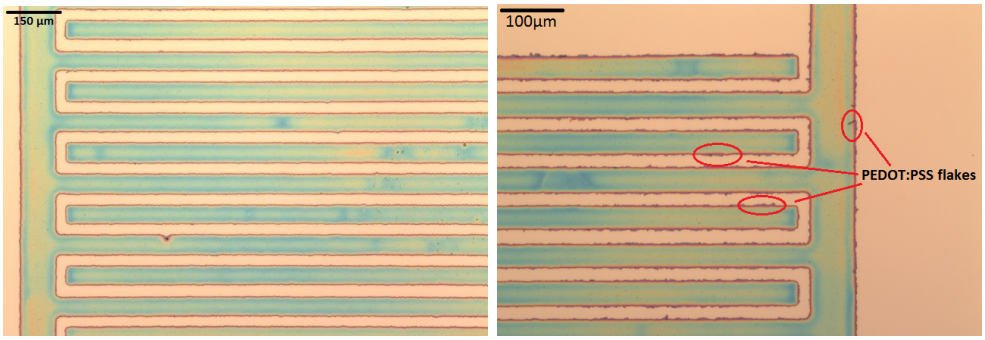

(a) (b)

Figure 4.3: Microscopic image of an interdigitated structure consisting of cross-linked PEDOT:PSS doped with ethylene glycol fabricated with a photolithographic. The lines have a 30 µm spacing and are used for the transistor described in section 4.4. a) with 100 nm thickness: good lift off b) 150 nm thickness: flakes and rags at the structure edges.

ference concerning lift of quality or sheet resistance. The only limitation for the substrate is its resistance to the developer used in the lithography process.

Structuring a PEDOT:PSS layer with a photolithographic lift off process has several advantages compared to patterning with shadow masks and spraycoating. One of the most important advantages is the increased resolution. With a lithography process a much higher resolution can be achieved. Even structures with a size in the range of micrometers are possible [73] while with shadow masks resolutions in the order of tens of micrometers are possible at the best. Another big advantage are the much smoother layers, as spraycoated layers generally have a high roughness. Also due to the cross-linking the layers get insensitive to chemicals or water used in later process steps, while non cross-linked

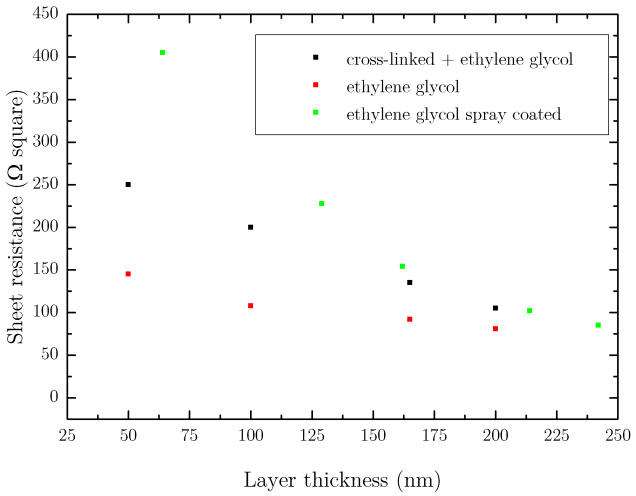

Figure 4.4: Sheet resistance of spincoated and cross-linked PEDOT:PSS layers compared to not cross-linked spincoated and spraycoated layers. All layers are doped with ethylene glycol.

spraycoated layers are sensitive to most polar solvents making a coating of the electrodes with materials dissolved in such solvents difficult, if not impossible.

The biggest disadvantage is the limitation of the thickness of spincoated layers in a lift off process. At a thickness above 150 nm the cohesion of the layer gets so strong, that a good lift off is not possible anymore. Flakes and rags of PEDOT:PSS will remain at the edges of the structures which can cause shortcuts (see figure 4.3 b)).

4.4 Transistors

Transistors are not only the basis for the modern computer technology, they are also used in a wide variation of sensors. In cases of sensors usually the quantity to be measured influences the behaviour of the dielectric used in the transistor. This changes the characteristics of the transistor, giving the possibility to determine the quantity. Usually such transistor based sensors like ISFETs are fabricated using metal electrodes As a prove of concept transistors were fabricated with PEDOT:PSS electrodes using the previously described lithography process. The transistor consist of a interdigitated finger structure with 30 µm spacing (see figure 4.3). As substrate silicon wafers with 65 nm oxide on top as well as polyimide (Kapton) samples were used. The semiconductor was in both cases P3HT, spincoated onto the PEDOT:PSS electrodes from a $1\,\mathrm{wt} - \%$ solution dissolved in dichlorobenzene (DCB) with a spin speed of 1000 rpm resulting in a 73 nm thick layer.

A so called electrolyte gated setup was used to characterize the transistors. In such a setup the dielectric is covered with an liquid electrolyte in which the gate electrode is immersed. Details about such kind of measurement setups can be found elsewhere [8]. This kind of setup was chosen to evaluate a future use in ion-selective sensors using Polyvinyl chloride (PVC) membranes (see section 6.5).

For transistors fabricated on silicon wafers a self-made Ag/AgCl - Electrode was used as gate. In case of samples fabricated on Kapton PEDOT:PSS electrodes were used. The devices on Kapton can therefor considered as all carbon devices. Figure 4.6 shows the transfer curves of two different transistors from the same batch on a silicon substrate. Both transistors are measured with a constant drain voltage V_{dr} of $-1\,\mathrm{V}$ and a voltage sweep of the gate voltage V_{EG}

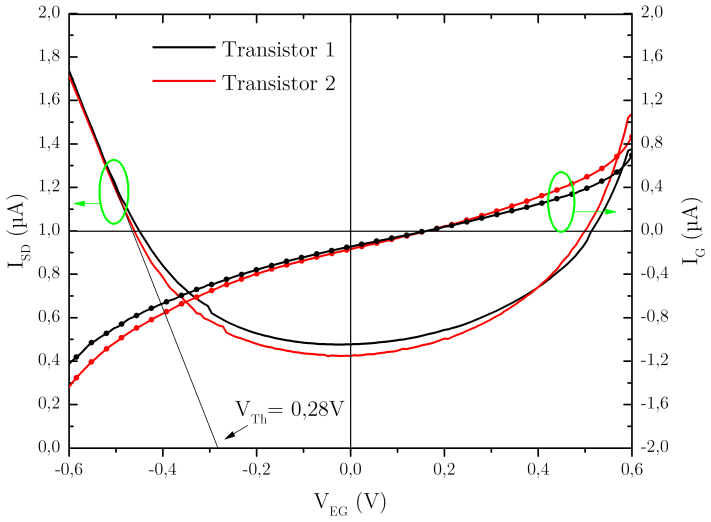

Figure 4.5: Transfer curves of two different transistor from the same batche made with PEDOT:PSS electrodes using P3HT as dielectric

from $-0.6\,\mathrm{V}$ to $0.6\,\mathrm{V}$ with a step size of $80\,\mathrm{mV}$. The used electrolyte is in this case deionized water.

From these transfer curves the on-off-ratio as well as the threshold voltage can be determined. Usually the concentration of the anayltes are determined by the change of the threshold voltage (see [76] and [77] for details). For this reason and because of the low quality of the transistors, only the transfer curves have been acquired and no output characteristics. Both transistors show a on-off ratio of about 4, while V_{th} is close to $0.28\,\mathrm{V}$.

Figure 4.6 shows the transfer curve of a transistor fabricated with the same parameters as the transistors displayed in figure 4.6. The main difference is the use of a Kapton substrate and an electrode also fabricated with crosslinked

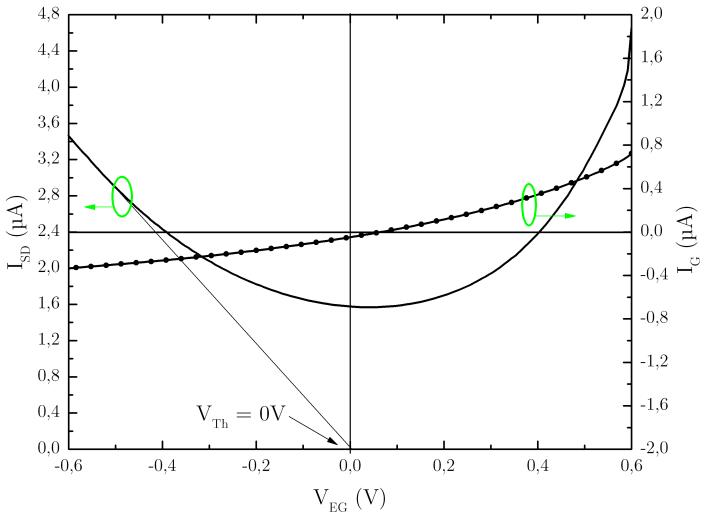

Figure 4.6: Transfer curves of a transistor made with PEDOT:PSS electrodes on a Kapton substrate using P3HT as dielectric and a gate electrode also fabricated with PEDOT:PSS

PEDOT:PSS. The transistor has a threshold voltage V_{th} of 0 V and an on-off ratio of 2.

While the presented transistors show low on-off ratios compared to standard silicon based devices they still prove as a proof of concept that it is possible to fabricate transistors with the proposed technique. The transistor shown in figure 4.6 can here be described as an all carbon device as substrate, contacts and electrodes as well as dielectric and gate electrode are fabricated by the use of carbon based organic materials. Possible reasons for the low transistor performance are the P3HT (which is known to degrade in water and oxygen rich environments) used as semiconductor and leakage path formed during the lithography process. The possible problems with P3HT as semiconductor mate-

rial could be avoided by using carbon nanotubes instead (see section 6.5). The presence of leakage path is likely as transistors fabricated on silicon wafers as well as devices fabricated on Kapton show a relatively high drain current I_{SD} of around 0.5 A and 1.6 A respectively. A further optimization of the fabrication process should be able to minimize the leakage path and therefore increase the on-off ratio.

5 Spraycoated organic photodetectors

The following chapter will focus on the fabrication of spraycoated organic indium tin oxide free photodetectors. These results have already been published in AIP Advances in 2014 [150]. Parts of the text can be found there.

5.1 Introduction

Organic photovoltaic devices like organic solar cells and organic photodetectors have been attracting a great amount of research [26, 79]. They offer promising features as they allow flexible lightweight applications and roll-to roll production of low-cost large area components. To develop their full potential, this kind of devices has to be fabricated using scalable fabrication technologies like spray coating, ink-jet printing or screen printing which are already known from the printing or painting industry. This way high cost fabrication technologies like PVD can be avoided. A drawback of these technologies is that they usually require a solution processability of the used materials. So far the production of most organic devices still contains fabrication steps that rely on PVD, especially for the electrical contacts. A good example is the indium tin oxide (ITO) commonly used as transparent electrode material.

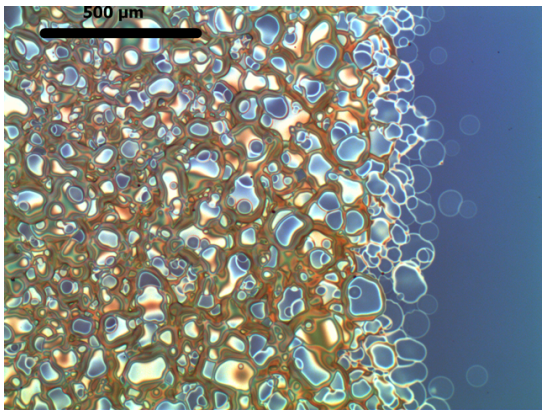

Figure 5.1: Microscopic picture of an spraycoated P3HT:PCBM layer

However, ITO is brittle, thus causing problems in processing flexible devices. Furthermore, the limited availability of indium causes a steady increase of its cost. This has raised the demand for ITO-free devices. For this reason alternative transparent electrode materials like graphene [80], carbon nanotubes [81], metal nanowire networks [82–85] as well as metal grids [86] and conductive polymers like poly(3,4-ethylenedioxythiophene): poly(styrenesulfonate) (PEDOT:PSS) [28, 87] have been investigated. All of the mentioned alternatives, besides metal grids, also have the advantage of relying on solution processable materials, which allows to replace the sputter process usually used for the ITO deposition with a printing or spray coating technique.

PEDOT:PSS is a promising candidate as electrode material, due to its easy processabilty, nontoxicity and relatively high conductivity [87, 88]. An additional advantage is the possibility to further increase its conductivity by chemical doping (see chapter 4 for details). Previous works demonstrated the feasibility of fabricating such ITO free photodiodes [28] and solar cells [70, 89] with high conductive PEDOT:PSS as anode and an active layer made of

poly(3-hexylthiophen) (P3HT) and [6,6]-phenyl-C61-butyric acid methyl ester (PCBM). However, these devices - produced by means of a lab scale spin-coating technique - show low performance. In case of the photodiodes a high dark current and therefore a low on-off ratio has been reported [28]. The use of spray-technologies [90] would allow to exploit the afore mentioned high throughput large area production capabilities of this technique which is one of the main advantages of organic electronics, at the same time avoiding the drawbacks of lab scale production processes like spin coating or doctor blading as e.g. the high waste of material. The feasibility of such an approach has been first demonstrated with ITO-free spray coated solar cells [91]. Regarding photodiodes, only devices with an inverted top absorbing structure have been demonstrated so far [53, 68]. These devices also have been successfully integrated in organic/inorganic hybrid CMOS-detectors [116]. Also it was demonstrated that it is relatively easy to replace one of the used materials to achieve for example infrared sensitivity [116]. However, such inverted structures make use of e.g. plasma processes to increase the wettability of the hydrophobic P3HT:PCBM active layer which could negatively affect the device.

In this chapter a way to fabricate spray coated ITO-free organic photodiodes with a non inverted structure and patterned PEDOT:PSS anodes as transparent electric contacts will be demonstrated. By replacing lithography processes with a shadow mask approach for the patterning of the electrodes, the manufacturing process can be easily transferred to large scale production. A comparative study of standard and ITO-free devices is included.

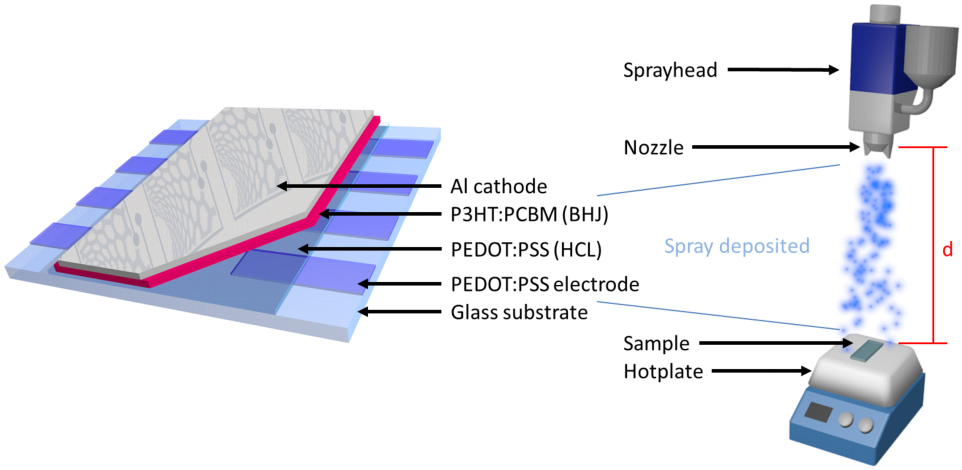

Figure 5.2: Schematic of spray setup and a spray coated sample with PEDOT:PSS anode on glass substrate

5.2 Fabrication

The whole fabrication process of the devices except the evaporation of the back electrode is done by spray coating. This part is therefore the last production step which is not yet replaced by a solution based fabrication process like spray coating or ink-jet printing.

All devices were fabricated on float glass or prepatterned indium tin oxide coated (ITO) glass samples (Xin Yan Technology Ltd, $R_S = 15\,\Omega/\square$). To clean the samples they were first sonicated in acetone and isopropanol for 10 minutes and subsequently blow dried with nitrogen. To provide a sufficient surface coverage of the samples with the water based PEDOT:PSS solution and to remove any remaining organic contamination on the surface they were treated with oxygen plasma for 1 minute after the cleaning process.

To fabricate the PEDOT:PSS electrodes in ITO free devices the samples were heated to 120 °C and spray coated with a conduction enhanced PEDOT:PSS solution. The solution consisting of PEDOT:PSS (Clevios PH 1000), deionized water, ethylenglycol (Merck) for increasing the conductivity and the wetting agent Dynol 604 (Sigma-Aldrich) with a weight ratio of 1:1:0.4:0.01 was stirred for two hours at room temperature and filtered with a 0.45 µm filter before usage. The addition of the wetting agent was necessary as the heating of the sample is reducing the effect of the plasma treatment. The sample was coated for 60 seconds with a nozzle-to-substrate-distance of 20 cm (see figure 5.2 and section 3.4). A shadow mask was used to pattern the film, thus avoiding the use of complex lithography processes. The sample is covered with the shadow mask and only coated at spots where a hole in the mask exists. Afterwards the samples were annealed at 140 °C for 10 minutes to remove any residual moisture in the layer.

After cooling the samples to room temperature a hole conducting layer (HCL) consisting of PEDOT:PSS (Clevios P VP CH 8000) was spray-deposited. The nozzle-to-substrate-distance was 25 cm, while the spray time was varied between samples to achieve different thicknesses for optimization purposes. Afterwards the samples underwent a second annealing step at 140 °C for 10 minutes to again remove the remaining water. The photo active layer consisting of a blend made with P3HT (Rieke Metals) and PCBM (Solenne B.V.) with a weight ratio of 1:0.75 dissolved in 1,2-dichlorobenzene (Sigma-Aldrich) was subsequently sprayed on top, forming a bulk heterojunction (BHJ). Again a series with different spray times and therefore different layer thicknesses was sprayed for optimization. A last annealing step at 140 °C for 10 minutes in a nitrogen filled glovebox followed. Finally a 100 nm aluminum electrode was deposited by thermal evaporation. As previously described in section 2.3.1 the P3HT tends to

degrade when getting in contact with water and oxygen, therefore all devices were encapsulated using an UV-curing epoxy (Dymax OP4) and a thin glass sheet. Further details on spray coating and used materials can be found in section 3.4.

For the reference devices with ITO anode, a previously optimized stack with (HCL:10s (50 nm), BHJ: 20s (600 nm)) was fabricated using the very same fabrication procedure.

5.3 Results

To characterize the fabricated devices the I-V-characteristics of the device, the external quantum efficiency, the cut of frequency, the sheet resistance of the PEDOT:PSS anode as well as the spray coated layer thickness have been measured.

The I-V characterization of the devices was carried out using a Keithley 2602A source meter and a halogen lamp with a light power of 100 mW/cm^2. The external quantum efficiency (EQE) was obtained by using a Newport 74125 Monochromator with a 300 W Xenon arc lamp and a Merlin 70105 Lock-In amplifier. Finally, the cut-off frequency of the devices was evaluated as follows: a Keithley 3390 arbitrary waveform generator produced a square wave voltage with $D = 50\%$ duty cycle modulating the optical emission of a green LED (max. 500 µW/cm^2 at 525 nm); the photocurrent of the OPDs was amplified via a FEMTO transconductance amplifier with a gain of 10^4 and the voltage waveforms were analyzed with a LeCroy WavePRO 7zi oscilloscope. The sheet resistance of the PEDOT:PSS anode was measured using a custom-made 4-point prober.

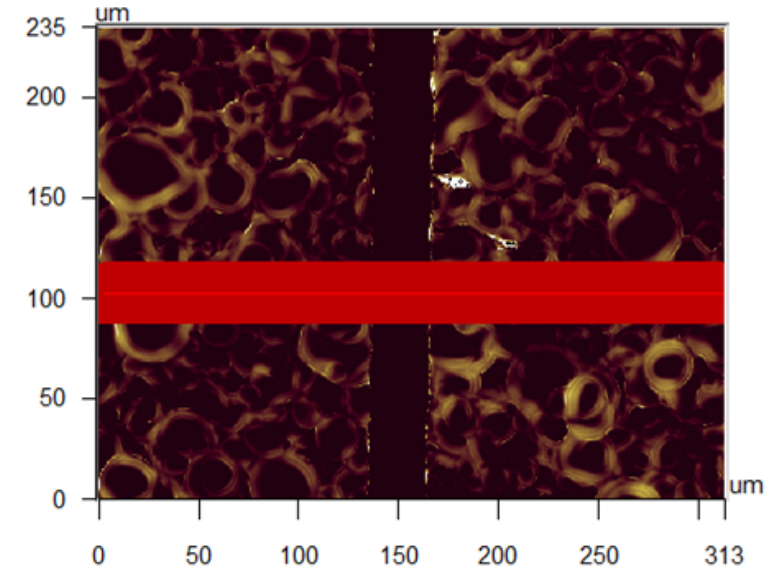

(a)

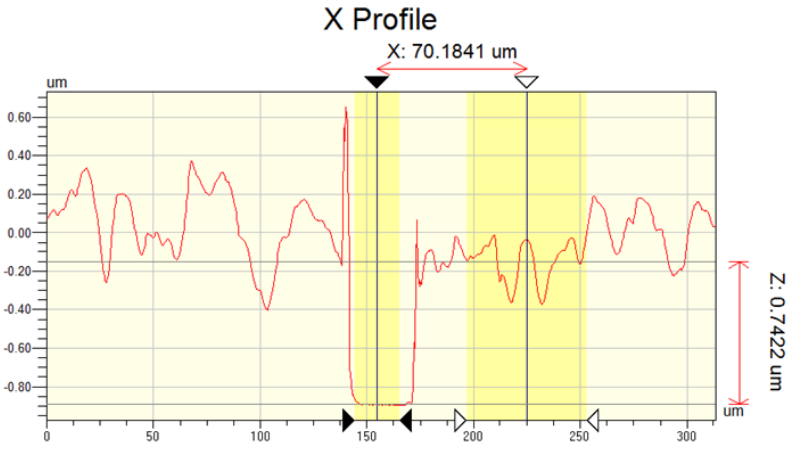

(b)

Figure 5.3: a) WLI image of a spray coated layer. Instead of a single profile, an average profile on the shaded area was measured, in order to give an effective-thickness of the spray-coated layer. b) Average profile of a spray-coated blend layer

The thickness of the spray coated layers was determined by means of white light interferometry (WLI). As for WLI an opaque sample is necessary. For this reason glass samples with sprayed layers were scratched and a thin (15 nm) aluminum layer was evaporated on top to reflect the white light. Then a Veeco NT9080 (20.2x magnification) white light interferometer was used to determine the thickness of the layers. Since the spray-coated layers are relatively rough, the measurement was averaged on 50 µm in the x direction (the yellow shaded area in the shown profiles, figure 5.1 b)) and 25 µm in the y direction (the red area in figure 5.1 a))

5.3.1 I-V-characteristics

To determine the I-V characteristics of the fabricated devices a voltage sweep from −4 V to 2 V with a step wide of 0.075 V was applied to the devices while being in the dark and under illumination. To assume a good electrical contact silver conductive paste was applied to the cathode and the anodes.

Figure 5.4 and 5.5 are showing the I-V characteristics of devices fabricated with varying thicknesses of the HCL and BHJ active layer (see figures 5.3 a and b) compared to devices with a BHJ layer thickness of 600 nm and a HCL thickness of 75 nm. The thickness of the HCL (50 nm to 120 nm) is determined by the spray time. In fact the droplet formation during the spray deposition process results in a layer thickness which can vary strongly. In the case of the BHJ active layer, the thickness can be acquired more accurately as the average layer thickness is much higher (300 nm to 750 nm) and droplet size is significantly smaller due to the different material properties.

If the thickness of the HCL is increased a strong decrease of the dark current occurs. This can be seen in figure 5.4. The dark current drops for nearly one

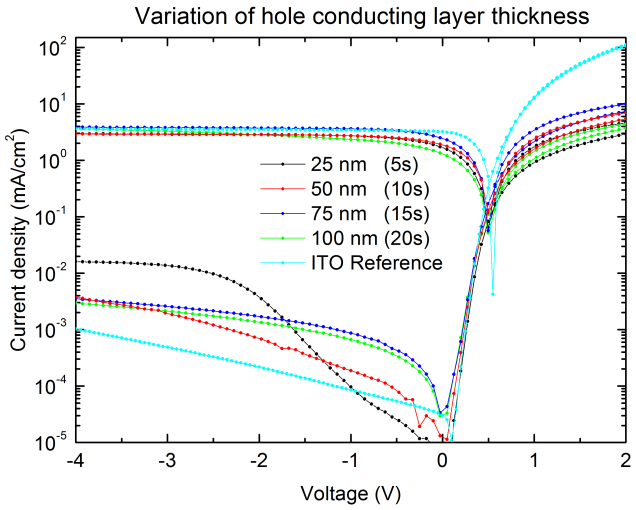

Figure 5.4: Logarithmic plot of the I-V-characteristics of samples with varying HCL thickness (BHJ thickness for all samples 600 nm)

order of magnitude. In contrast to this the photo current of devices is first increasing and then decreasing with increasing HCL thickness. As previously mentioned, the PEDOT:PSS layer is a hole conductor. Therefore the reduced recombination of electrons diffusing to the anode and the increased roughness are believed to be the reasons for this behaviour [16, 32, 34, 92, 93]. Once the HCL thickness reaches a level at that all electrons are blocked, the effect will saturate and the photocurrent will decrease, as the serial resistance increases with HCL thickness as well. This is reflected on the similar behaviour shown by the forward current, while the increasing resistance also leads to a decreasing dark current. Compared to a device with ITO electrode the forward current is lower while the photocurrent is basically the same. The reason for this is the lower sheet resistance (R_S) of the ITO electrode of 15 $\Omega/\square$ (value given by the

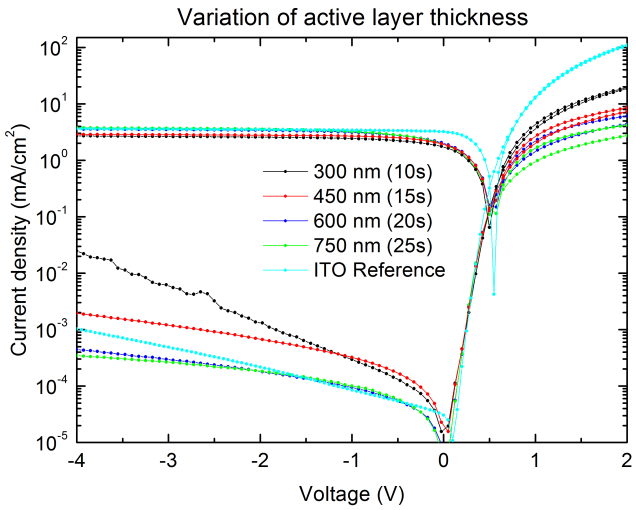

Figure 5.5: Logarithmic plot of the I-V-characteristics of samples with varying BHJ thickness (HCL layer thickness of 50 nm)

manufacturer) compared to the PEDOT:PSS electrode with measured value of $\approx 100\,\Omega/\square$. The dark current for ITO based devices is significantly lower than that of the PEDOT:PSS based devices. It is believed that the higher roughness of the spray coated PEDOT:PSS anode compared to ITO anode is the reason for this behaviour. Still one has to keep in mind that the BHJ thickness chosen for the devices is optimized for ITO electrodes and not for PEDOT:PSS. For devices fabricated with varying BHJ thickness a HCL thickness of 50 nm has been chosen as this seems to be the optimal thickness.

Leaving the HCL thickness constant and increasing the BHJ layer thickness (figure 5.5 b) leads to a slight increase in the photocurrent and a drop of the dark current until saturation is reached. In contrary to this the forward current drops constantly with increasing BHJ thickness. It is believed that the rise of

the photocurrent is caused by a higher proportion of the incident light that is absorbed. This is caused by the higher absorption of the thicker films. The photocurrent saturates as at a certain point the complete light is absorbed. On the other hand, the simultaneously increasing serial resistance is responsible for the decreasing dark current which becomes even lower than that of the ITO reference. The constant decrease of the forward current with increasing thickness is also believed to be caused by the rising serial resistance. Here no rise similar to that when increasing HCL thickness is present as the forward current is independent from the illumination. This affects the performance of the photodetectors in a positive way, since the on-off ratio of the devices with the thickest BHJ layer is reaching values of nearly 4 orders of magnitude, which is what we measured for the reference diode on ITO. It is worth mentioning that thick active layers, although positively impacting the on-off ratio, hinder a fast operation of the devices (see below).

5.3.2 External Quantum Efficiency

The external quantum efficiency (EQE) of a solar cell or a photo detector represents the ratio between incoming photons and charge carriers extracted from the device for each wavelength. It is used as a figure of merit for photodetectors to determine how efficient they can be operated at different wavelength. It can be calculated according to the following equation.

$$EQE_{SC}(\lambda) = \frac{N_e}{N_P} = \frac{I_D}{I_R} EQE_R(\lambda) \tag{5.1}$$

With $EQE_{SC}(\lambda)$ being the external quantum efficiency of the measured device, the number of impinging photons N_P, the number of extracted charges N_e, the photo current of device I_D, the photo current of reference I_R and the

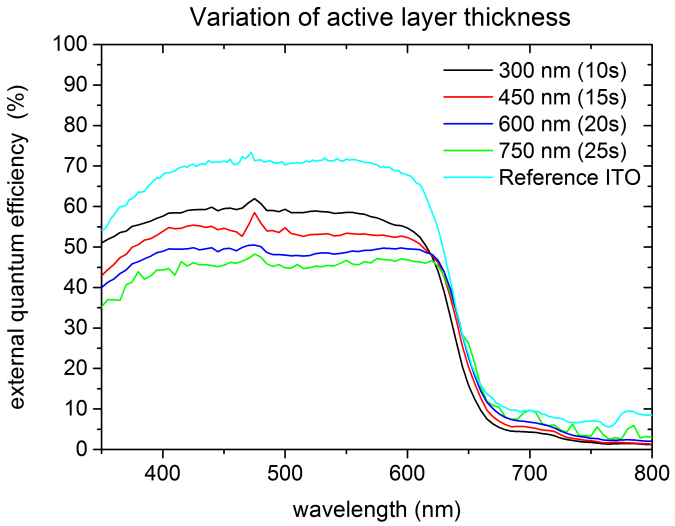

Figure 5.6: External quantum efficiency (EQE) measured at −4 V bias voltage of devices with varying BHJ thickness (HCL thickness 50 nm) compared to a device (cyan) with ITO anode (HCL:10s (50 nm), BHJ: 20s (600 nm))

external quantum efficiency of the reference $EQE_R(\lambda)$. As can be derived from the equation, a reference detector with a known quantum efficiency is needed for this purpose. In case of this work a calibrated silicon photodiode from Newport was used.

Figure 5.6 shows the EQE of devices fabricated with varying active layer thickness and constant HCL thickness, while figure 5.7 shows devices with varying HCL and constant active layer thickness. Both are measured under a reverse bias of −4 V. In the figure can be seen that increasing the thickness of the BHJ active layer leads to a reduction in the EQE and to a substantial modification of its shape. In fact, if on the one hand, a thicker BHJ layer guarantees a higher number of collected photons, on the other hand, the probability of

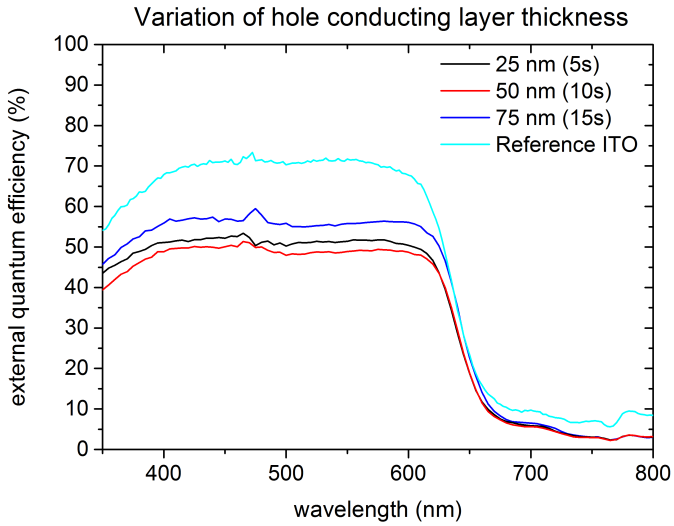

Figure 5.7: External quantum efficiency (EQE) measured at −4 V bias voltage of devices with varying HCL thickness (BHJ thickness for all samples 600 nm) compared to a device (cyan) with ITO anode (HCL:10s (50 nm), BHJ: 20s (600 nm))

recombination at defects and therefore loss is enhanced by the longer average distance from the point in which the charge is generated up to the contacts. The higher serial resistance which occurs with rising layer thickness adds additional losses. The variation in the HCL thickness did not show any clear trend and the differences found are related to process uncertainties.

A comparison between the ITO-free fabricated devices and the ITO reference with the optimal HCL/BHJ stack shows an average difference of about 10 % in EQE, roughly coincident with the difference in transmittance between the conductive PEDOT:PSS electrode and the ITO. The obtained values of EQE are consistent with the ones found in the literature for ITO-free OPDs[28].

Another figure of merit of photo detectors is the responsivity of the devices. It can be estimated from the wavelength of the incident light and the quantum efficiency according to the following equation:

$$R = \frac{\eta e \lambda}{hc} \tag{5.2}$$

With R being the responsivity, the elementary charge e, the quantum efficiency η at the wavelength λ, h being Plancks constant and the speed of light c.

The responsivity for the fabricated devices was found to be between 0.19 A/W and 0.25 A/W at 530 nm for devices with PEDOT:PSS electrode, compared to 0.30 A/W for the ITO reference. The found values are well comparable to that of standard silicon photodiodes which show responsivities between 0.2 A/W and 0.3 A/W [94].

5.3.3 Cut-off Frequency

The cut-off frequency is an important figure of merit for photodiodes. It limits the maximum signal frequency which can be detected by the photodiode. When the light illuminating the photodiode changes with a higher frequency the response of the diode gets too small for an accurate detection. For photodiodes the cut-off frequency is usually defined as the frequency at which the response falls below 3 dB or 50 % compared to the response under constant illumination.

The spray-coated diodes on a structured ITO glass gave, on average, cut-off frequencies around 3 kHz (Figure 5.8) at a light power density of 200 µW/cm^2 at 525 nm (comparable to the sunlight intensity at this wavelength) and were used again as reference to be compared with the fully-spray coated ones.

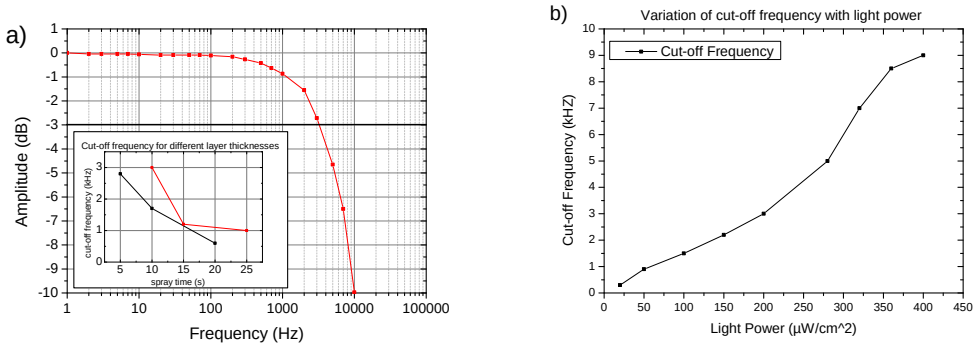

Figure 5.8: a) Bode plot of ITO reference device. The inset shows the decrease of cut-off frequency with increasing HCL and BHJ spray time (red BHJ variation, black HCL variation) at 200 µW/c^{2}m light power density. b) Plot cut-off frequency of the best device depending on incident light power density

As shown in the inset of figure 5.8, the cut-off frequency is strongly influenced by the overall thickness of the device. Increasing either the BHJ layer or the HCL thickness gives a clear trend of a severe reduction in the cut-off frequency.

Two phenomena seem to be responsible for this behaviour. Firstly, as previously stated, to a thicker layer corresponds a longer travel distance for the carriers, meaning that carriers with the same velocity would take, on average, a higher time to get to the contacts. Secondly, since the voltage applied to the electrodes is the same for all devices, the resulting electric field is lower for the thicker ones.

A lower electric field leads to a lower average carrier velocity, hence, at the same time both the velocity is lower and the travel distance is higher: it follows that with an increasing thickness of the layers, the carrier average travel time is increased, with a consequent reduction of the highest possible operating frequencies. As mentioned above photodiodes optimized in order to achieve a high

on-off ratio are limited in their dynamic response, which reduces their field of application to stationary ones.

Figure 5.8 b) shows how light intensity influences the cut-off frequency for the best performing spray coated diode. A region of quasi-linearity can be noted between $100\,\mu W/cm^2$ and $350\,\mu W/cm^2$, showing a threshold effect for low light intensity and a saturation phenomena for high light intensity. Work performed by others [74] indicates that at higher light intensities even higher cut of frequencies can be achieved.

5.4 Conclusion

We have demonstrated the fabrication of ITO free P3HT:PCBM-based organic photodiodes using a spray coating manufacturing process. The fabricated devices reach an external quantum efficiency of 62 % and on-off-ratios of nearly 4 orders of magnitude.

A maximum cut-off frequency of 9 kHz has been reached at a light power of $400\,\mu W/cm^2$, as well as a responsivity of 0.25 A/W at 530 nm. Future work will be devoted to increase the operational frequency of these spray-deposited photodiodes as well as their quantum efficiency.

The reached values are comparable to that of ITO free OPDs fabricated with other materials or fabrication techniques as depicted in table 5.1. While the achieved on-off ratio of ≈ 100000 is very good, compared to the other devices fabricated with other technologies, it is difficult to compare EQE. As can be seen in the table the measurement conditions vary strongly. The dark current is also very low, only surpassed by Baierl *et al.* [53], who used spray coating as fabrication technique but an inverted stack architecture for their devices.

Table 5.1: Comparisson of ITO free organic photodiodes fabricated with different technologies

Ref	On-Off ratio (at $-1V$)	EQE at 500 nm (%)	Dark current at $-1V$ (mA/cm^2)	Fabrication technique
Huang [28]	≈ 10	50	10^{-3}	Spincoating
Pace [95]	≈ 100	32 (-1V bias)	10^{-3}	Inkjet
Azzellino [96]	≈ 10000	65 (-0,9V bias)	10^{-3}	Inkjet
Baierl [53]	≈ 100000	70 (-4V bias)	10^{-5}	Spray/ inverted
Falco [71]	≈ 100000	65 (-5V bias)	10^{-4}	Spray/CNT
This work	≈ 100000	59 (-4V bias)	10^{-4}	Spray

6 Spraycoated organic potentiometric sensors

In this chapter the fabrication of fully spray coated all solid state potentiometric sensors will be described. The results presented in this chapter have been achieved in collaboration with Eva Jaworska, Giuseppe Scarpa, Krzysztof Maksymiuk and Agata Michalska and have already been published in Analyst [145]. Parts of the text can be found there. The author of this work was responsible for the entire fabrication process.

6.1 Chemical sensing with potentiometric sensors

A potentiometric sensor is a chemical sensor that measures the concentration of certain analytes by the change of the potential between a so called working electrode and a reference electrode. A subgroup of these kinds of sensors are potentiometric ion sensors (also called ion-selective electrodes (ISEs)). In such a sensor the electrodes are usually covered with an ion selective membrane, giving the possibility to measure the concentration of a specific ion. The concentration of the analyte is derived from the potential change under no-current-conditions. Because of its small size, portability, low cost and low energy consumption compared to other analytical techniques ISEs are interesting for a wide field of

applications [97]. The most successful ISEs are based on polymeric membranes and are commonly used as chemical sensors in clinical analysis [98].

Common ISEs contain an internal buffer solution. This leads to a lot of drawbacks like difficult storing, danger of leakage, problems with sterilization and a high need of maintenance. An attractive option of such systems would be the use in miniaturized systems like lab-on-chip devices, which would require a high grade of miniaturization of the device. As it is difficult to miniaturize classic ISEs because of the internal buffer solution there is an ongoing development of all-solid-state ion-selective electrodes (ASS-ISE) which lack such a buffer solution [99]. ASS-ISE show similar analytical parameters as the previously mentioned ISEs including the stability of potential values over time [100].

The most simple version of an ASS-ISE is the so called coated wire arrangement which was already developed in the 1970s [101, 102]. It is basically consisting of a solid electrical conductor, i.e. a platinum wire, covered with an ion-selective membrane. The main drawback of such a setup is a high amount of manual work during the fabrication, a high material consumption, the low reproducibility and drifting of the electrode potential caused by the bad charge transfer between the electrically conducting wire and the ionically conducting membrane [101].

In many cases simple disposable sensors are needed. Due to the high cost of fabrication the above mentioned solution is not feasible for such a purpose. An approach to overcome this is the fabrication of ASS-ISE by screen printing using conductive polymers (CPs) or CNTs as electrode material. Still screen printing requires some manual steps, increasing the costs and allowing a variation in the fabrication process caused by human influence [103–106]. Alternatively the layers in such a device could be fabricated by spray coating, which is a well established fabrication technique in industry (see section 3.4). In this work a

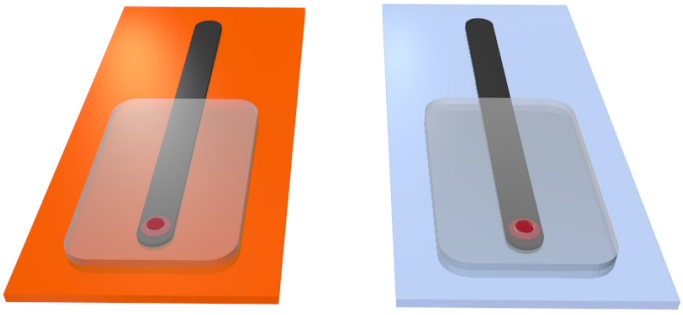

Figure 6.1: Schematic drawing of spraycoated ion-selective electrodes on Kapton and PET substates consisting of MWCNT electrodes covered with an PVC based membrane

method to fabricate ion-selective electrodes solely by spray coating will be presented. The setup of the electrodes is as follows. On a supporting substrate consisting of polyimide (Kapton) or PET a CNT layer working as electrical lead support and transducer layer is sprayed. A defined area of the CNT layer is spray coated with an ion-selective membrane. An insulating plasticized PVC layer is sprayed on the remaining CNT area which is used as electrical lead to define the membrane area (see figure 6.1 and 6.3 for ample setup). As model systems potassium-, hydrogen ion- and chloride-selective electrodes using plasticized PVC membranes were prepared.

6.2 Ion-selective PVC based membranes

The most important component of an ISE is the ion-selective membrane. It has the biggest influence on the quality of the sensor. A bad or non suitable

membrane will result in a sensor with low sensitivity or low reproducibility and, in the worst case, in a non functional sensor. Its main function is, as can be derived from the name, to"'filter"' a specific ion out of the usually watery solutions containing several different ionic species. Otherwise the potentiometric sensor would only be able to measure the sheer existence of ions, not the exact concentration of the specific ion of interest.

An ion-selective polymeric membrane is ideally immiscible in water and consists of the following components [107, 108]:

- Polymeric matrix
- Plasticizer
- Lipophilic ion
- Ionophore
- Lipophilic salt

Polymeric matrix The polymeric matrix is usually made of a polymer that doesn't react with any of the chemicals in the sensed solution and is immiscible in water. It stabilizes the membrane. So far the most common matrix material for ion-selective ISEs is PVC [109, 110].

Plasticizer The plasticizer ensures a high mobility of the membrane ingredients. To provide a homogenous distribution of all ingredients it has to be compatible with all of them. It has a strong influence on the selectivity of the membrane as it influences the ion-exchange characteristics of the membrane, which is depending on the polarity and dielectric constant [111]. The plasticizer used in the membrane presented in this work is bis(2-ethylhexyl) sebacate (DOS).

Lipophilic ion For a Nernstian response of the ISE it is necessary that no ions with opposite charge of the target ion are extracted together with the target ion from the sample solution into the membrane. For this reason the membrane should only be permeable for ions with the same charge sign of the target ion. This membrane characteristic is called permselectivity or Donnan exclusion. Non-exchangeable lipophilic ions in the membrane keep the ISE operational by keeping the total concentration of target ions in the membrane much higher than the amount of ions with an opposing charge extracted from the sample solution. Cation-selective ISE-membranes normally contain as lipophilic site a tetraphenylborate derivate and anion-selective membranes a tetraalkylammonium salt [110].

Ionophore A very high influence on the selectivity of the ion selective membrane has the ionophore or ion carrier. The ionophore forms a reversible complex together with the target ion and transports it throughout the membrane. In an ideal case this complex formation is selective only to the target ions. In a non ideal case this complex formation also happens with ions similar to the target ions, so called interfering ions. To keep the leaching rate of the ionophore into the sample solution as low as possible it should contain numerous lipophilic groups.

Lipophilic salt Lipophilic salts are usually added to the ion selective membranes to decrease the electrical resistance of the membrane. Additionally it increases the ionic strength in the membrane, making the membrane more selective for divalent or monovalent ions [112].

6.3 Fabrication

As mentioned previously all layers in the fabricated devices were deposited by spray coating. For spray coating, a pneumatically controlled Krautzberger M10 spray head was used, with nitrogen as the atomizing gas (see section 3.4). As the aim of the work was the fabrication of a model system for disposable sensors suitable for mass production, flexible Kapton and PET samples were chosen as substrates. Both materials are widely available and are commonly used in industry. Due to the availability and the low costs these materials are also promising candidates for potentially disposable ion-selective electrodes. The following layers were successively spray coated on top of the sample. The layer stack is depicted in figure 6.3. The patterns were achieved by the use of different shadow masks resembling the pattern needed for each layer (see figure 6.2). Similar to optical lithography, these shadow masks block the sprayed material in areas where it is not desired. A new pattern can be quickly implemented by simply replacing the shadow mask. A drawback of spray coating when used in small scale with a stationary setup is the amount of material required. If the spray head is not moved across the sample, only the center of the sprayed area shows homogenous layer thickness. However, this can be overcome easily by the use of non-stationary spraying devices and/or up-scaling the fabrication for example in roll-to-roll processes.

During spray coating the samples were placed on a hot plate under the spray gun and coated with the different materials at different sample-to-nozzle distances as described in section 3.4. In case of the CNT layer, the coating was done in several cycles with intervals to allow drying of the layers. Otherwise, large droplets would be formed on the sample causing inhomogeneous layers. The thickness of the layers is defined by the number of spray cycles as thickness

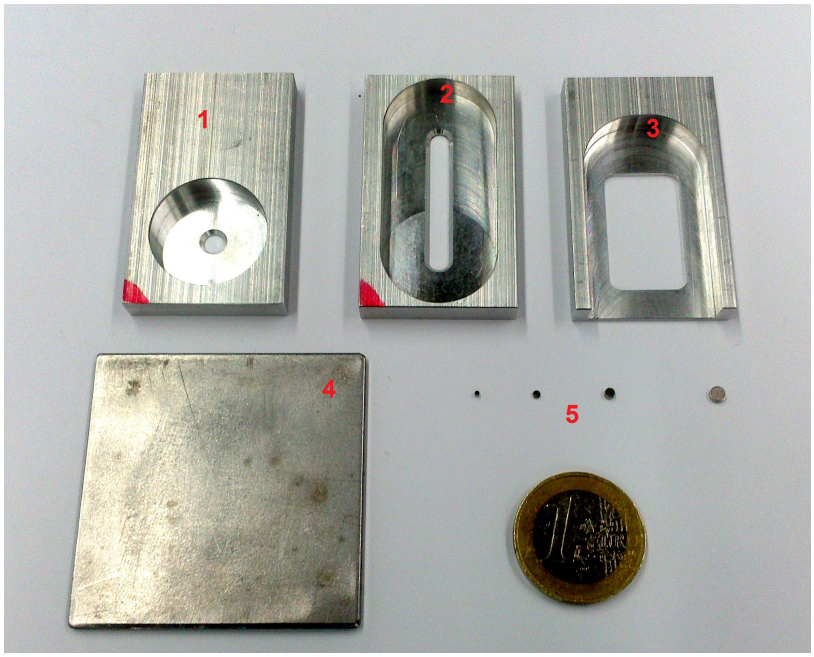

Figure 6.2: Spraymasks used to define the pattern of the different layers: 1. Mask for ion-selective membrane; 2. mask for CNT electrode; 3. mask for passivation layer; 4. stainless steel support plate; 5. magnets in different sizes (1 mm, 1.5 mm, 2 mm and 3 mm)

linearly increases with spray time. In case of the CNT layer, the coating was performed in several cycles with break intervals to allow drying of the layers. This was not necessary for the ion-selective membrane/PVC protective layer as the tetrahydrofuran (THF), used as solvent, evaporates considerably faster than the water used in the CNT ink, allowing a continuous coating of the substrates. The whole spray setup is depicted in figure 6.3 a.

To avoid any physical stress during the fabrication process the substrates were mounted onto a ferromagnetic steel support by the use of magnets. Additional magnets were later used to fix the masks to the sample and also used as fixed

shadow masks to protect the ion-selective membrane from being covered with the passivation layer later in the fabrication process. The fabrication steps were happening in the following order:

1. ink fabrication
2. membrane cocktail fabrication
3. substrate preparation
4. spray coating of CNT layers
5. spray coating of ion selective membrane
6. spray coating of passivation layer

In the following sections the single steps will be described in more detail.

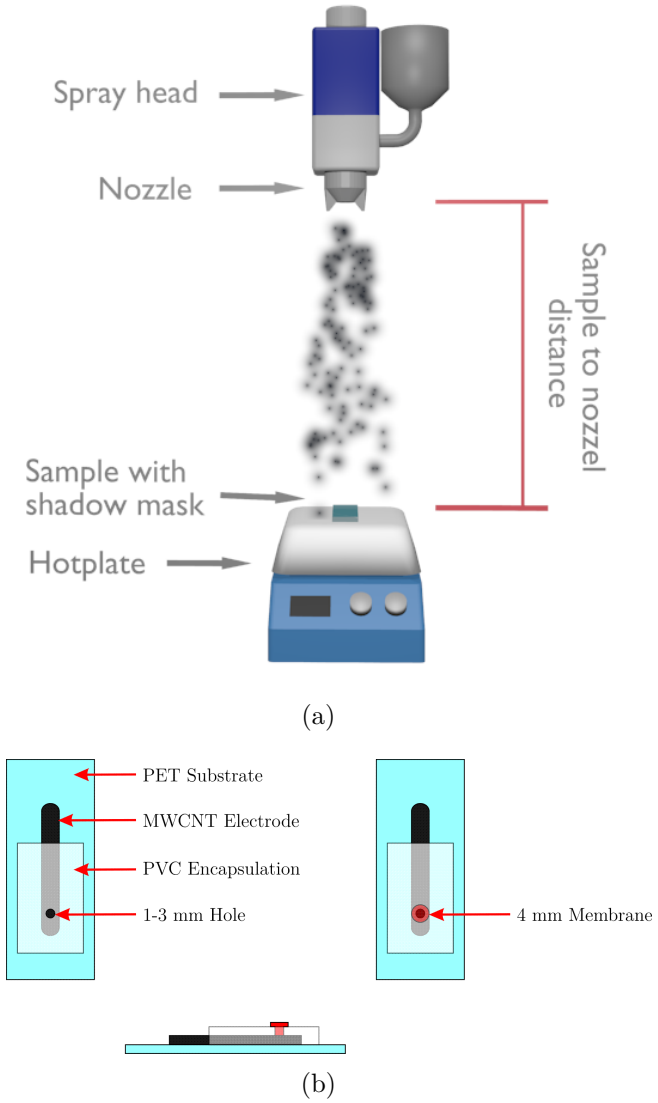

Figure 6.3: a) schematic of the used spray setup consisting of a Krautzberger M10 sprayhead and a hotplate. b) schematic drawing of the achieved sensor setup

6.3.1 Fabrication of CNT ink

The material that is used in spray coating (also called ink) needs to fulfil certain requirements to allow a reliable coating process. One of the most important requirements is that the ink is free from agglomerations that can cause blockings of the nozzle. This would lead to irreproducibilities in the fabrication process. As CNTs form bundles and tend to agglomerate in water a dispersant is needed [113]. Also enough kinetic energy has to be applied to separate the CNT bundles without literally shredding the single CNTs into pieces. For the fabrication of CNT ink 6 g of the dispersant sodium dodecyl sulfate (SDS) were dissolved in 60 ml water and stirred for 1 h. Subsequently, 30 mg of multi-wall carbon nanotubes (MWCNT) (0.05 wt%, Sigma-Aldrich) were added and the mixture was sonicated with a horn sonicator (Branson Digital Sonifier 450) three times for 5 min each, with 5 min breaks in between for cooling. Then, the solution was centrifuged for 1.5 h at 15 000 rpm to remove residual agglomerations from the solution. After centrifugation, the top 75% of the solution was used as ink. Ink fabricated this way has a shelf life time of up to several months but was used immediately after fabrication.

6.3.2 Fabrication of ion-selective membranes

The membrane 'cocktails' were mixed one day before electrode fabrication and stirred at room temperature overnight. K^+-selective membranes contained (by weight): 1.2% NaTFPB, 2.8% valinomycin, 64.4% DOS and 31.6% PVC. Total amount (200 mg) was dissolved in 20 ml of THF. The insulation mask membrane contained (by weight): 40% PVC and 60% DOS. Total 400 mg were dissolved in 40 ml of THF. H^+-selective membrane contained (by weight): 1.0% of tridodecyl amine, 0.6% KTChPB, 63.8% DOS and 34.6% of PVC. Total amount

(200 mg) was dissolved in 20 ml of THF. Cl^-selective membrane contained (by weight): 5% TDDM-Cl, 32.9% PVC and 62.1% DOS. Total amount (200 mg) was dissolved in 20 ml of THF.

6.3.3 Substrate preparation

Before the actual spray coating samples were cleaned. For this purpose 50 mm x 20 mm PET (Hostaphan from Mitsubishi) or polyimide (Kapton HM from DuPont) sheets were placed in an ultrasonic bath with isopropanol for 20 min and blown dry with nitrogen. Before spray coating, both types of substrates were placed into oxygen plasma (150 W, Femto plasma asher by Diener electronics) for 1 min to increase the surface wettability (see section 3.5).

6.3.4 Spray coating of CNTs layers

The substrates were placed onto a hot plate and heated up to 30 °C, and then coated with 1 bar atomizing gas pressure and 25 cm nozzle-to-substrate distance 25 times for 30 s with 15 s drying steps in between. A line pattern with 4 mm width and 30 mm length was fabricated by using a shadow mask (see figure 6.2 1.). After spray coating, the substrates were dried for 1 h at room temperature. To remove the SDS, the substrates were placed in water for 15 min, afterwards in isopropanol for 10 min and finally blown dry with nitrogen. A SEM image of the resulting layer can be seen in figure 6.5.

Spray coating of ion-selective membrane/PVC protective layer On top of the CNT electrode a circle with a 4 mm diameter of the ion-selective membrane was deposited with a substrate-to-nozzle-distance of 15 cm and 1 bar atomizing gas pressure for 40 s at room temperature, resulting in a layer with a thickness

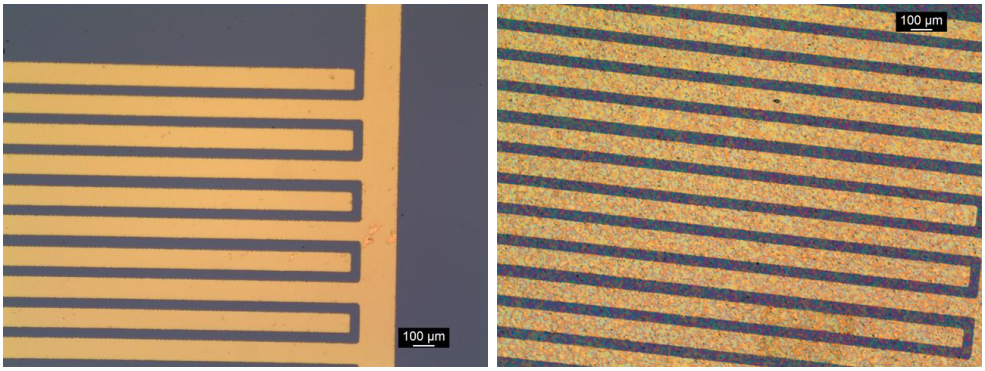

(a) (b)

Figure 6.4: Microscopic images of a) dropcasted and b) spray coated membranes on gold interdigitated transistor structures used in section 6.5

of close to 40 µm. Finally, the PVC passivation layer was deposited on top with a substrate-to-nozzle distance of 17 cm and 1 bar atomizing gas pressure for 60 s also at room temperature, resulting in a layer thickness close to 60 µm. During this step the ion-selective membrane was covered by a circular shadow mask with a 3 mm diameter, forming an active window of 7.06 mm^2. The 0.5 mm overlap of both layers ensures that no gap between the membrane and the protective layer is present. Thus, ion-selective electrodes obtained before the measurement were conditioned in 10^{-3} M KCl for 1 h. In between the measurements, electrodes were stored in air.

Figure 6.4 shows microscopic pictures of dropcasted and spray coated ion selective membranes. One can notice that drop-casted films show a considerably more homogenous surface than spray coated films. Still as long as a high enough spray time is chosen (see section 3.4) the spray coated layer can be considered as a closed layer with high roughness. Also a high surface roughness is potentially

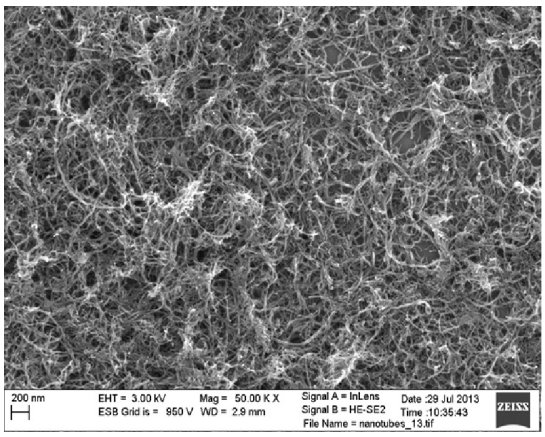

Figure 6.5: SEM image of a spray coated CNT network

advantageous as through the higher surface area a higher ion transport should be possible as more binding sites are present.

6.4 All solid state ion-selective electrodes

At first the resulting CNT layers were characterized. Figure 6.5 shows a scanning electron microscope (SEM) image of a spray coated CNT layer. As can be seen in figure 6.5 the layers are composed of a porous network of tangled MWCNTs. The thickness of these networks was close to 200 nm. 4-point-probe measurements carried out on the CNT layers resulted in a sheet resistance of about $40\,\mathrm{k\Omega/\square}$. While still having a relatively high sheet resistance the electrodes are still suitable for the use as electrode.

Figure 6.6 shows the potentiometric response of spray coated potassium selective electrodes on Kapton and PET substrates. For both kinds of substrates a linear response is present within an activity from $0.1\,\mathrm{M}$ to $10^{-6}\,\mathrm{M}$ with a Nerstian slope equal to $59.8 \pm 0.4\,\mathrm{mV/dec}$ ($R^2 = 0,9998$) for Kapton

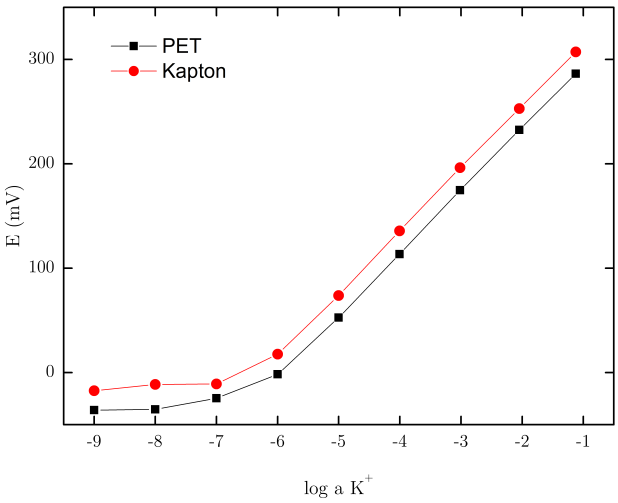

Figure 6.6: Potentiometric responses of spray-coated, potassium selective electrodes prepared using PET (black) or Kapton (red) substrates, recorded in KCl solutions with different concentrations

and $59.6 \pm 0.5\,\mathrm{mV/dec}$ ($R^2 = 0,9996$) for PET. Thus detection limits equal to $10^{-6.5}\,\mathrm{M}$ were obtained. The results received with spray coated sensors are therefore well comparable to classical ASS-ISE potassium sensors [100]. They are well comparable to other planar screen-printed [114] or manually coated [115] setups using CNTs or graphene as transducers or electrical contacts. Also they show more favourable detection limits compared with paper-based sensors using CNTs as transducers and electrical leads [116].

Selectivity coefficients ± standard deviation (SD) are obtained with separate solution method, using experimental slope values for activities ranging from $0.1\,\mathrm{M}$ to $10^{-4}\,\mathrm{M}$ measured on Kapton and PET are displayed in table 6.1.

Table 6.1: selectivity coefficients ± SD for activities between 0.1 M to 10^{-4} M of Kapton and PET samples

	Kapton	PET
$\log K_{K,Na}$	-3.3 ± 0.4	-2.8 ± 0.3
$\log K_{K,Mg}$	-4.4 ± 0.4	-3.4 ± 0.3
$\log K_{K,Ca}$	-4.6 ± 0.3	-3.6 ± 0.4
$\log K_{K,H}$	-4.5 ± 0.3	-4.0 ± 0.6

Although the obtained selectivity coefficients are well comparable with those obtained for other (nominally disposable) systems (e.g. ref. [116, 117]) prepared using PVC-based membranes, there were some differences between sensors prepared on Kapton or PET substrates. Despite the fact that the sensors were pretreated/tested in parallel, Kapton substrate-based sensors repeatedly proved to be characterized by slightly higher selectivity for divalent interfering ions, compared with PET. In our opinion, this effect, consistently observed in tested sensors, can be related to the substrate effect, particularly as relatively thin ion-selective membranes were used (ca. four times thinner compared with standard membrane thickness used [100]).

The preliminary conclusions drawn from conducted experiments related to reproducibility of the automatic manufacturing production method are highly encouraging. The differences in E^0 potential value between sensors prepared in one manufacturing batch (regardless of the type of substrate used) were in the range of a few mV. The response time of spray coated sensors was dependant on the activity of the sample solution; however, it was observed that sensors prepared using Kapton substrate were characterized with shorter response time compared with those of PET, reaching about 20 s and about 70 s, respectively,

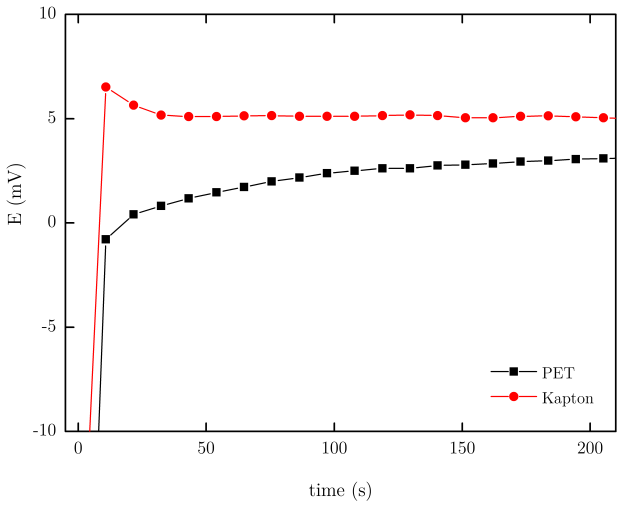

Figure 6.7: Response time of tested sensors for electrolyte concentration changes using PET (black) and Kapton (red) substrates

as shown in figure 6.7 for an electrolyte concentration change from 10^{-2} M to 10^{-3} M.

The reproducibility of potential readings of nominally disposable spray-coated potentiometric sensors (within one day) was tested in a non-optimized setup simply, in a beaker. Mean values of potentials recorded for each activity during four consecutive calibrations performed within the broad KCl activity range (from 0.1 M to 10^{-9} M) are presented in figure 6.6 and 6.8. They clearly show that both kinds of support used are resulting in sensors characterized with similar potential values and a high reproducibility of the values recorded (SD of values recorded 9 mV). The results presented clearly confirm that although the herein proposed system is prepared using a relatively small amount of chemicals

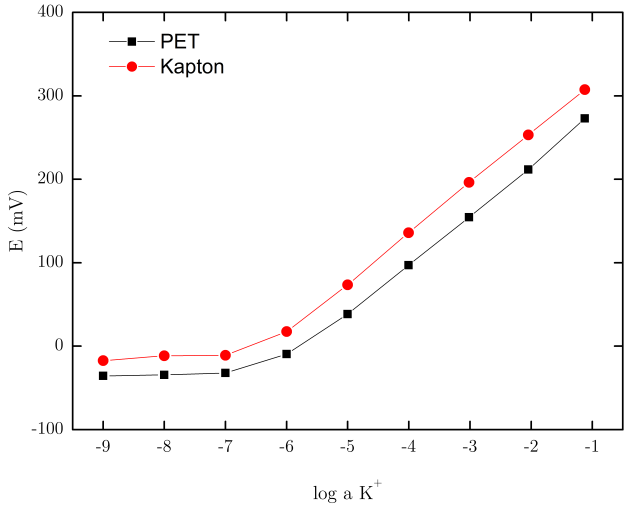

Figure 6.8: Mean potential values course of four calibrations performed during one day for spray-coated sensors using either PET (black) or Kapton (red) substrates

per sensor (relatively thin layers of automatically applied materials), the sensor offers sufficient long-term stability to enable multiple measurements.

Moreover, the potentiometric performance of the sensors tested both shortly after preparation (e.g. <2 weeks, including the transport between cooperating groups of laboratories) or after significantly longer storage (under refrigeration, due to the valinomycin ionophore used) was the same within the range of experimental error, which is promising for practical applications.

The reproducibility of potential values is well comparable to that obtained in similar tests performed for traditional sensors (glassy carbon supporting electrode) with one of the most trusted transducers poly(3-octylthiophene) [118].

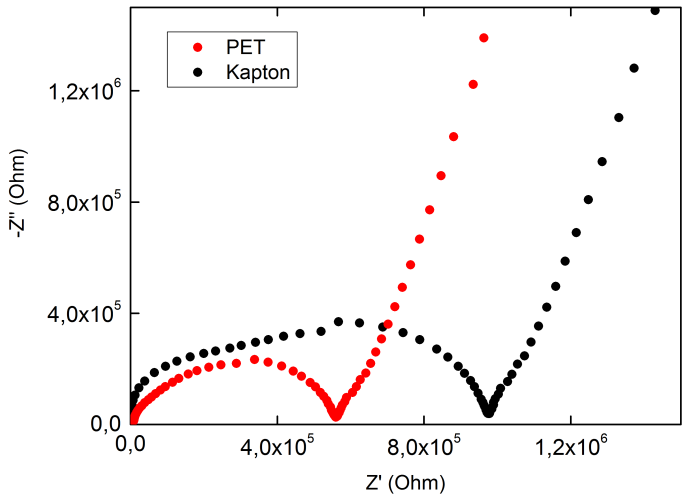

Figure 6.9: Complex plane impedance plots of tested spray coated K^+-electrodes prepared using PET (black) and Kapton (red) recorded in 0.1 M KCl solution, using 50 mV amplitude at 0.3 V potential, in the frequency range from 0.01 Hz to 10^{-5} Hz and the equivalent circuit proposed for the Kapton support electrode

This result is highly promising from the point of view of possible practical application of the simplified sensors proposed herein.

The stability of potentiometric responses within longer time periods was also studied. Although such tests are generally rarely performed for nominally disposable sensors, in our opinion, this is an important long-term stability test for any newly proposed arrangement. The SD of the mean value of potentials recorded was changing with electrolyte concentration, lower SD values were obtained for the linear range of responses (close to 7 mV), slightly higher values were obtained for lower activities (Figure 6.8).

The usual set of tests applied for novel-type, potentiometric, all-solid-state sensors includes impedance spectroscopy [100]. Figure 6.9 presents complex plane impedance plots for the sensors withKapton and PET support, respectively. For the Kapton support, the spectrum contains a single semicircle at higher frequencies followed by a linear part recorded at lower frequencies (a slope close to 45 degrees), and then the slope of dependence increases with decreasing frequency. For the PET substrate, the picture is more complicated, suggesting the overlapping of two semicircles at high frequencies. This effect can result from additional resistance in the presence of the PET support. It can be observed that the shapes of plots for Z^0 higher than $6 \times 10^{-5}\,\Omega$ (Kapton) and $3 \times 10^{-5}\,\Omega$ (PET) are similar. The plot obtained for PET support appears to be shifted to $3 \times 10^{-5}\,\Omega$ higher resistances compared with that of the Kapton, suggesting the same properties in the case of both supports, related to the membrane, CNT transducer, and their interfaces. The shape of the ISE response suggests that it can be analyzed using the simplified equivalent circuit, proposed in [115] for the glassy carbon and plastic electrodes with CNT layer (figure 6.9). This circuit consists of solution resistance, RS, and parallel-connected R and C_g, representing the membrane resistance (as the most resistive component of the sensor) and geometric capacitance of the sensor (membrane), respectively. Z_W represents the Warburg impedance resulting from diffusion limitations in the membrane, whereas C_b corresponds to the bulk capacitance of the CNT layer responsible for its transducing properties. For the data presented, figure 6.10 shows the results of a fitting procedure, which was applied to the experimental data for the sensor with Kapton support, leading to good concordance with the experimental data. The R resistance and Cg are typical values obtained for PVC-based membrane ($4.8 \times 10^{-5}\,\Omega$ and $1.7 \times 10^{-10}\,\mathrm{F}$, respectively), whereas C_b around $2 \times 10^{-6}\,\mathrm{F}$ is typical for carbon supports [119].

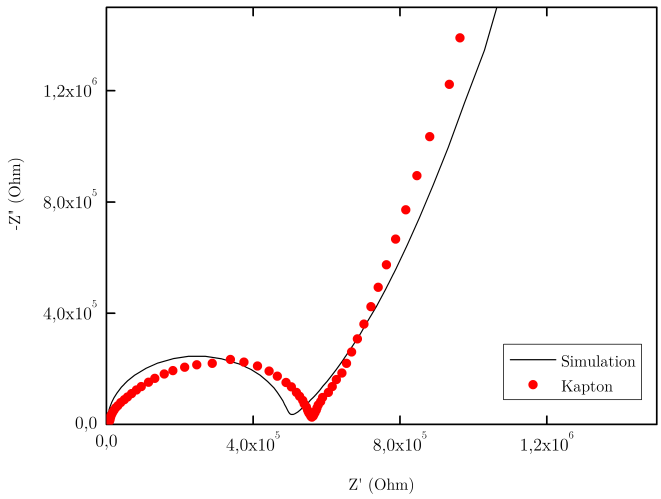

Figure 6.10: Complex plane impedance plots of tested spray coated K^+-electrodes prepared using Kapton (red) recorded in 0.1 M KCl solution (figure 6.9), using 50 mV amplitude at 0.3 V potential, in the frequency range from 0.01 Hz to 10^{-5} Hz compared to (black line) fit to equivalent circuit presented in 6.9 using fitting tools of CH-Instruments software

The same methodology was used to prepare H^+ -selective electrodes (on PET substrates) using tridodecylamine as the ionophore. Thus, obtained sensors were characterized with linear responses of slope equal to 53.7 ± 1.1 mV/dec ($R^2 = 0.997$) for a hydrochloric acid concentration change from 0.1 M to 10^{-5} M. Thus, the obtained sensor was used to determine H^+-concentration of three different types of orange juices. The results obtained using herein-prepared, nominally disposable H^+ sensitive sensors were within the range of experimental error comparable with those of measurements performed in parallel experiments with glass electrode determination in an unoptimized experimental setup

Table 6.2: Log a H^+ results of spray coated H^+-selective sensors compared to standard glass based sensors measured in different kinds of orange juice

	Spray coated	Glass
Juice 1	3,83	3,85
Juice 2	3,72	3,74
Juice 3	3,91	3,95

in beakers (see table 6.2). These results clearly show that herein-proposed sensors can be used as cost-effective devices (relatively low chemical consumption for preparing sensors) in the analysis of real samples. A model anion-selective sensor Cl^--selective electrode was also prepared (on PET substrate). Thus, obtained sensors were characterized with linear responses within the KCl concentration range from $0.1\,\text{M}$ to $10^{-5}\,\text{M}$ with a slope equal to $56.3 \pm 1.3\,\text{mV/dec}$ ($R^2 = 0.994$). The selectivity of the thus-obtained sensor was tested for model interferents Br^- and NO_3^- anions.

Obtained selectivity coefficients (for ions that are known to be severe interferents for chloride-ion selective sensors; separate solution methods within the activity range from $10^{-1}\,\text{M}$ to $10^{-3}\,\text{M}$) were equal to log $K_{Cl,Br}$ 1.3 and log K_{Cl,NO_3} 1.6. These values are more favourable than those previously reported for other classically sized, all-solid-state, chloride-selective electrodes of similar membranes [120], clearly showing that the herein-proposed method can be used to prepare sensors responsive to various ions.

6.5 Transistors with spray coated ion-selective membranes

In the previous section the fabrication of completely spray coated ion-selective electrodes was presented. In this section ion-selective field effect transistors (ISFET) based on carbon nanotube field effect transistors (CNT-FET) with a spray coated ion-selective membrane on top will be presented.

ISFET have attracted a growing amount of scientific research [121–123]. This rising interest is based on the advantages of ISFETs compared to classical ISEs that are short response time, low output impedance, small size, mass production and the solid state nature of most ISFETs [124]. Also ISFETs allow an integration of compensation and data processing into a single chip [125]. Field-effect transistors based on carbon nanotubes (CNT-FET) provide a good platform for further development in the field of ISFETs. Their solution processability allows a scalable and cost effective way to fabricate flexible or disposable sensors on a wide variety of substrates. Also it has already been shown that unfunctionalyzed CNT-FETs exhibit a high sensitivity towards the ionic strength of the used electrolyte [77, 126–128]. Ion-selective CNT-FETs with dropcasted membranes on the CNT layer have already been published, showing that the overall process is possible [76]. The integration of a spray coated design would allow further automatization of the fabrication process as the drop casting process so far requires manual work.

The transistors were fabricated on silicon wafers with a 200 nm thick thermal oxide on top using the same lift-off technique and masked as already described in section 3.1, 4.3 and 4.4. In this case the interdigitated transistor structure consists of a 40 nm thick gold layer with a 5 nm Cr adhesion layer underneath. On top of this layer a CNT layer was spincoated with 1000 rpm, resulting in a

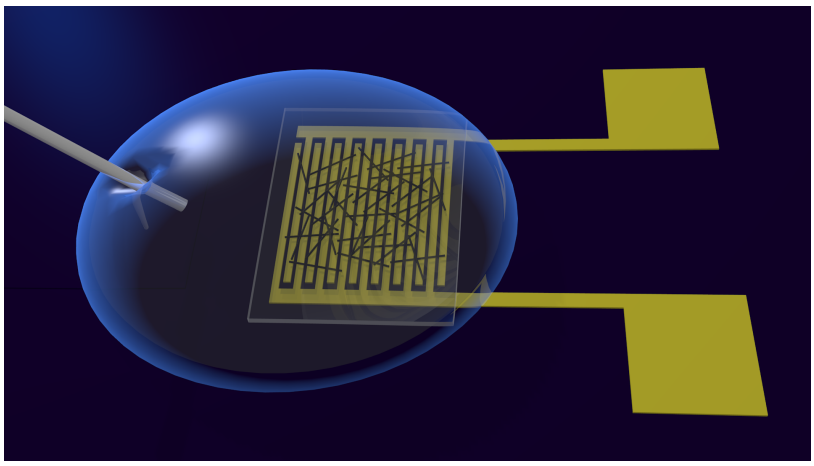

Figure 6.11: Schematic 3D drawing of an electrolyte-gated CNT-transistor with spray coated ion selective membrane

thin CNT network with roughly 15 CNTs per μm^2. The CNT solution in this case was based on single wall CNTs with 92.5 % of semiconducting CNTs. The ink fabrication process is similar to that described above. On top of the CNT network different kinds of ion-selective membranes were sprayed. In this case K^+ and pH selective membranes were used as a model system. The parameters for spray coating are the same as in section 6.3. As the ISFET are used in a electrolyte gated configuration it has to be made sure that after the spray coating of the membrane no contact between CNTs and electrolyte is present. Otherwise the result would be a transistor with a non-selective response to pH and ion concentration in the electrolyte, due to the intrinsic ion- as well as pH-sensitivity of the CNTs. A schematic of such an electrolyte gated CNT-FET with ion-selective membrane is shown in figure 6.11.

Figure 6.12 shows two transfer curves of the same CNT-FET one with and one without membrane. The CNT-FET with membrane has also undergone a

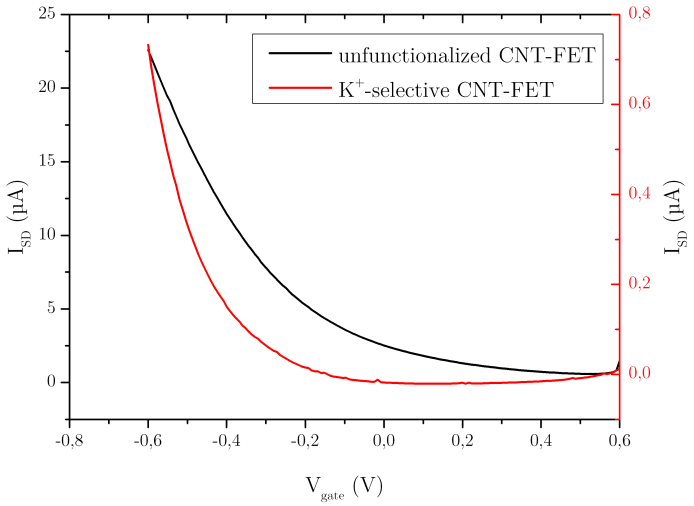

Figure 6.12: Transfercurves of CNT-FETs before (black) and after (red) membrane modification of the CNT network

conditioning step necessary for operation (see section 6.4). The transfer curves show a shift towards more negative gate voltages after membrane addition. The transistor coated with a membrane still shows an on/off ratio of more than 100 and an on-current in the μA-range.

6.5.1 Potassium-selective membrane modified CNT-FET

The change of the analytes concentration within the electrolyte is determined by the change of the threshold voltage. Details on the measurement procedure can be found elsewhere [77]. Figure 6.13 shows the threshold voltages V_{th} of a K^+-selective ISFET for the primary ion K^+. The x-axis represents the logarithm of the ion activity in Mol. For solutions with a potassium concentration ranging from 0.1 M to 10^{-6} M a constant linear response of 57.2 ± 3.2 mV/dec can be de-

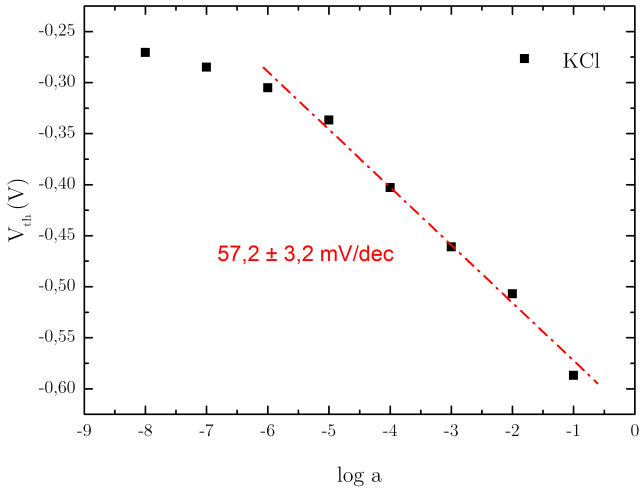

Figure 6.13: Threshold voltages of an K^+-selective ISFET for the primary ion K^+

termined. This value is, keeping in mind the standard deviation, nearly identical with the values measured with ISEs on Kapton and PET ($59.8 \pm 0.4\,\mathrm{mV/dec}$ and $59.6 \pm 0.5\,\mathrm{mV/dec}$ respectively) measured in section 6.4. Also the detection range from $0.1\,\mathrm{M}$ to $10^{-6}\,\mathrm{M}$ is identical.

Also the selectivity coefficients were determined with the fixed interference method which is usually closer to reality than the separate solution method used in section 6.4 [129]. The obtained values of $\log K_{K,Na} = -6,54$ and $\log K_{K,Ca} = -5,73$ are significantly higher than the ones achieved with ISEs (3,3 and 4,6 respectively, on Kapton). A possible reason for this, besides the measurement method, is a substrate effect as already differences between PET and Kapton are present and the ISFETs were fabricated on silicon wafers. The obtained values are well comparable to values that can be found in literature, in some

cases even better [116, 117]. Still one has to keep in mind that the amount of measured samples is rather small, therefore variations in the fabrication process are possible.

6.5.2 H^+-selective membrane modified CNT-FET

Figure 6.14 shows the threshold voltages of a H^+-selective ISFET at different pH values. The thickness of the membrane is supposed to be 40 µm, equal to the membranes described in the previous sections. A linear increase of V_{th} with decreasing pH can be seen between pH values of 11 and 5. For pH values lower than 5 the threshold voltage V_{th} drops again. The slope of the rise between 5 and 11 pH is -86.6 ± 2.8 mV.

For CNT-FETs with cation-selective membranes usually a shift of V_{th} towards more positive values can be expected with decreasing cation concentration [77]. A possible explanation for the observed opposite behaviour at pH values bigger than 5 is the presence of a second pH-sensitive interface at the platinum wire used as gate electrode. Platinum is known to form oxides when getting in contact with water. These oxides are highly pH sensitive [130]. The same effect has also been observed in devices without membrane or devices without CNTs and is the aim of current investigations. This response depends on the strength and ingredients of the used buffer solution. The buffer solutions used in this case were prepared by setting the pH value of a highly concentrated KOH solution with different amounts of HCl to the desired values.

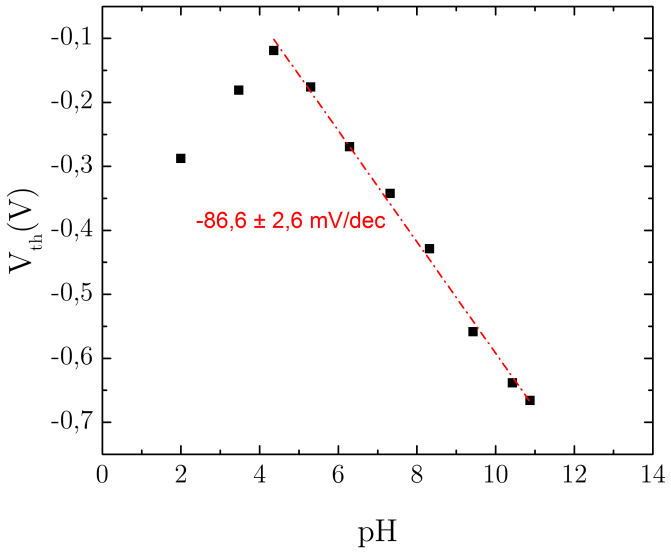

Figure 6.14: Threshold voltages of a pH-selective ISFET with spraycoated H^+-selective membrane at different pH values

6.6 Conclusion

The presented results show clearly that fabricating ion-selective electrodes solely by spray coating is an effective way to fabricate reliable potentiometric sensors. Achieved sensors are stable and show a response and selectivity comparable to values achieved in literature. Also the fabrication of CNT-FET based ISFETs with a spraycoated ion -selective membrane has been demonstrated. Results achieved with ISFETs are well comparable to that achieved with spray coated ISEs.

7 Nanotexturing of organic semiconductors

The following chapter will focus of the nanotexturing of organic solar cells. First a short overview on nanotexturing is given, then different kinds of nanostructuring, namely nanoimprinting and nano transferprinting of organic semiconductors will be described in more detail. Parts of the results presented in this chapter have already been published in the Proceedings of the 2015 IEEE 15th International Conference on Nanotechnology (IEEE-NANO) [154].

7.1 Nanotexturing in organic solar cells

Nanostructuring or nanotexturing in organic solar cells has been performed with a multitude of techniques. The following section will give a short overview on a selection of common technologies used for this purpose. A wider review about this topic can be found elsewhere [132–134].

Tandem setups for solar cells have been the aim of a growing amount of attention in the recent years. Still most organic solar cells have a setup comparable to that of the organic photodetectors descibed in section 5: A flexible or rigid substrate covered with a transparent conductive electrode (front electrode), followed by a hole or electron blocking layer, the active layer containing

the organic semiconductors and a metal electrode on top (back electrode). This setup allows an easy exchange of layer material as well as a modification of one the single layers i.e. by applying a nanotexture. The aim of introducing nanotextures into organic solar cells usually is an increase of the cells efficiency. This can be achieved in multiple ways.

Kang *et al.* [135] for example used nTP (see section 3.3) to fabricate transparent metal electrodes consisting of nanogrids as a replacement for ITO electrodes. This way it was possible to achieve similar efficiencies as with ITO. A different approach was followed by Chou *et al.* [136]. In their work they used an optimized gold nanomesh fabricated by NIL (see section 3.2) to increase the efficiency by nearly 50 % exploiting a cavity effect.

Jin *et al.* [137] are using holographic lithography to structure the front electrode of their cells a grating with a 350 nm pitch. The enhancement of the power conversion efficiency exhibits of 35% is believed to be caused by an absorption enhancement resulted by the excitation of propagating surface-plasmon polariton (SPP) modes at the corrugated metal/organic interface.

A different way to use a plasmonic effect is the introduction of metal nanoparticles into this device. As the nanoparticles are usually smaller or equally sized compared to the wavelength of the incoming light one speaks of localized surface plasmons. Gold or silver nanoparticles are commonly used for this purpose, but other metals like copper and aluminum are also possible. In most cases the nanoparticles are incorporated into the PEDOT:PSS hole conduction layer. I. e. Kim *et al.* [138] used by electrodeposition fabricated silver nanoparticles located in the PEDOT:PSS layer of solar cells, with a P3HT:PCBM active layer, to boost the efficiency of their cells from 3.05 % to 3.69 %. A similar approach was followed by Morfa *et al.* [139] who used a vapour phase deposition process to deposit silver nanoparticles onto the ITO electrode. They improved the effi-

ciency of their cells from 1.3 % to 2.2 % using P3HT:PCBM as active layer. Wu *et al.* [140] used solution processable gold nanoparticles also incorporated into the PEDOT:PSS layer in a P3HT:PCBM solar cell to enhance their solar cell efficiency from 3.57 % to 4.24 %.

It has been shown by Wu *et al.* [141] and Wadams *et al.* [142] that nanoparticles don't have to be spherical. They used silver nanotriangels and gold nanorods respectively.

Instead of structuring the front electrode it is also possible to structure the back electrode to introduce a grating into the solar cell. Li *et al.* [143] achieved an enhancement from 3.09 % to 3.68 % of the power conversion efficiency by the introduction of a silver back grating using a P3HT:PCBM blend as active layer. You *et al.* [144] demonstrated a rise from 7.20 % to 7.73 % with a similar process but using a different material system (PTB7: $PC_{71}BM$). In both cases the gratings were fabricated by nanoimprinting the active layer with a soft PDMS stamp and evaporating the metal electrode onto the pre-structured layer, thus forming a metal grating. Ko et all showed that nanostructurs in solar cell can increase absorption in specific regions by up to 10% using a technique called pattern replication in nonwetting templates (PRINT) for fabrication [145, 146]. While achieved efficiency of around 0.6 % to 1 % is relatively low, the results are promising. De Oliveira Hansen *et al.* [147] even integrated a grating structure into the back electrode of a flexible solar cell based on a P3HT:PCBM blend, archiving an efficiency enhancement of 34 %. The used technique in this case was e-beam lithography.

This work will focus on the fabrication of organic solar cells with a active layer made of an P3HT:PCBM blend and metallic back grating. The fabrication of the grating will be performed with a technique comparable to that used by Li and You and their coworkers [143, 144]. The grating will be formed by

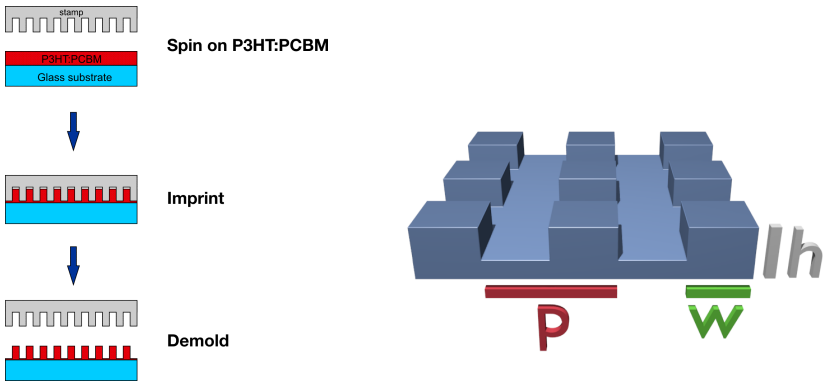

(a) (b)

Figure 7.1: a) Schematic overview on the imprint process for the P3HT:PCBM layer. b) Drawing of the stamp structure

the evaporation of a Ca/Ag back electrode onto a already structured organic semiconductor. The main difference is the structuring mechanism of the organic semiconductor which will be performed by the means of nTP.

7.2 Nanotexturing of organic semiconductors by nanoimprinting

As a first approach glass samples covered with a P3HT:PCBM layer were imprinted and the transmission of the resulting structured layer was measured. The aim of this test was to find out if the structured polymer can support a nanostructure or if the structures will collapse. One has to keep in mind that the used organic semiconductors are not designed to be nanotextured like stamp replication polymers like OmrmoStamp or like imprint resists. Float glass samples were first sonicated in acetone and isopropanol for 10 minutes and subse-

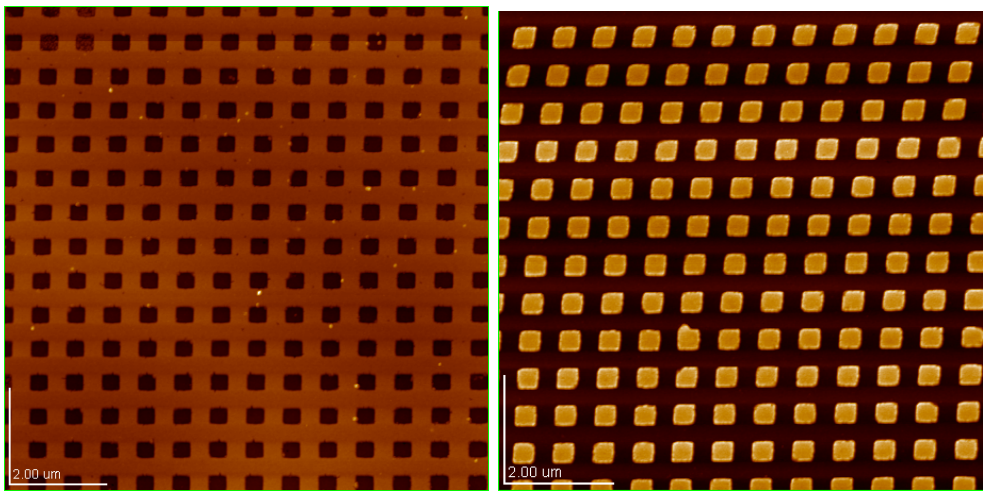

(a) (b)

Figure 7.2: AFM images of a stamp replica with 350 nm × 350 nm square pillars made of OrmoStamp. a) first generation copy with inverted (or negative) structure. b) second generation copy with original (positive) structure.

quently blow dried with nitrogen. Afterwards a 1 minute plasma treatment was performed to increase wettability and remove any residual organic contaminations. Subsequently the samples were spincoated with a P3HT:PCBM solution at a spin speed of 400 rpm, resulting in a layer thickness of 320 nm. The imprint process was performed immediately afterwards with a pressure of 8 bar at a temperature of 140 °C for 10 min (see section 3.2 for details on nanoimprinting). The imprinting process is depicted in figure 7.1 a. Imprinting the sample directly after spincoating is critical as in this case the layer is not dried completely and therefore still soft. After imprinting the sample is transferred quickly into inert gas atmosphere were the stamp is removed to prevent degradation.

The blend used for spincoating was consisting of P3HT and PCBM with a ratio of 1:0.75 by weight. Both materials were dissolved in DCB to form a solution with a concentration of 2 % by weight and stirred at a temperature of 50 °C over night. Before usage the solution was filtered with a 0.25 µm filter to remove any residual particles. The stamp used for the imprinting process was a semi-flexible (see section 3.3.2) stamp with a thin glass backing and an active (structured) area of 1 cm. This area is covered with square pillars with an edge length w of 350 nm, a pitch p of 700 nm and a structure height h of 275 nm (see figure 7.1 b). AFM images of such stamps are shown in figure 7.2.

Figure 7.3 shows an atomic force microscope (AFM) image of an imprint carried out according to the above described procedure. As one can see the pattern in the P3HT:PCBM layer closely resembles that of the imprint stamp. With 702 nm the pitch of the cell is very close to the original value of 700 nm. Also the pillar wide of 357 nm is very close to the structures on the stamp which are 350 nm wide. The structure was stable over several weeks.

7.2.1 Transmission measurements

After fabricating the above mentioned nanostructured P3HT:PCBM layers transmission measurements were performed on these samples. Figure 7.4 shows the transmission of an imprinted sample measured at a wavelength between 300 nm and 1000 nm. Samples are measured against a glass reference to subtract the substrate influence.

The transmission of imprinted samples show a significantly decreased transmission, especially at wavelengths below 500 nm and above 600 nm. At a wavelength of 650 nm a shoulder is present in the transmission of structured layers. The bandgap of the P3HT used in the layers is 1.9 eV (see section2.3.1) which

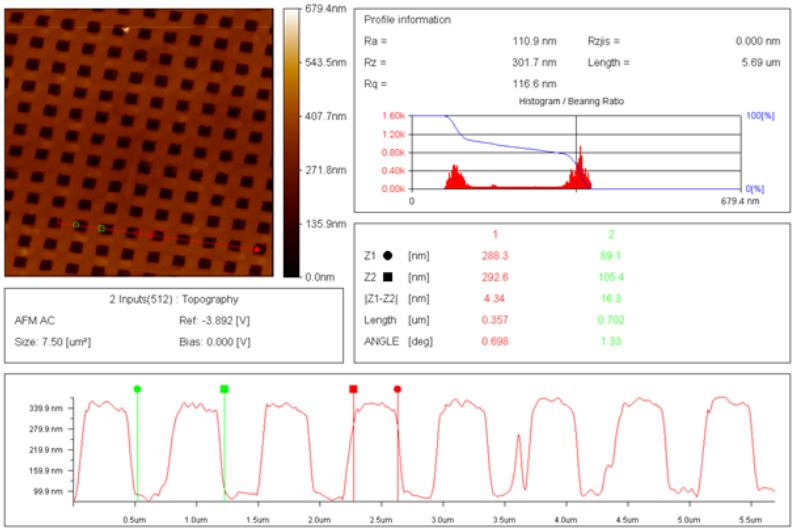

Figure 7.3: Atomic force microscope image of an imprint into a P3HT:PCBM layer

corresponds to a wavelength of 650 nm, while the PCBM with a bandgap of 2.7 eV (see section 2.3.2) corresponding to 450 nm. As optical absorption of photons with an energy below the bandgap is unlikely, the layer is supposed to be transparent at a wavelength above 650 nm. Measurements were performed with an integration sphere, which allows angle independent transmission measurements.

7.2.2 Conclusion

As mentioned above it has been proven that a structuring of a P3HT:PCBM by the means of nanoimprinting is possible. The fabricated structures are stable over several weeks under ambient conditions without any supporting structure such as a supporting metal layer. No collapsing of the structure has been ob-

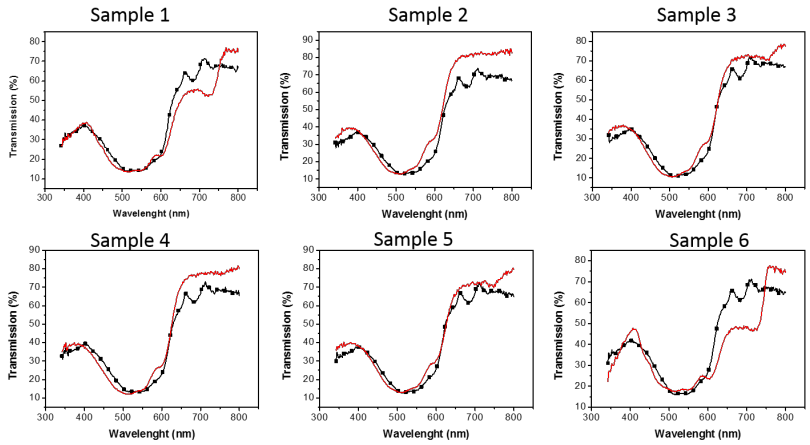

Figure 7.4: Transmission measurements carried out on imprinted P3HT:PCBM blend films with a thickness of 320 nm on a glass substrate. Red: imprinted sample area. Black: flat sample area

served, demonstrating that P3HTR:PCBM films are a suitable material system for nanostructuring. Structured films show an overall decreased transmission which is believed to be partly based on reflection.

7.3 Transferprinting of organic semiconductors

One way to implement the structures in the solar cell more gently is nanotransfer printing. The big advantage of this process is that it doesn't rely on high temperatures and high pressure like nanoimprinting (see sections 3.2, 3.3 and 7.2). Another big advantage is that due to the lack of need of huge apparatus the process can be carried out in a glove box under inert gas atmosphere. This way the organic semiconductors like P3HT are prevented from degrading in the oxygen and water vapour rich environment. For the transfer process a transfer stamp is needed which is, after a surface treatment, covered with the material

to transfer. To transfer the material the stamp is brought in conformal contact with the target substrate. Then heat is applied to increase adhesion to the target substrate. Then the stamp is removed from the substrate, leaving the transferred layer on the substrate.

A transfer of structure layers is also possible. Here a stamp with the desired structure is needed. When the structured stamp is covered by spin coating the structures will get filled with the applied material and a flat layer will form on top of the structure. This process only works for relatively low structure heights and depends on the viscosity, surface tension and the amount of the applied material, as well as the spin speed during spin coating.

7.3.1 Transfer of flat films

As a first step a transfer process for flat films was developed. For this purpose flat transfer stamps where obtained from unstructured 2" silicon or quartz wafers treated with an anti sticking layer. On top of these 3 g PDMS (Sylgard 184 silicone elastomer (Dow Corning) and a curing agent mixed with a ration of 10:1 Sylgard:curing agent by mass) was purred and cured at 90 °C for 2 h (see section 2.3.4) resulting in a 3 mm thick layer. The cured PDMS layer was cut into 2 cm × 2 cm parts. After cutting the pieces were peeled of the wafers and transferred onto 1.2 mm thick glass supports for convenient handling and to minimize the bending of the stamp during processing. During this transfer it was made sure that the side of the stamp which was in contact with the wafer during curing is now pointing upwards to assume a surface equally flat as a polished wafer. Afterwards a plasma treatment step was necessary to allow the stamps to be wettable with material to be transferred (see section 3.5 for

details). Spin coating on untreated layers resulted in not conformal layers or no layers at all.

The plasma treatment step turned out to be one of the most critical ones during the whole transfer process of P3HT:PCBM layers. A too strong treatment resulted in a high adhesion of the material to transfer on the stamp. On the other hand, if the treatment is to short, a conformal covering of the transfer stamp is difficult. A treatment with a higher applied power than 90 W or a longer treatment time than 30 seconds results in no transfer at all. If the treatment time is shorter than 12 s and the applied power is lower than 45 W a sufficient covering of the stamp is not possible. The ideal treatment parameters for transferring P3HT:PCBM layers were found to be a 18 s treatment time with an applied power of 60 W. All samples were additionally kept in a Faraday cage during the treatment. The found values are similar to values found by other groups [148].

For the transfer of PEDOT:PSS layers (Clevios P VP AI4083) the plasma parameters are not as critical. Long treatment times don't seem to increase adhesion to the stamp but improve the wetting of the hydrophobic stamp with the water based PEDOT:PSS solution. For PEDOT:PSS layers the treatment time used is 1 min with an applied power of 90 W, also in a Faraday cage.

After the plasma treatment the samples were spin coated with the desired material. Subsequently an annealing step at 140 °C for 10 minutes was conducted. Before the annealing process the stamps have to be removed from the glass support without being bended to avoid a bonding of the stamp to the glass support. After a short cooling step of 5 minutes the stamps were transferred to the designated sample and heated to 100 °C for 5 minutes. Finally, after cooling the samples down to room temperature, the stamps can be removed, leaving the transferred layer on the substrate.

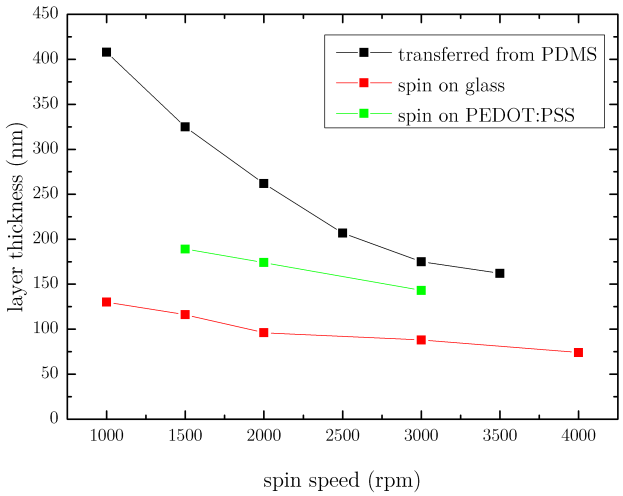

Figure 7.5: Thicknesses of spin coated P3HT:PCBM layers (spin coated from a 2 % by weight solution with DCB as solvent and a weight ratio of P3HT:PCBM of 1:0.75) on glass substrates compared to layers spin coated on PEDOT:PSS covered substrates as well as layers transferred from PDMS

After transfer process development the thickness of P3HT:PCBM layers spin coated on glass substrates and substrates covered with a PEDOT:PSS layer have been compared to transferprinted layers (see figure 7.3.1). Layers were spin coated from a 2 % by weight solution with DCB as solvent and a weight ratio of P3HT:PCBM of 1:0.75. The transferred layers were spin coated onto flexible and plasma treated PDMS stamps before transfer. As can be seen a strong variation of the layer thickness depending on the spin coated substrate is present. Transferred layers (spin coated on PDMS before the transfer) show a nearly four times higher layer thickness at low spin speeds compared to glass substrates. The difference decreases with increasing spin speed. Layers spin

coated onto PEDOT:PSS covered samples have a thickness which is roughly twice as high as that of layers on glass samples.

7.3.2 Transfer of structured films

After developing a transfer process the very same process has been used to transfer structured layers. Different from the previous described process the flexible PDMS stamps are not fabricated using a wafer as master but using a structured SiO_2 master with a 350 nm square pillar structure similar to that described in section 7.2. The main difference is a smaller pillar height, which is only 40 nm. The thickness of the PEDOT:PSS and P3HT:PCBM layers to be transferred is only 20 nm to 100 nm and 100 nm to 350 nm respectively, a structure higher than the layer thickness would lead to a non conformal covering of the structured area. Also stamps with an inverted structure (holes instead of pillars) were used.

As a first approach structured PEDOT:PSS (Clevios P VP AI4083) layers were transferred onto substrates consisting of float glass. Results of such transfers are shown in figure 7.6. As can be seen in the images the transferred layer with holes shows a very good pattern transfer which closely matches the pattern of the original stamp (see figure 7.2). All holes are transferred completely and no collapse of the holes is visible. The transfer of the pillars on the other hand is not as good. The transferred pillars show round edges and a dome like shape.

It has to be mentioned that the transfer of flat and structured PEDOT:PSS layers using the previously described method also works for large areas. In this work layers with a lateral dimension of 25 mm by 25 mm have been successfully transferred, as well as layers with a nanotextured area of 10 mm by 10 mm.

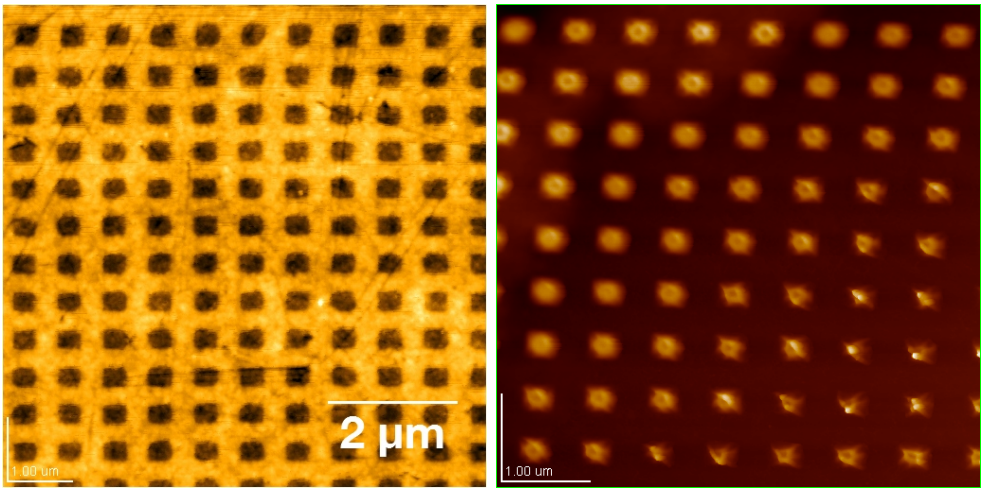

(a) (b)

Figure 7.6: AFM images of transfer-printed PEDOT:PSS layers on glass samples. a) using a stamp with pillars and b) using a stamp with holes.

In a second approach layers consisting of P3HT and PCBM with a weight ratio of 1:0.75 have been transferred. In this case only stamps with pillars were used for transfer, therefore only layers with holes have been fabricated. Figure 7.7 shows AFM images of such transferred layers. As master for the transfer stamps the same template as for the PEDOT:PSS layers have been used. The pattern dimensions are therefore identical. As the image in figure 7.7 a) shows a good pattern transfer is present. The transferred structure closely resembles that of the transfer stamp. The AFM image with lower resolution in figure 7.7 b) shows that the pattern transfer appears to have the same quality over large area.

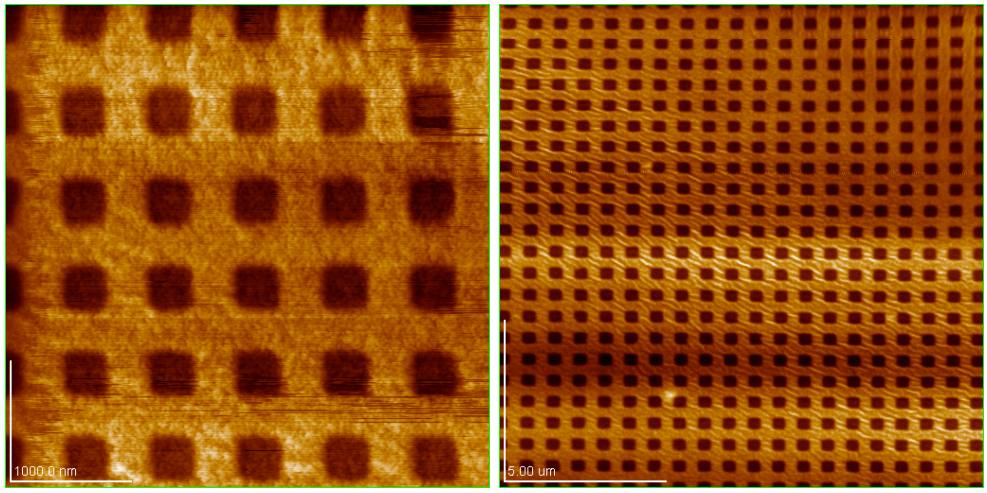

(a) (b)

Figure 7.7: AFM images of transfer-printed of P3HT:PCBM layers on PEDOT:PSS coated glass samples with different resolutions

7.3.3 Nanotextured organic solar cells fabricated by nanotransferprinting

After fabricating single nanotextured layers by the means of nanotransferprinting the next logical step is the fabrication of whole organic solar cells. For this purpose a layer stack was chosen similar to that of the spray coated organic photodetectors demonstrated in chapter 5. The layer stack is as follows: A glass substrate with a transparent electrode on top (here ITO) is covered with a 40 nm thick hole conducting layer, which consists of PEDOT:PSS. On top of these follows the nanotstructured active layer made of P3HT and PCBM (ratio 1:0,75) which is fabricated by the means of nanotransferprinting. A metal electrode consisting of a 20 nm Ca layer and a 100 nm Ag layer is evaporated on top by thermal evaporation. Finally the device is encapsulated using a UV

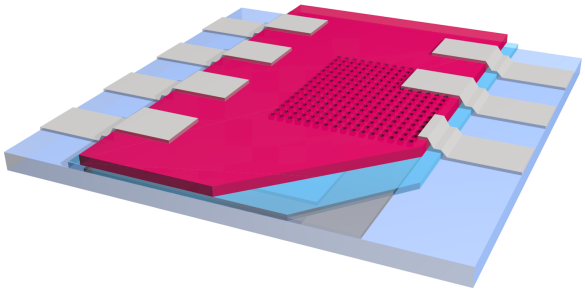

Figure 7.8: Drawing of a nantextured organic solar cell with an active layer fabricated by nanotransferprinting

curing epoxy and a thin glass sheet. The whole layer stack is depicted in figure 7.1.

Figure 7.9 shows the exemplary i-v-characteristics of a transferred nanotextured organic solar cell (red) compared to a transferred flat cell (black) from the first fabricated batch of nanotextured organic solar cells. The batch consists of 20 working solar cells. 5 of these cells are nanotextured while 15 are flat. All cells have a non optimized active layer thickness close to 300 nm. As one can see from the exemplary curves, the short circuit current of structured cells is higher when compared to that of flat cells. The open circuit voltage also shows a very small change to slightly higher values. While the open circuit voltage is mainly depending on the material composition [149], the short circuit current is mainly depending on the absorbed light. Therefore an increased absorption in the active layer caused by the integrated nanotexture is likely.

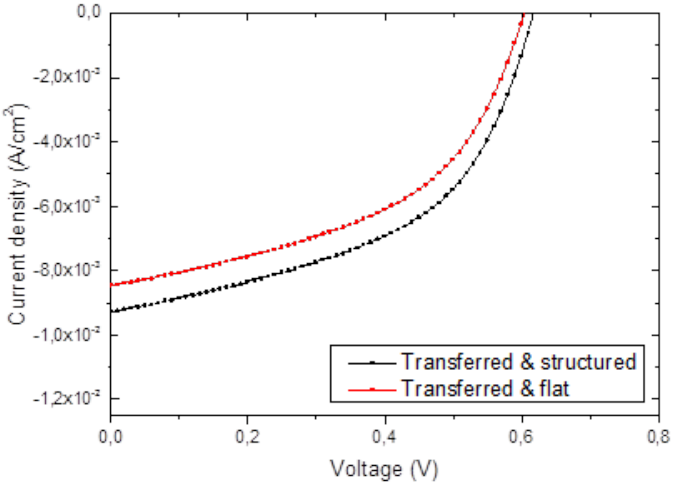

Figure 7.9: I-v-characteristics of a transferred nanotextured organic solar cell (red) compared to a transferred flat cell (black)

Table 7.1 shows the average power conversion efficiency (η), the short circuit voltage (J) and the fill factor of the nanotextured cells compared to that of not textured cells. While the average fill factor is only increased by 1.42 % when introducing the nanotexture, the short circuit voltage shows an increase of 0.81 mA/cm. This results in an average increase of 13,7 % in the power conversion efficiency of nanotextured cells compared to flat cells. These values are comparable to values achieved by Li [143] and You [144]. Therefore it is believed that the increase of efficiency is caused by a SPP resonance effect, which results in a higher absorption and therefore higher charge carrier generation within the active layer.

In a second approach cells with an optimized active layer thickness of 180 nm and two different kinds of nanotextures were fabricated and compared to flat

Table 7.1: Average power conversion efficiency values of nanotextured transferprinted organic solar cells compared to transferprinted flat organic solar cells.

	$\eta(\%)$	$J(mA/cm^2)$	FF(%)
flat	2,46	8,43	47,96
structured	2,80	9,24	49,38
difference	0,34	0,81	1,42

cells from the same batch. The second batch consisted out of 15 cells, 12 flat and 3 structured. Two of these structured cells are fabricated with holes as in the previously mentioned batch and one with a pillar structure on top.

Exemplary plots of i-v-characteristics of devices from this batch are shown in figure 7.10. The behaviour of the different cells is similar to that of the first batch in figure 7.9. While the open circuit voltage is nearly the same for all devices, the short circuit current is varying. Solar cells with a hole structure in the active layer show a significantly higher current than cells with pillars or flat cells.

Table 7.2 shows the average efficiency and fill factor of structured cells with pillars and holes compared to flat cells. Cells with a hole structure show a 16.8 % higher efficiency than flat cells while cells with a pillar structure show a 10.8 % higher efficiency than flat cells. It is therefore believed that the plasmonic effect (see 7.1) is less present if the grating is pointing out of the active layer as it is the case with the pillar structure.

Additionally to the I-V-characteristics of the devices the external quantum efficiency (EQE) was obtained. In figure 7.11 the EQE of transferprinted cells with pillar and hole structures are compared to that of transferprinted flat cell and spin coated cells.

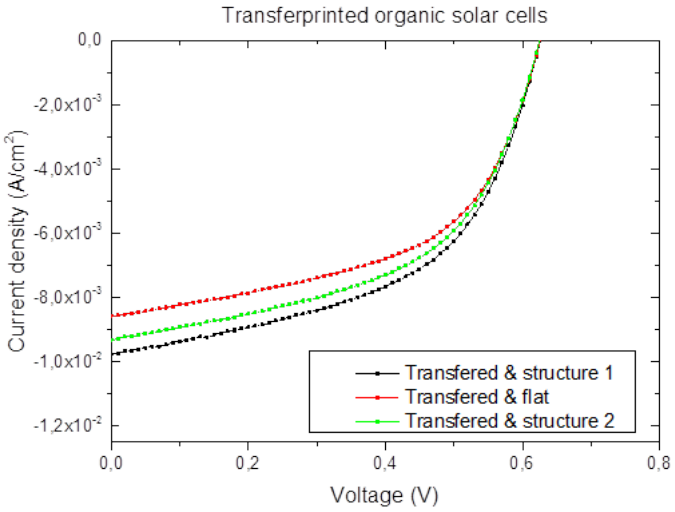

Figure 7.10: I-v-characteristics of a transferred nanotextured organic solar cell with holes (red) and pillars (green) compared to a transferred flat cell (black)

As one can see the quantum efficiency of all devices is nearly identical for wavelengths shorter than 470 nm. At longer wavelengths the behaviour changes. While the quantum efficiency of spincoated and flat transfered cells starts to drop already at a wavelength of 550 nm the quantum efficiency of both kinds of structured cells stays high until close to 600 nm. The cells with hole structure show a slightly higher quantum efficiency than the ones with pillars.

Table 7.2: Average power conversion efficiency values of nanotextured transferprinted organic solar cells compared to different transferprinted flat organic solar cells.

	$\eta(\%)$	FF(%)
flat	2,75	52,6
pillars	3,04	52,6
holes	3,20	53,7
difference flat-pillars	0,29	0,0
difference flat-holes	0,45	1,1

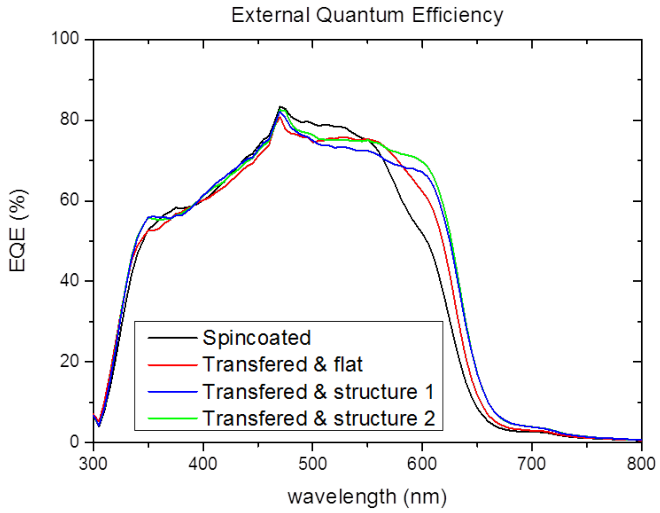

Figure 7.11: External quantum efficiency of transferprinted nanotextured organic solar cells with different structures compared to flat and spin coated cells.

7.4 Conclusion

The fabrication of nanotextured organic semiconductors by the means of nanotransferprinting has been demonstrated. Layers consisting of PEDOT:PSS and a blend of P3HT:PCBM with a weight ratio of 1:0.75 have been transferred with nanotextured stamps with hole and pillar nanostructures. Due to the evaporation of a Ca/Ag back electrode on the structured layers a metallic grating is formed.

These layers have been used to fabricate nanostructured organic solar cells. These structured cells show a higher power conversion efficiency compared to not structured cells. Structures with holes show a 13,7% higher power conversion efficiency with non optimized active layer thickness and 16.8% with optimized active layer thickness of 180 nm.

8 Conclusion and outlook

The aim of this work was the demonstration of alternative fabrication methods for organic devices. This has been achieved by the fabrication of different kinds of organic devices with several non-standard fabrication methods.

In a first chapter the fabrication of transparent conductive electrodes using the conductive polymer PEDOT:PSS has been demonstrated. Furthermore this material has then been used to fabricate fully carbon transistors using a lithography process.

Also the fabrication of ITO free P3HT:PCBM-based organic photodiodes using a spray coating manufacturing process has been demonstrated. The fabricated devices reach an external quantum efficiency of 62 % and on-off-ratios of nearly 4 orders of magnitude.

A maximum cut-off frequency of 9 kHz has been reached at a light power of 400 µW/cm^2 as well as a responsivity of 0.25 A/W at 530 nm. Future work will be devoted to increase the operational frequency of these spray-deposited photodiodes as well as their quantum efficiency. The achieved results are comparable to that of ITO free OPDs fabricated with other materials or fabrication techniques.

It has been also demonstrated that fabricating ion-selective electrodes solely by spray coating is an effective way to fabricate reliable potentiometric sensors. Achieved sensors are stable and show a response and selectivity comparable to

values achieved in literature. The fabrication of CNT-FET based ISFETs with a spraycoated ion -selective membrane has been demonstrated. Results achieved with ISFETs are well comparable to that achieved with spray coated ISEs.

In a following chapter the fabrication of nanotextured organic semiconductors by the means of nanotransferprinting has been demonstrated. Layers consisting of PEDOT:PSS and a blend of P3HT:PCBM have been transferred with nanotextured stamps with hole and pillar nanostructures to form together with an evaporated Ca/Ag layer metallic back electrodes on organic solar cells.

These structured cells show a higher power conversion efficiency compared to not structured cells. With a non optimized active layer thickness, structures with holes show a 13,7% higher power conversion efficiency, with an optimized active layer thickness of 180 nm a 16.8% higher power conversion efficiency is reached.

Several fabrication methods usable in organic devices have been presented. It has been shown that photodetectors, as well as transistors are possible with PEDOT electrodes. The possibility of fabricating full solid state potentiometric sensors with spraycoating has been demonstrated as well as the increase of the efficiency of organic solar cells by transferprinting nanostructured organic layers.

Future work should focus on the further improvement of the lithographic process used to fabricate the PEDOT:PSS transistors to increase the on off-ratio of these devices. Also additional ways to increase the conductivity of the PEDOT:PSS electrodes used for organic photodiodes should be investigated to increase the performance of these devices.

An additional interesting field for further research would be the integration of the all carbon transistors presented in chapter 4 with the ISFET from chapter 6 to fabricate disposable cheap fully carbon and transparent devices.

Symbols

Symbols	Unit	Description
a_{sc}	cm^2	solar cell area
c	$\frac{m}{s}$	speed of light
$D(E)$		density of states for electrons
d	cm	substrate-to-nozzle distance
d_{sheet}	nm	layer thickness
$E - E_0$	eV	energy relative to the center of $D(E)$
e	C	elementary charge
E_1	eV	energy of the valence band
E_2	eV	energy of the conduction band
E_G	eV	energy of the band gap
$EQE_R(\lambda)$	%	external quantum efficiency of reference
$EQE_{SC}(\lambda)$	%	external quantum efficiency of device
η_0	Nsm^{-2}	viscosity of the imprint resist
η_{sc}	%	power conversion efficiency
η		quantum efficiency
F	N	imprint force
FF	%	fill factor
h	$J \cdot s$	Planck constant

h_0	m	imprint resist thickness
h_f	m	residual layer height
I	A	current
I_D	A	photo current of device
I_R	A	photo current of reference
I_s	A	reverse bias saturation current
I_{pp}	A	maximum power point current
I_{sc}	A	short circuit current
L	m	length of the imprinted structure
λ	nm	wavelength
N		density of monomer states
n	cm^{-3}	concentration of conducting electrons
NA		numerical aperture
N_e		number of extracted charge carriers
n_i	cm^{-3}	material's intrinsic concentration of charge carriers
M_{pp}	W	maximum power point
n		ideality factor
N_P		number of impinging photons
p	cm^{-3}	concentration of conducting electron holes
P_L	W/cm^2	light power
CD	nm	critical dimension
κ_1		system factor
p	bar	carrier gas pressure
R	$\frac{A}{W}$	responsivity
R_{sheet}	Ωcm	sheet resistance
σ		width of the Gaussian density of state distribution
s	m	width of the imprinted structure

T	C	substrate temperature
t	s	spray time
t_f	s	imprint time
T_g	C	glass transition temperature
T_{opt}	%	optical transmission
V_{br}	V	breakdown voltage
V_d	V	threshold voltage
V_D	V	voltage across the diode
V_{dr}	V	drain voltage
V_{EG}	V	gate voltage
V_{oc}	V	open circuit voltage
V_{pp}	V	maximum power point voltage
V_T	V	thermal voltage

Acronyms

AFM	atomic force microscope.
CNT	carbon nanotube.
CNT-FET	carbon nanotube field effect transistors.
CPs	conductive polymers.
DCB	dichlorobenzene.
DI-water	deionized-water.
DMSO	dimethyl sulfoxide.
DOS	bis(2-ethylhexyl) sebacate.
EG	ethylene glycol.
EQE	external quantum efficiency.
GPS	3-glycidoxypropyltrimethoxysilane.
HCL	hole conducting layer.
HH	head–head.
HOMO	highest occupied molecular orbital.
HT	head–tail.
ASS-ISE	all-solid-state ion-selective electrodes.
ISEs	ion-selective electrodes.
ISFET	ion-selective field effect transistors.
ITO	indium tin oxide.

LUMO	lowest unoccupied molecular orbital.
MWCNT	multi-wall carbon nanotubes.
NIL	Nanoimprint lithography.
nTP	Nanotransfer printing.
OFET	organic field effect transistors.
OLED	organic light emitting diode.
OPD	organic photodiode.
OSC	organic solar cell.
P3HT	poly(3-hexylthiophene).
PCBM	[6,6]-phenyl-C61-butyric acid methyl ester.
PDMS	Polydimethylsiloxane.
PEC	polyelectrolyte complex.
PEDOT:PSS	Poly(3,4-ethylenedioxythiophene):poly(styrenesulfonate).
PET	Polyethylene terephthalate.
PRINT	pattern replication in nonwetting templates.
PVC	Polyvinyl chloride.
RFID	radio-frequency identification.
rr-P3HT	regioregular P3HT.
rra-P3HT	regiorandom P3HT.
SD	standard deviation.
SDS	sodium dodecyl sulfate.
SEM	scanning electron microscope.
	.
THF	tetrahydrofuran.
TT	tail–tail.
WLI	white light interferometry.

List of Figures

List of Tables

References

[1] A. Einstein. "Über einen die Erzeugung und Verwandlung des Lichtes betreffenden heuristischen Gesichtspunkt". In: *Annalen der Physik* 322.6 (1905), pp. 132–148.

[2] F. G. Brunetti, R. Kumar, and F. Wudl. "Organic electronics from perylene to organic photovoltaics: painting a brief history with a broad brush". In: *J. Mater. Chem.* 20.15 (2010), p. 2934.

[3] Y. Yang and F. Wudl. "Organic Electronics: From Materials to Devices". In: *Advanced Materials* 21.14-15 (Apr. 2009), pp. 1401–1403.

[4] P. Kumar and S. Chand. "Recent progress and future aspects of organic solar cells". In: *Prog. Photovolt: Res. Appl.* 20.4 (Aug. 2011), pp. 377–415.

[5] H. Shirakawa, E. J. Louis, A. G. MacDiarmid, C. K. Chiang, and A. J. Heeger. "Synthesis of electrically conducting organic polymers: halogen derivatives of polyacetylene, (CH) x". In: *J. Chem. Soc., Chem. Commun.* 16 (1977), p. 578.

[6] L. Torsi, M. Magliulo, K. Manoli, and G. Palazzo. "Organic field-effect transistor sensors: a tutorial review". In: *Chemical Society Reviews* 42.22 (2013), p. 8612.

[7] V. Subramanian, P. Chang, J. Lee, S. Molesa, and S. Volkman. "Printed organic transistors for ultra-low-cost RFID applications". In: *IEEE Transactions on Components and Packaging Technologies* 28.4 (2005), pp. 742–747.

[8] K. Melzer, A. M. Münzer, E. Jaworska, K. Maksymiuk, A. Michalska, and G. Scarpa. "Polymeric ion-selective membrane functionalized gate-electrodes: Ion-selective response of electrolyte-gated poly (3-hexylthiophene) field-effect transistors". In: *Organic Electronics* 15.2 (Feb. 2014), pp. 595–601.

[9] N. Thejo Kalyani and S. Dhoble. "Organic light emitting diodes: Energy saving lighting technology - A review". In: *Renewable and Sustainable Energy Reviews* 16.5 (June 2012), pp. 2696–2723.

[10] S. Günes, H. Neugebauer, and N. S. Sariciftci. "Conjugated Polymer-Based Organic Solar Cells". In: *Chemical Reviews* 107.4 (Apr. 2007), pp. 1324–1338.

[11] B. Kippelen and J.-L. Brédas. "Organic photovoltaics". In: *Energy & Environmental Science* 2.3 (2009), p. 251.

[12] W. J. D. Beenken. "Excitons in conjugated polymers: Do we need a paradigma change?" In: *Phys. Status Solidi (a)* 206.12 (Aug. 2009), pp. 2750–2756.

[13] R. Österbacka, C. P. An, X. M. Jiang, and Z. V. Vardeny. "Two-Dimensional Electronic Excitations in Self-Assembled Conjugated Polymer Nanocrystals". In: *Science* 287.5454 (Feb. 2000), pp. 839–842.

[14] D. Hertel and H. Bässler. "Photoconduction in Amorphous Organic Solids". In: *ChemPhysChem* 9.5 (Mar. 2008), pp. 666–688.

[15] G. D. Scholes and G. Rumbles. "Excitons in nanoscale systems". In: *Nature Materials* 5.9 (Sept. 2006), pp. 683–696.

[16] C. Deibel and V. Dyakonov. "Polymer-fullerene bulk heterojunction solar cells". In: *Reports on Progress in Physics* 73.9 (2010), pp. 096401–.

[17] H. Bässler. "Charge Transport in Disordered Organic Photoconductors a Monte Carlo Simulation Study". In: *phys. stat. sol. (b)* 175.1 (1993), pp. 15–56.

[18] R. Schmechel. "Gaussian disorder model for high carrier densities: Theoretical aspects and application to experiments". In: *Phys. Rev. B* 66.23 (2002), p. 235206.

[19] F. Liu, Y. Gu, X. Shen, S. Ferdous, H.-W. Wang, and T. P. Russell. "Characterization of the morphology of solution-processed bulk heterojunction organic photovoltaics". In: *Progress in Polymer Science* 38.12 (Dec. 2013), pp. 1990–2052.

[20] R. Elsenbaumer, K. Jen, and R. Oboodi. "Processible and environmentally stable conducting polymers". In: *Synthetic Metals* 15.2-3 (July 1986), pp. 169–174.

[21] S. S. Pandey, W. Takashima, S. Nagamatsu, T. Endo, M. Rikukawa, and K. Kaneto. "Regioregularity vs Regiorandomness: Effect on Photocarrier Transport in Poly(3-hexylthiophene)". In: *Japanese Journal of Applied Physics* 39.Part 2, No. 2A (Feb. 2000), pp. L94–L97.

[22] P. Schilinsky. "Loss analysis of the power conversion efficiency of organic bulk heterojunction solar cells". PhD thesis. Carl von Ossietzky Universität Oldenburg, 2005.

[23] R. Kroon, M. Lenes, J. C. Hummelen, P. W. M. Blom, and B. de Boer. "Small Bandgap Polymers for Organic Solar Cells (Polymer Material Development in the Last 5 Years)". In: *Polymer Reviews* 48.3 (2008), pp. 531–582.

[24] M. Caironi, T. Agostinelli, D. Natali, M. Sampietro, R. Cugola, M. Catellani, and S. Luzzati. "External quantum efficiency versus charge carriers mobility in polythiophene/methanofullerene based planar photodetectors". In: *Journal of Applied Physics* 102.2 (2007), p. 024503.

[25] J. C. Hummelen, B. W. Knight, F. LePeq, F. Wudl, J. Yao, and C. L. Wilkins. "Preparation and Characterization of Fulleroid and Methanofullerene Derivatives". In: *The Journal of Organic Chemistry* 60.3 (Feb. 1995), pp. 532–538.

[26] G. Yu, J. Gao, J. C. Hummelen, F. Wudl, and A. J. Heeger. "Polymer Photovoltaic Cells: Enhanced Efficiencies via a Network of Internal Donor-Acceptor Heterojunctions". In: *Science* 270.5243 (1995), pp. 1789–1791.

[27] J. Xue and S. R. Forrest. "Carrier transport in multilayer organic photodetectors: I. Effects of layer structure on dark current and photoresponse". In: *Journal of Applied Physics* 95.4 (2004), pp. 1859–1868.

[28] J. Huang, X. Wang, Y. Kim, A. J. deMello, D. D. C. Bradley, and J. C. deMello. "High efficiency flexible ITO-free polymer/fullerene photodiodes". In: *Physical Chemistry Chemical Physics* 8.33 (2006), pp. 3904–3908.

[29] F. Zhang, M. Johansson, M. Andersson, J. Hummelen, and O. Ingans. "Polymer Photovoltaic Cells with Conducting Polymer Anodes". In: *Advanced Materials* 14.9 (May 2002), pp. 662–665.

[30] V. D. Mihailetchi, P. W. M. Blom, J. C. Hummelen, and M. T. Rispens. "Cathode dependence of the open-circuit voltage of polymer:fullerene bulk heterojunction solar cells". In: *Journal of Applied Physics* 94.10 (Nov. 2003), pp. 6849–6854.

[31] L. Groenendaal, F. Jonas, D. Freitag, H. Pielartzik, and J. R. Reynolds. "Poly(3,4-ethylenedioxythiophene) and Its Derivatives: Past, Present, and Future". In: *Advanced Materials* 12.7 (Apr. 2000), pp. 481–494.

[32] A. Elschner, S. Kirchmeyer, W. Lovenich, U. Merker, and K. Reuter. *PEDOT: Principles and Applications of an Intrinsically Conductive Polymer*. CRC Press, 2010, p. 147.

[33] A. Elschner, F. Bruder, H.-W. Heuer, F. Jonas, A. Karbach, S. Kirchmeyer, S. Thurm, and R. Wehrmann. "PEDT/PSS for efficient hole-injection in hybrid organic light-emitting diodes". In: *Synthetic Metals* 111-112 (June 2000), pp. 139–143.

[34] B. Friedel, P. E. Keivanidis, T. J. K. Brenner, A. Abrusci, C. R. McNeill, R. H. Friend, and N. C. Greenham. "Effects of Layer Thickness and Annealing of PEDOT:PSS Layers in Organic Photodetectors". In: *Macromolecules* 42.17 (Sept. 2009), pp. 6741–6747.

[35] H.-H. Moretto, M. Schulze, and G. Wagner. "Silicones". In: *Ullmann's Encyclopedia of Industrial Chemistry* (June 2000).

[36] E. Baumann. "Ueber einige Vinylverbindungen". In: *Ann. Chem. Pharm.* 163.3 (1872), pp. 308–322.

[37] M. W. Allsopp and G. Vianello. "Poly(Vinyl Chloride)". In: *Ullmann's Encyclopedia of Industrial Chemistry* (June 2000).

[38] D. P. Sanders. "Advances in Patterning Materials for 193 nm Immersion Lithography". In: *Chemical Reviews* 110.1 (Jan. 2010), pp. 321–360.

[39] S. Y. Chou, P. R. Krauss, and P. J. Renstrom. "Imprint Lithography with 25-Nanometer Resolution". In: *Science* 272.5258 (Apr. 1996), pp. 85–87.

[40] M. Beck, M. Graczyk, I. Maximov, E.-L. Sarwe, T. Ling, M. Keil, and L. Montelius. "Improving stamps for 10 nm level wafer scale nanoimprint lithography". In: *Microelectronic Engineering* 61-62 (July 2002), pp. 441–448.

[41] E. Menard and J. Rogers. *Handbook of Nanotechnology*. Ed. by B. Bhushan. Springer-Verlag, 2007, pp. 239–298.

[42] A. Carlson, A. M. Bowen, Y. Huang, R. G. Nuzzo, and J. A. Rogers. "Transfer Printing Techniques for Materials Assembly and Micro/Nanodevice Fabrication". In: *Advanced Materials* 24.39 (Oct. 2012), pp. 5284–5318.

[43] M. Mühlberger, I. Bergmair, A. Klukowska, A. Kolander, H. Leichtfried, E. Platzgummer, H. Loeschner, C. Ebm, G. Grötzner, and R. Schäftner. "UV-NIL with working stamps made from Ormostamp". In: *Microelectronic Engineering* 86.4-6 (Apr. 2009), pp. 691–693.

[44] H. Schift, C. Spreu, M. Saidani, M. Bednarzik, J. Gobrecht, A. Klukowska, F. Reuther, G. Gruetzner, and H. H. Solak. "Transparent hybrid polymer stamp copies with sub-50-nm resolution for thermal and UV-nanoimprint lithography". In: *J. Vac. Sci. Technol. B* 27.6 (2009), p. 2846.

[45] A. Klukowska, A. Kolander, I. Bergmair, M. Mühlberger M.hlberger, H. Leichtfried, F. Reuther, G. Grötzner, and R. Schäftner. "Novel transparent hybrid polymer working stamp for UV-imprinting". In: *Microelectronic Engineering* 86.4-6 (Apr. 2009), pp. 697–699.

[46] H. Lan. "Updates in Advanced Lithography". In: InTech, July 2013. Chap. Soft UV Nanoimprint Lithography and Its Applications, pp. 196–197.

[47] S. W. Lee and S. S. Lee. "Shrinkage ratio of PDMS and its alignment method for the wafer level process". In: *Microsystem Technologies* 14.2 (May 2007), pp. 205–208.

[48] H. Hillborg, J. Ankner, U. Gedde, G. Smith, H. Yasuda, and K. Wikström. "Crosslinked polydimethylsiloxane exposed to oxygen plasma studied by neutron reflectometry and other surface specific techniques". In: *Polymer* 41.18 (Aug. 2000), pp. 6851–6863.

[49] D. Bodas and C. Khan-Malek. "Formation of more stable hydrophilic surfaces of PDMS by plasma and chemical treatments". In: *Microelectronic Engineering* 83.4-9 (Apr. 2006), pp. 1277–1279.

[50] C. K. Chan, L. J. Richter, B. Dinardo, C. Jaye, B. R. Conrad, H. W. Ro, D. S. Germack, D. A. Fischer, D. M. DeLongchamp, and D. J. Gundlach. "High performance airbrushed organic thin film transistors". In: *Appl. Phys. Lett.* 96.13 (2010), p. 133304.

[51] N. A. Azarova, J. W. Owen, C. A. McLellan, M. A. Grimminger, E. K. Chapman, J. E. Anthony, and O. D. Jurchescu. "Fabrication of organic thin-film transistors by spray-deposition for low-cost, large-area electronics". In: *Organic Electronics* 11.12 (Dec. 2010), pp. 1960–1965.

[52] S. F. Tedde, J. Kern, T. Sterzl, J. Fürst, P. Lugli, and O. Hayden. "Fully Spray Coated Organic Photodiodes". In: *Nano Letters* 9.3 (Mar. 2009), pp. 980–983.

[53] D. Baierl, B. Fabel, P. Lugli, and G. Scarpa. "Efficient indium-tin-oxide (ITO) free top-absorbing organic photodetector with highly transparent polymer top electrode". In: *Organic Electronics* 12.10 (Oct. 2011), pp. 1669–1673.

[54] A. Abdellah, B. Fabel, P. Lugli, and G. Scarpa. "Spray deposition of organic semiconducting thin-films: Towards the fabrication of arbitrary shaped organic electronic devices". In: *Organic Electronics* 11.6 (June 2010), pp. 1031–1038.

[55] H. Noda, T. Umeda, H. Mizukami, A. Fujii, and M. Ozaki. "Fabrication of Organic Photovoltaic Cells with Interpenetrating Heterojunction of Conducting Polymer and C_{60} by Spray Method". In: *Japanese Journal of Applied Physics* 45.4A (2006), pp. 2792–2793.

[56] K.-J. Kim, Y.-S. Kim, J.-U. Park, W.-S. Kang, B.-H. Kang, S.-H. Yeom, D.-E. Kim, J.-H. Kim, and S.-W. Kang. "Substrate Heated Spray-Deposition Method for High Efficient Organic Solar Cell: Morphology Inspection". In: *Japanese Journal of Applied Physics* 49.1 (2010), pp. 018002–.

[57] C. Girotto, D. Moia, B. P. Rand, and P. Heremans. "High-Performance Organic Solar Cells with Spray-Coated Hole-Transport and Active Layers". In: *Advanced Functional Materials* 21.1 (2011), pp. 64–72.

[58] E. Jaworska, M. Schmidt, G. Scarpa, K. Maksymiuk, and A. Michalska. "Spray-coated all-solid-state potentiometric sensors". In: *Analyst* 139 (2014), pp. 6011–6016.

[59] B. Chapman. *Glow Discharge Processes, Sputtering and Etching*. JOHN WILEY & SONS, New York, 1980.

[60] Y. H. Kim, C. Sachse, M. L. Machala, C. May, L. Müller-Meskamp, and K. Leo. "Highly Conductive PEDOT:PSS Electrode with Optimized Solvent and Thermal Post-Treatment for ITO-Free Organic Solar Cells". In: *Advanced Functional Materials* 21.6 (2011), pp. 1076–1081.

[61] X. Crispin, F. L. E. Jakobsson, A. Crispin, P. C. M. Grim, P. Andersson, A. Volodin, C. van Haesendonck, M. Van der Auweraer, W. R. Salaneck, and M. Berggren. "The Origin of the High Conductivity of Poly(3,4-ethylenedioxythiophene):Poly(styrenesulfonate) (PEDOT:PSS) Plastic Electrodes". In: *Chem. Mater.* 18.18 (Aug. 2006), pp. 4354–4360.

[62] J. Huang, P. F. Miller, J. S. Wilson, A. J. de Mello, J. C. de Mello, and D. D. C. Bradley. "Investigation of the Effects of Doping and Post-Deposition Treatments on the Conductivity, Morphology, and Work Function of Poly(3,4-ethylenedioxythiophene)/Poly(styrene sulfonate) Films". In: *Adv. Funct. Mater.* 15.2 (Feb. 2005), pp. 290–296.

[63] J. Ouyang, C.-W. Chu, F.-C. Chen, Q. Xu, and Y. Yang. "High-Conductivity Poly(3,4-ethylenedioxythiophene):Poly(styrene sulfonate) Film and Its Application in Polymer Optoelectronic Devices". In: *Adv. Funct. Mater.* 15.2 (Feb. 2005), pp. 203–208.

[64] S. Kirchmeyer and K. Reuter. "Scientific importance, properties and growing applications of poly(3,4-ethylenedioxythiophene)". In: *J. Mater. Chem.* 15.21 (2005), p. 2077.

[65] J.-H. Huang, D. Kekuda, C.-W. Chu, and K.-C. Ho. "Electrochemical characterization of the solvent-enhanced conductivity of poly(3,4-ethylenedioxythiophene) and its application in polymer solar cells". In: *J. Mater. Chem.* 19.22 (2009), p. 3704.

[66] H. Yan and H. Okuzaki. "Effect of solvent on PEDOT/PSS nanometer-scaled thin films: XPS and STEM/AFM studies". In: *Synthetic Metals* 159.21-22 (Nov. 2009), pp. 2225–2228.

[67] D. Khodagholy, T. Doublet, M. Gurfinkel, P. Quilichini, E. Ismailova, P. Leleux, T. Herve, S. Sanaur, C. Bernard, and G. G. Malliaras. "Highly Conformable Conducting Polymer Electrodes for In Vivo Recordings". In: *Advanced Materials* 23.36 (Aug. 2011), H268–H272.

[68] D. Baierl, B. Fabel, P. Gabos, L. Pancheri, P. Lugli, and G. Scarpa. "Solution-processable inverted organic photodetectors using oxygen plasma treatment". In: *Organic Electronics* 11.7 (July 2010), pp. 1199–1206.

[69] D. Baierl, L. Pancheri, M. Schmidt, D. Stoppa, G.-F. Dalla Betta, G. Scarpa, and P. Lugli. "A hybrid CMOS-imager with a solution-processable polymer as photoactive layer". In: *Nature Communications* 3 (Nov. 2012), p. 1175.

[70] S.-I. Na, S.-S. Kim, J. Jo, and D.-Y. Kim. "Efficient and Flexible ITO-Free Organic Solar Cells Using Highly Conductive Polymer Anodes". In: *Advanced Materials* 20.21 (Nov. 2008), pp. 4061–4067.

[71] A. Falco, L. Cinà, G. Scarpa, P. Lugli, and A. Abdellah. "Fully-Sprayed and Flexible Organic Photodiodes with Transparent Carbon Nanotube Electrodes". In: *ACS Applied Materials & Interfaces* 6.13 (July 2014), pp. 10593–10601.

[72] J. Y. Lee. "Lifetime improvement of polymer light emitting diodes through a poly(3,4-ethylenedioxythiophene):silane hole transport layer". In: *Chemical Physics Letters* 393.1-3 (July 2004), pp. 260–263.

[73] D. Khodagholy, M. Gurfinkel, E. Stavrinidou, P. Leleux, T. Herve, S. Sanaur, and G. G. Malliaras. "High speed and high density organic electrochemical transistor arrays". In: *Appl. Phys. Lett.* 99.16 (2011), p. 163304.

[74] D. Baierl. "A Hybrid CMOS-Imager with integrated Solution-Processable Organic Photodiodes". PhD thesis. Technische Universität München, 2012.

[75] H. Do, M. Reinhard, H. Vogeler, A. Puetz, M. F. Klein, W. Schabel, A. Colsmann, and U. Lemmer. "Polymeric anodes from poly(3,4-ethylenedioxythiophene):poly(styrenesulfonate) for 3.5% efficient organic solar cells". In: *Thin Solid Films* 517.20 (Aug. 2009), pp. 5900–5902.

[76] C. C. Cid, J. Riu, A. Maroto, and F. X. Rius. "Ion-sensitive field effect transistors using carbon nanotubes as the transducing layer". In: *The Analyst* 133.8 (2008), p. 1001.

[77] K. Melzer, A. M. Münzer, E. Jaworska, K. Maksymiuk, A. Michalska, and G. Scarpa. "Selective ion-sensing with membrane-functionalized electrolyte-gated carbon nanotube field-effect transistors". In: *The Analyst* 139.19 (2014), p. 4947.

[78] M. Schmidt, A. Falco, M. Loch, P. Lugli, and G. Scarpa. "Spray coated indium-tin-oxide-free organic photodiodes with PEDOT:PSS anodes". In: *AIP Advances* 4.10 (2014), p. 107132.

[79] J. J. M. Halls, C. A. Walsh, N. Greenham, E. A. Marseglia, R. Friend, S. C. Moratti, and A. Holmes. "Efficient photodiodes from interpenetrating polymer networks". In: *Nature* 376.6540 (Aug. 1995), pp. 498–500.

[80] M. P. Ramuz, M. Vosgueritchian, P. Wei, C. Wang, Y. Gao, Y. Wu, Y. Chen, and Z. Bao. "Evaluation of Solution-Processable Carbon-Based Electrodes for All-Carbon Solar Cells". In: *ACS Nano* 6.11 (Nov. 2012), pp. 10384–10395.

[81] M. W. Rowell, M. A. Topinka, M. D. McGehee, H.-J. Prall, G. Dennler, N. S. Sariciftci, L. Hu, and G. Gruner. "Organic solar cells with carbon nanotube network electrodes". In: *Applied Physics Letters* 88.23 (2006), p. 233506.

[82] S. De, T. M. Higgins, P. E. Lyons, E. M. Doherty, P. N. Nirmalraj, W. J. Blau, J. J. Boland, and J. N. Coleman. "Silver Nanowire Networks as Flexible, Transparent, Conducting Films: Extremely High DC to Optical Conductivity Ratios". In: *ACS Nano* 3.7 (June 2009), pp. 1767–1774.

[83] J. van de Groep, P. Spinelli, and A. Polman. "Transparent Conducting Silver Nanowire Networks". In: *Nano Letters* 12.6 (May 2012), pp. 3138–3144.

[84] H. Wu, D. Kong, Z. Ruan, P.-C. Hsu, S. Wang, Z. Yu, T. J. Carney, L. Hu, S. Fan, and Y. Cui. "A transparent electrode based on a metal nanotrough network". In: *Nature Nanotechnology* (May 2013).

[85] D.-S. Leem, A. Edwards, M. Faist, J. Nelson, D. D. C. Bradley, and J. C. de Mello. "Efficient Organic Solar Cells with Solution-Processed Silver Nanowire Electrodes". In: *Advanced Materials* 23.38 (2011), pp. 4371–4375.

[86] J. Zou, H.-L. Yip, S. K. Hau, and A. K.-Y. Jen. "Metal grid/conducting polymer hybrid transparent electrode for inverted polymer solar cells". In: *Applied Physics Letters* 96.20 (2010), p. 203301.

[87] H. Do, M. Reinhard, H. Vogeler, A. Puetz, M. F. Klein, W. Schabel, A. Colsmann, and U. Lemmer. "Polymeric anodes from poly(3,4 - ethylenedioxythiophene): poly(styrenesulfonate) for 3.5% efficient organic solar cells". In: *Thin Solid Films* 517.20 (Aug. 2009), pp. 5900–5902.

[88] Y. Zhou, F. Zhang, K. Tvingstedt, S. Barrau, F. Li, W. Tian, and O. Inganas. "Investigation on polymer anode design for flexible polymer solar cells". In: *Applied Physics Letters* 92.23 (2008), p. 233308.

[89] Y.-S. Hsiao, W.-T. Whang, C.-P. Chen, and Y.-C. Chen. "High-conductivity poly(3,4-ethylenedioxythiophene):poly(styrene sulfonate) film for use in ITO-free polymer solar cells". In: *Journal of Materials Chemistry* 18.48 (2008), pp. 5948–5955.

[90] A. Abdellah, K. S. Virdi, R. Meier, M. Däblinger, P. Müller-Buschbaum, C. Scheu, P. Lugli, and G. Scarpa. "Successive Spray Deposition of P3HT/PCBM Organic Photoactive Layers: Material Composition and Device Characteristics". In: *Advanced Functional Materials* 22.19 (2012), pp. 4078–4086.

[91] S.-I. Na, B.-K. Yu, S.-S. Kim, D. Vak, T.-S. Kim, J.-S. Yeo, and D.-Y. Kim. "Fully spray-coated ITO-free organic solar cells for low-cost power generation". In: *Solar Energy Materials and Solar Cells* 94.8 (Aug. 2010), pp. 1333–1337.

[92] R. Po, C. Carbonera, A. Bernardi, and N. Camaioni. "The role of buffer layers in polymer solar cells". In: *Energy Environ. Sci.* 4.2 (2011), pp. 285–310.

[93] H. Ma, H.-L. Yip, F. Huang, and A. K.-Y. Jen. "Interface Engineering for Organic Electronics". In: *Advanced Functional Materials* 20.9 (May 2010), pp. 1371–1388.

[94] T. Saito. "Advances in Photodiodes". In: InTech, 2011. Chap. Spectral Properties of Semiconductor Photodiodes.

[95] G. Pace, A. Grimoldi, D. Natali, M. Sampietro, J. E. Coughlin, G. C. Bazan, and M. Caironi. "All-Organic and Fully-Printed Semitransparent Photodetectors based on Narrow Bandgap Conjugated Molecules". In: *Advanced Materials* (Sept. 2014).

[96] G. Azzellino, A. Grimoldi, M. Binda, M. Caironi, D. Natali, and M. Sampietro. "Fully Inkjet-Printed Organic Photodetectors with High Quantum Yield". In: *Advanced Materials* 25.47 (Sept. 2013), pp. 6829–6833.

[97] J. Bobacka. "Conducting Polymer-Based Solid-State Ion-Selective Electrodes". In: *Electroanalysis* 18.1 (Jan. 2006), pp. 7–18.

[98] E. Bakker, D. Diamond, A. Lewenstam, and E. Pretsch. "Ion sensors: current limits and new trends". In: *Analytica Chimica Acta* 393.1-3 (June 1999), pp. 11–18.

[99] B. Nikolskii and E. Materova. "Solid Contact in Membrane Ion-Selective Electrodes". In: *Ion-Selective Electrode Reviews* (1985), pp. 3–39.

[100] A. Michalska. "All-Solid-State Ion Selective and All-Solid-State Reference Electrodes". In: *Electroanalysis* 24.6 (May 2012), pp. 1253–1265.

[101] R. W. Cattrall and H. Freiser. "Coated wire ion-selective electrodes". In: *Analytical Chemistry* 43.13 (Nov. 1971), pp. 1905–1906.

[102] A. Michalska. "Optimizing the analytical performance and construction of ion-selective electrodes with conducting polymer-based ion-to-electron transducers". In: *Anal Bioanal Chem* 384.2 (Dec. 2005), pp. 391–406.

[103] P. C. Hauser, D. W. Chiang, and G. A. Wright. "A potassium-ion selective electrode with valinomycin based poly(vinyl chloride) membrane and a poly(vinyl ferrocene) solid contact". In: *Analytica Chimica Acta* 302.2-3 (Feb. 1995), pp. 241–248.

[104] G. S. Cha, D. Liu, M. E. Meyerhoff, H. C. Cantor, A. R. Midgley, H. D. Goldberg, and R. B. Brown. "Electrochemical performance, biocompatibility, and adhesion of new polymer matrixes for solid-state ion sensors". In: *Analytical Chemistry* 63.17 (Sept. 1991), pp. 1666–1672.

[105] M. Fibbioli, W. E. Morf, M. Badertscher, N. F. de Rooij, and E. Pretsch. "Potential Drifts of Solid-Contacted Ion-Selective Electrodes Due to Zero-Current Ion Fluxes Through the Sensor Membrane". In: *Electroanalysis* 12.16 (Nov. 2000), pp. 1286–1292.

[106] L. Y. Heng and E. A. H. Hall. "Producing "Self-Plasticizing" Ion-Selective Membranes". In: *Analytical Chemistry* 72.1 (Jan. 2000), pp. 42–51.

[107] P. Buhlmann and L. D. Chen. *Supramolecular Chemistry: From Molecules to Nanomaterials*. Ed. by J. W. Steed and P. A. Gale. Vol. 5. Wiley, 2012, pp. 2539–2576.

[108] A. Ceresa. "Ion-Selective Polymeric Membrane Electrodes for Potentiometrie Trace Level Measurements". PhD thesis. Swiss Federal Institute of Technology, Zurich, 2001.

[109] G. Moody, E. Saad, and J. Thomas. "The development of polymer matrix membranes for ion-selective electrodes". In: *Sel. Electrode Rev.* 10 (1988), pp. 71–106.

[110] R. Armstrong and G. Horvai. "Properties of PVC based membranes used in ion-selective electrodes". In: *Electrochimica Acta* 35.1 (Jan. 1990), pp. 1–7.

[111] U. Fiedler. "Influence of the dielectric constant of the medium on the selectivities of neutral carrier ligands in electrode membranes". In: *Analytica Chimica Acta* 89.1 (Mar. 1977), pp. 111–118.

[112] M. Nägele, Y. Mi, E. Bakker, and E. Pretsch. "Influence of Lipophilic Inert Electrolytes on the Selectivity of Polymer Membrane Electrodes". In: *Analytical Chemistry* 70.9 (May 1998), pp. 1686–1691.

[113] A. Abdelhalim, A. Abdellah, G. Scarpa, and P. Lugli. "Fabrication of carbon nanotube thin films on flexible substrates by spray deposition and transfer printing". In: *Carbon* 61 (Sept. 2013), pp. 72–79.

[114] F. X. Rius-Ruiz, G. A. Crespo, D. Bejarano-Nosas, P. Blondeau, J. Riu, and F. X. Rius. "Potentiometric Strip Cell Based on Carbon Nanotubes as Transducer Layer: Toward Low-Cost Decentralized Measurements". In: *Analytical Chemistry* 83.22 (Nov. 2011), pp. 8810–8815.

[115] E. Jaworska, W. Lewandowski, J. Mieczkowski, K. Maksymiuk, and A. Michalska. "Simple and disposable potentiometric sensors based on graphene or multi-walled carbon nanotubes - carbon - plastic potentiometric sensors". In: *The Analyst* 138.8 (2013), p. 2363.

[116] M. Novell, M. Parrilla, G. A. Crespo, F. X. Rius, and F. J. Andrade. "Paper-Based Ion-Selective Potentiometric Sensors". In: *Analytical Chemistry* 84.11 (June 2012), pp. 4695–4702.

[117] A. Michalska and K. Maksymiuk. "All-plastic, disposable, low detection limit ion-selective electrodes". In: *Analytica Chimica Acta* 523.1 (Oct. 2004), pp. 97–105.

[118] E. Jaworska, M. Wojcik, A. Kisiel, J. Mieczkowski, and A. Michalska. "Gold nanoparticles solid contact for ion-selective electrodes of highly stable potential readings". In: *Talanta* 85.4 (Sept. 2011), pp. 1986–1989.

[119] E. Jaworska, W. Lewandowski, J. Mieczkowski, K. Maksymiuk, and A. Michalska. "Critical assessment of graphene as ion-to-electron transducer for all-solid-state potentiometric sensors". In: *Talanta* 97 (Aug. 2012), pp. 414–419.

[120] A. Hulanicki and A. Michalska. "All-solid-state chloride-selective electrode with poly(pyrrole) solid contact". In: *Electroanalysis* 7.7 (July 1995), pp. 692–693.

[121] J. Janata. "Historical review. Twenty years of ion-selective field-effect transistors". In: *The Analyst* 119.11 (1994), p. 2275.

[122] A. Sibbald. "Chemical-sensitive field-effect transistors". In: *IEE Proceedings I Solid State and Electron Devices* 130.5 (1983), p. 233.

[123] P. Bergveld. "Thirty years of ISFETOLOGY". In: *Sensors and Actuators B: Chemical* 88.1 (Jan. 2003), pp. 1–20.

[124] C. Jimenez-Jorquera, J. Orozco, and A. Baldi. "ISFET Based Microsensors for Environmental Monitoring". In: *Sensors* 10.1 (Dec. 2009), pp. 61–83.

[125] A. S. Piet Bergveld. *Analytical and Biomedical Applications of Ion-selective Field-effect Transistors*. Elsevier, pp. 75–99.

[126] A. M. Münzer, M. Heimgreiter, K. Melzer, A. Weise, B. Fabel, A. Abdellah, P. Lugli, and G. Scarpa. "Back-gated spray-deposited carbon nanotube thin film transistors operated in electrolytic solutions: an assessment towards future biosensing applications". In: *Journal of Materials Chemistry B* 1.31 (2013), p. 3797.

[127] A. M. Münzer, W. Seo, G. J. Morgan, Z. P. Michael, Y. Zhao, K. Melzer, G. Scarpa, and A. Star. "Sensing Reversible Protein-Ligand Interactions with Single-Walled Carbon Nanotube Field-Effect Transistors". In: *The Journal of Physical Chemistry C* 118.31 (Aug. 2014), pp. 17193–17199.

[128] T. Haeberle, A. M. Münzer, F. Buth, J. Antonio Garrido, A. Abdellah, B. Fabel, P. Lugli, and G. Scarpa. "Solution processable carbon nanotube network thin-film transistors operated in electrolytic solutions at various pH". In: *Appl. Phys. Lett.* 101.22 (2012), p. 223101.

[129] E. Bakker, E. Pretsch, and P. Bühlmann. "Selectivity of Potentiometric Ion Sensors". In: *Analytical Chemistry* 72.6 (Mar. 2000), pp. 1127–1133.

[130] P. Kurzweil. "Metal Oxides and Ion-Exchanging Surfaces as pH Sensors in Liquids: State-of-the-Art and Outlook". In: *Sensors* 9.6 (June 2009), pp. 4955–4985.

[131] M. Schmidt, P. Lugli, G. Ulisse, C. Ciceroni, and F. Brunetti. "Nanopatterning of P3HT:PCBM for organic solar cell realization". In: *2015 IEEE 15th International Conference on Nanotechnology (IEEE-NANO)* (July 2015).

[132] Q. Gan, F. J. Bartoli, and Z. H. Kafafi. "Plasmonic-Enhanced Organic Photovoltaics: Breaking the 10% Efficiency Barrier". In: *Advanced Materials* 25.17 (2013), pp. 2385–2396.

[133] E. Menard, M. A. Meitl, Y. Sun, J.-U. Park, D. J.-L. Shir, Y.-S. Nam, S. Jeon, and J. A. Rogers. "Micro- and Nanopatterning Techniques for Organic Electronic and Optoelectronic Systems". In: *Chemical Reviews* 107.4 (Apr. 2007), pp. 1117–1160.

[134] H. A. Atwater and A. Polman. "Plasmonics for improved photovoltaic devices". In: *Nature Materials* 9.3 (Feb. 2010), pp. 205–213.

[135] M.-G. Kang, M.-S. Kim, J. Kim, and L. J. Guo. "Organic Solar Cells Using Nanoimprinted Transparent Metal Electrodes". In: *Advanced Materials* 20.23 (Dec. 2008), pp. 4408–4413.

[136] S. Y. Chou and W. Ding. "Ultrathin, high-efficiency, broad-band, omni-acceptance, organic solar cells enhanced by plasmonic cavity with subwavelength hole array". In: *Optics Express* 21.S1 (Nov. 2013), A60.

[137] Y. Jin, J. Feng, X.-L. Zhang, M. Xu, Y.-G. Bi, Q.-D. Chen, H.-Y. Wang, and H.-B. Sun. "Surface-plasmon enhanced absorption in organic solar cells by employing a periodically corrugated metallic electrode". In: *Appl. Phys. Lett.* 101.16 (2012), p. 163303.

[138] S.-S. Kim, S.-I. Na, J. Jo, D.-Y. Kim, and Y.-C. Nah. "Plasmon enhanced performance of organic solar cells using electrodeposited Ag nanoparticles". In: *Appl. Phys. Lett.* 93.7 (2008), p. 073307.

[139] A. J. Morfa, K. L. Rowlen, T. H. Reilly, M. J. Romero, and J. van de Lagemaat. "Plasmon-enhanced solar energy conversion in organic bulk heterojunction photovoltaics". In: *Appl. Phys. Lett.* 92.1 (2008), p. 013504.

[140] J.-L. Wu, F.-C. Chen, Y.-S. Hsiao, F.-C. Chien, P. Chen, C.-H. Kuo, M. H. Huang, and C.-S. Hsu. "Surface Plasmonic Effects of Metallic Nanoparticles on the Performance of Polymer Bulk Heterojunction Solar Cells". In: *ACS Nano* 5.2 (Feb. 2011), pp. 959–967.

[141] B. Wu, T. Z. Oo, X. Li, X. Liu, X. Wu, E. K. L. Yeow, H. J. Fan, N. Mathews, and T. C. Sum. "Efficiency Enhancement in Bulk-Heterojunction Solar Cells Integrated with Large-Area Ag Nanotriangle Arrays". In: *The Journal of Physical Chemistry C* 116.28 (July 2012), pp. 14820–14825.

[142] R. C. Wadams, C.-w. Yen, D. P. Butcher, H. Koerner, M. F. Durstock, L. Fabris, and C. E. Tabor. "Gold nanorod enhanced organic photovoltaics: The importance of morphology effects". In: *Organic Electronics* 15.7 (July 2014), pp. 1448–1457.

[143] X. Li, W. E. Sha, W. C. Choy, D. D. S. Fung, and F. X. Xie. "Efficient Inverted Polymer Solar Cells with Directly Patterned Active Layer and Silver Back Grating". In: *The Journal of Physical Chemistry C* 116.12 (Mar. 2012), pp. 7200–7206.

[144] J. You, X. Li, F.-x. Xie, W. E. I. Sha, J. H. W. Kwong, G. Li, W. C. H. Choy, and Y. Yang. "Surface Plasmon and Scattering-Enhanced Low-Bandgap Polymer Solar Cell by a Metal Grating Back Electrode". In: *Adv. Energy Mater.* 2.10 (June 2012), pp. 1203–1207.

[145] D.-H. Ko, J. R. Tumbleston, L. Zhang, S. Williams, J. M. DeSimone, R. Lopez, and E. T. Samulski. "Photonic Crystal Geometry for Organic Solar Cells". In: *Nano Lett.* 9.7 (July 2009), pp. 2742–2746.

[146] M. J. Hampton, S. S. Williams, Z. Zhou, J. Nunes, D.-H. Ko, J. L. Templeton, E. T. Samulski, and J. M. DeSimone. "The Patterning of Sub-500 nm Inorganic Oxide Structures". In: *Advanced Materials* 20.14 (July 2008), pp. 2667–2673.

[147] R. M. de Oliveira Hansen, Y. Liu, M. Madsen, and H.-G. Rubahn. "Flexible organic solar cells including efficiency enhancing grating structures". In: *Nanotechnology* 24.14 (Mar. 2013), p. 145301.

[148] T. A. M. Ferenczi, J. Nelson, C. Belton, A. M. Ballantyne, M. Campoy-Quiles, F. M. Braun, and D. D. C. Bradley. "Planar heterojunction organic photovoltaic diodes via a novel stamp transfer process". In: *J. Phys.: Condens. Matter* 20.47 (Oct. 2008), p. 475203.

[149] I. Lange, J. Kniepert, P. Pingel, I. Dumsch, S. Allard, S. Janietz, U. Scherf, and D. Neher. "Correlation between the Open Circuit Voltage and the Energetics of Organic Bulk Heterojunction Solar Cells". In: *The Journal of Physical Chemistry Letters* 4.22 (Nov. 2013), pp. 3865–3871.

[150] H. Gerdes, M. Schmidt, J. Wellhausen, R. Bandorf, and G. Bräuer. "Investigations on high power impulse magnetron sputtering by optical emission spectroscopy of NiCr in different compositions (40/60 and 80/20)". In: *Proceedings of ICTF14 & RSD2008*. 2008, pp. 92–95.

[151] D. Baierl, M. Schmidt, G. Scarpa, P. Lugli, L. Pancheri, D. Stoppa, and G.-F. Dalla Betta. "Towards a hybrid CMOS-imager with organic semiconductors as photoactive layer". In: *7th Conference on Ph.D. Research in Microelectronics and Electronics* (July 2011), pp. 89–92.

[152] D. Weinbrenner, S. Yazji, M. Sachsenhauser, C. Westermeier, M. Schmidt, G. Scarpa, B. Nickel, I. Zardo, A. Cattani-Scholz, and G. Absteiter. "Thin-Film Morphology of Pentacene Films deposited on Organophosphonate Self-Assembled Monolayers". In: *2012 MRS Fall Meeting, Hynes Convention Center, Boston, Massachusetts, USA*. Nov. 2012.

[153] A. T. Exner, I. Pavlichenko, D. Baierl, M. Schmidt, G. Derondeau, B. V. Lotsch, P. Lugli, and G. Scarpa. "A step towards the electrophotonic nose: integrating 1D photonic crystals with organic light-emitting diodes and photodetectors". In: *Laser & Photonics Reviews* 8.5 (June 2014), pp. 726–733.

[154] M. Schmidt, G. Ullise, B. Fabel, F. Brunetti, and P. Lugli. "Nanotransfer Printing and Nanoimprinting of 3d structured P3HT:PCBM and PEDOT:PSS for organic solar cells". In: *11th International Conference on Nanosciences & Nanotechnologies (NN14)*. 2014.

[155] F. Brunetti et al. "Doped and textured graphene as electrode for organic solar cells". In: *IEEE Nano 2015 - 15th International Conference on Nanotechnology*. 2015.

[156] R. D. Nagel, T. Haeberle, M. Schmidt, P. Lugli, and G. Scarpa. "Large Area Nano-transfer Printing of Sub-50-nm Metal Nanostructures Using Low-cost Semi-flexible Hybrid Templates". In: *Nanoscale Research Letters* 11.1 (Mar. 2016).

Publications

H. Gerdes, M. Schmidt, J. Wellhausen, R. Bandorf, and G. Bräuer. "Investigations on high power impulse magnetron sputtering by optical emission spectroscopy of NiCr in different compositions (40/60 and 80/20)". In: *Proceedings of ICTF14 & RSD2008*. 2008, pp. 92–95.

D. Baierl, M. Schmidt, G. Scarpa, P. Lugli, L. Pancheri, D. Stoppa, and G.-F. Dalla Betta. "Towards a hybrid CMOS-imager with organic semiconductors as photoactive layer". In: *7th Conference on Ph.D. Research in Microelectronics and Electronics* (July 2011), pp. 89–92.

D. Baierl, L. Pancheri, M. Schmidt, D. Stoppa, G.-F. Dalla Betta, G. Scarpa, and P. Lugli. "A hybrid CMOS-imager with a solution-processable polymer as photoactive layer". In: *Nature Communications* 3 (Nov. 2012), p. 1175.

D. Weinbrenner, S. Yazji, M. Sachsenhauser, C. Westermeier, M. Schmidt, G. Scarpa, B. Nickel, I. Zardo, A. Cattani-Scholz, and G. Absteiter. "Thin-Film Morphology of Pentacene Films deposited on Organophosphonate Self-Assembled Monolayers". In: *2012 MRS Fall Meeting, Hynes Convention Center, Boston, Massachusetts, USA*. Nov. 2012.

A. T. Exner, I. Pavlichenko, D. Baierl, M. Schmidt, G. Derondeau, B. V. Lotsch, P. Lugli, and G. Scarpa. "A step towards the electrophotonic nose: integrating 1D photonic crystals with organic light-emitting diodes and photodetectors". In: *Laser & Photonics Reviews* 8.5 (June 2014), pp. 726–733.

E. Jaworska, M. Schmidt, G. Scarpa, K. Maksymiuk, and A. Michalska. "Spray-coated all-solid-state potentiometric sensors". In: *Analyst* 139 (2014), pp. 6011–6016.

M. Schmidt, A. Falco, M. Loch, P. Lugli, and G. Scarpa. "Spray coated indium-tin-oxide-free organic photodiodes with PEDOT:PSS anodes". In: *AIP Advances* 4.10 (2014), p. 107132.

M. Schmidt, G. Ullise, B. Fabel, F. Brunetti, and P. Lugli. "Nanotransfer Printing and Nanoimprinting of 3d structured P3HT:PCBM and PEDOT:PSS for organic solar cells". In: *11th International Conference on Nanosciences & Nanotechnologies (NN14)*. 2014.

F. Brunetti et al. "Doped and textured graphene as electrode for organic solar cells". In: *IEEE Nano 2015 - 15th International Conference on Nanotechnology*. 2015.

M. Schmidt, P. Lugli, G. Ulisse, C. Ciceroni, and F. Brunetti. "Nanopatterning of P3HT:PCBM for organic solar cell realization". In: *2015 IEEE 15th International Conference on Nanotechnology (IEEE-NANO)* (July 2015).

R. D. Nagel, T. Haeberle, M. Schmidt, P. Lugli, and G. Scarpa. "Large Area Nano-transfer Printing of Sub-50-nm Metal Nanostructures Using Low-cost Semi-flexible Hybrid Templates". In: *Nanoscale Research Letters* 11.1 (Mar. 2016).

Acknowledgments

A lot of people supported me during the writing process of this thesis and during the work before. These people I want to thank:

- Prof. Paolo Lugli for making this thesis possible by allowing me to work at the Institute for Nanoelectronics. I also want to thank him for his guidance and support.
- My co-authors Aniello Falco, Ewa Jaworska and Agatha Michalska.
- My family and Carmen for being a reliable support in the background and for pushing me to this point.
- Special thanks go to Katharina Melzer and Vejay Deepbath for being fabulous office mates, fun colleagues in the lab and for cheering me up during hard times. I miss you guys.
- Bernhard Fabel for being himself, the fruitful discussions and his guidance.
- Alexandra Muenzer for our little projects.
- All other current and former institute members for being great colleagues, creating a happy environment and all the fun we had: Simone, Armin, Omar, Daniela, Tobias, Robin, Ahmet, Alina, Alaa, Florin and last but not least Marius.